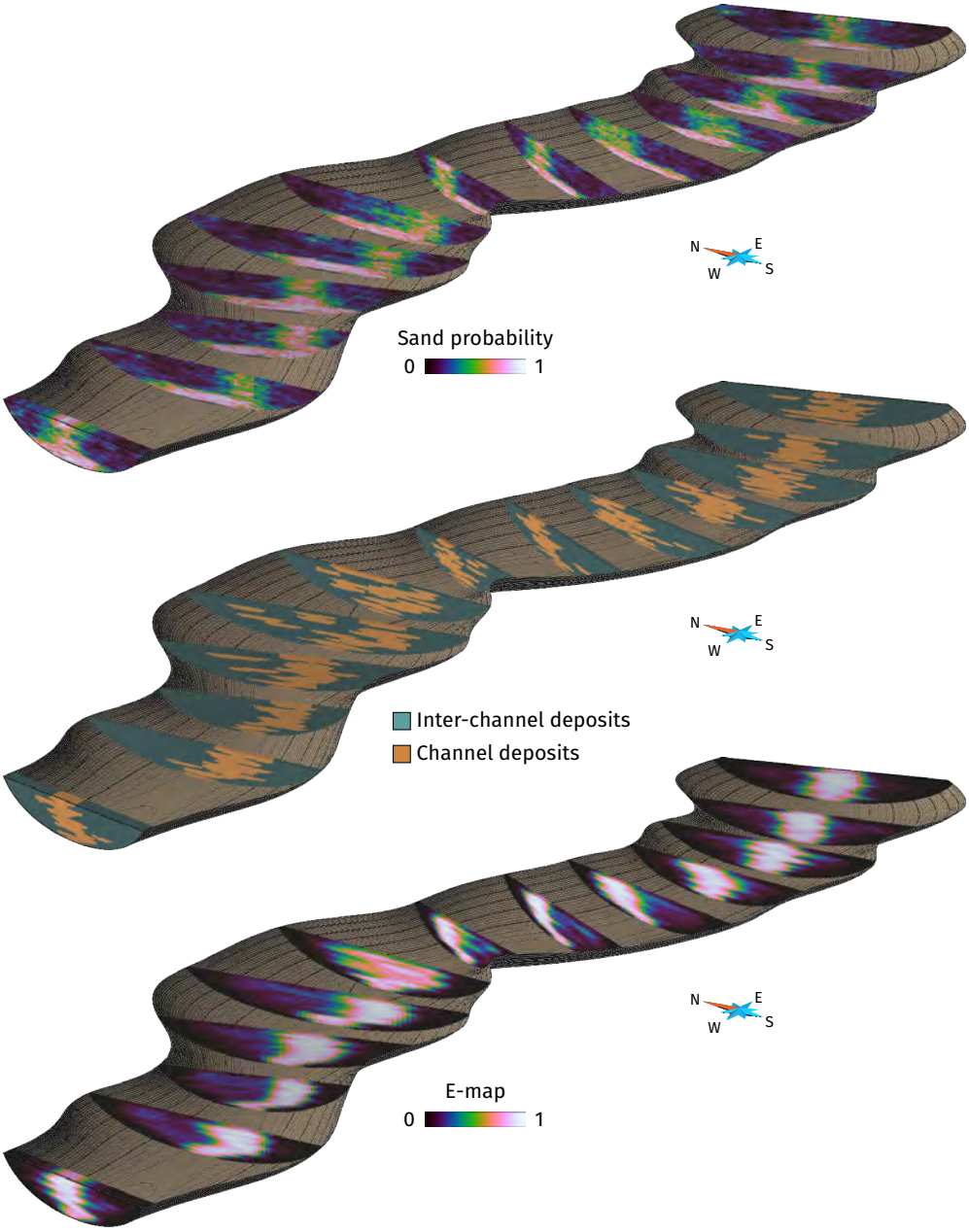

Figure 3.31 Details on the channel trend of the realization in figure 3.29 rasterized in the master channel grid. The sand property cube along the same sections is here for comparison. The E-map illustrates the mean channel distribution over the 100 unconditional realizations.

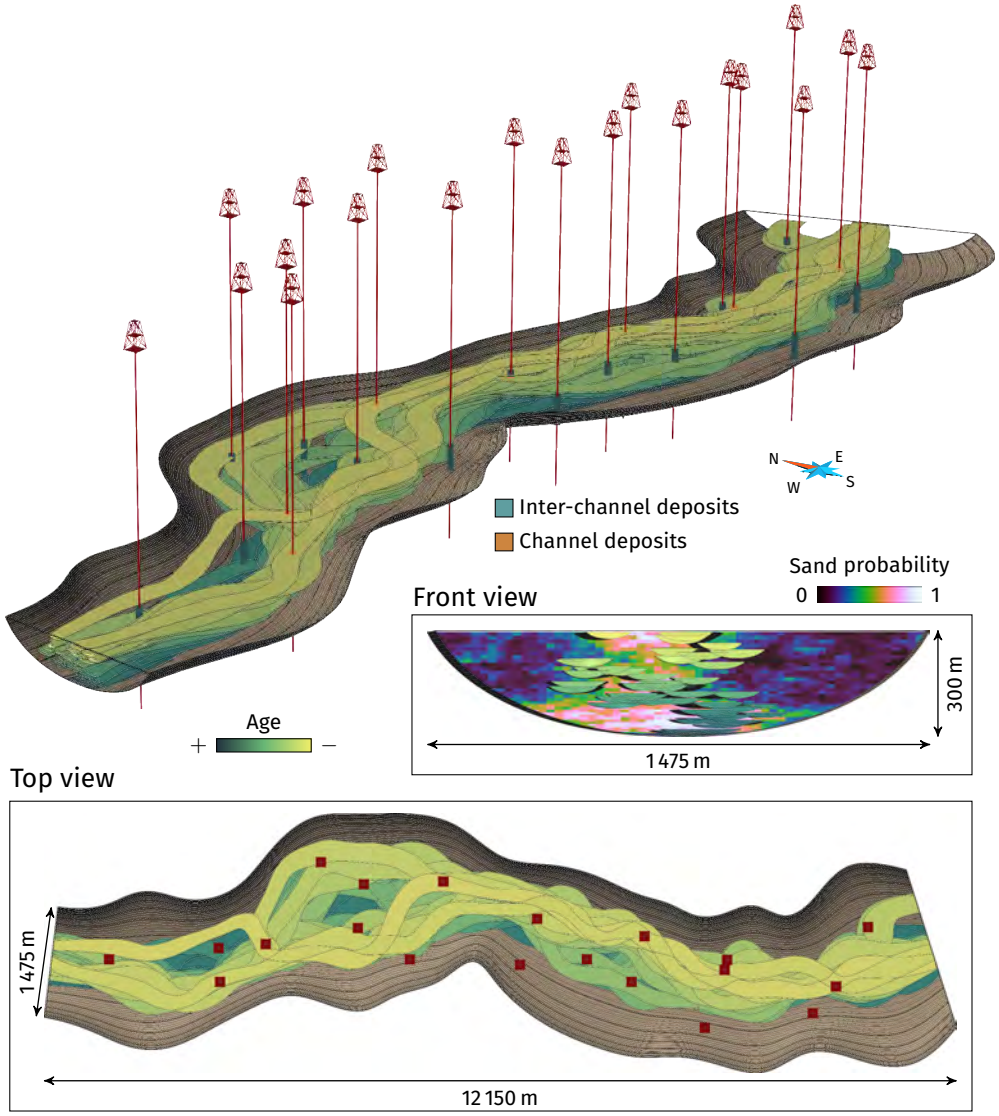

Figure 3.32 Example of a realization containing 40 channels conditioned to a sand probability cube and well sedimentary data within a master channel.

The purpose remains to preserve the channel morphology while respecting all those constraints. Figure 3.33 illustrates this aspect with the top channel of a realization. This channel must go through the entire master channel, without going outside the master channel margins, without conditioning one of the 14

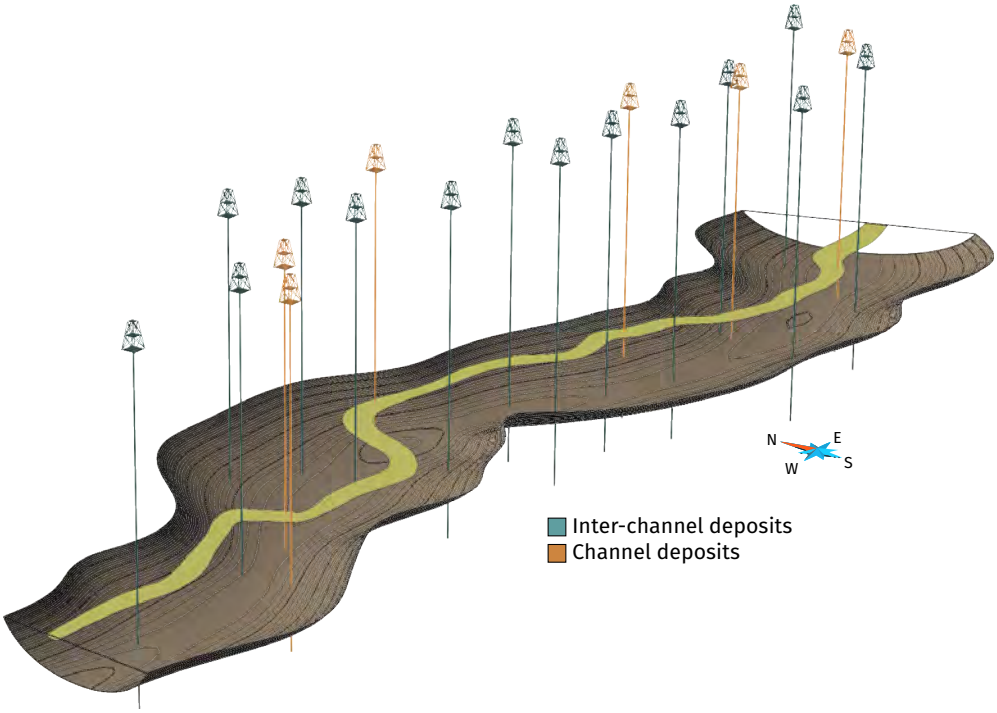

Top view

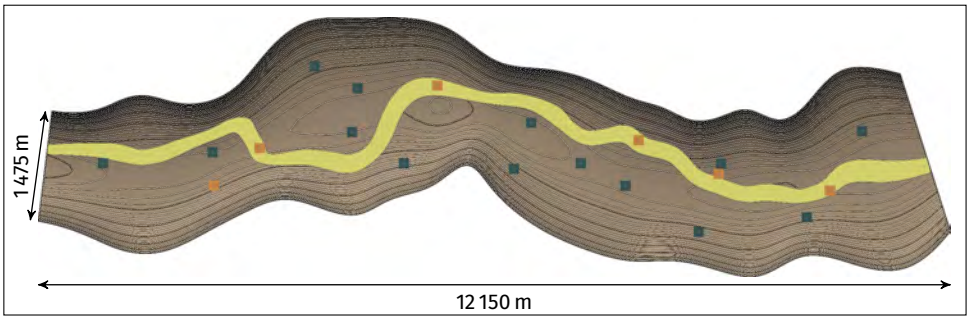

Figure 3.33 Channel at the top of the realization in figure 3.32. The wells are colored depending on their facies data for the channel.

inter-channel data and with 6 channel data that it may condition.

The channel centerlines never go outside the master channel margins, but locally the channel objects can go outside. This is often due to some inter-channel data close to the margins (figure 3.34): the space is maybe not enough

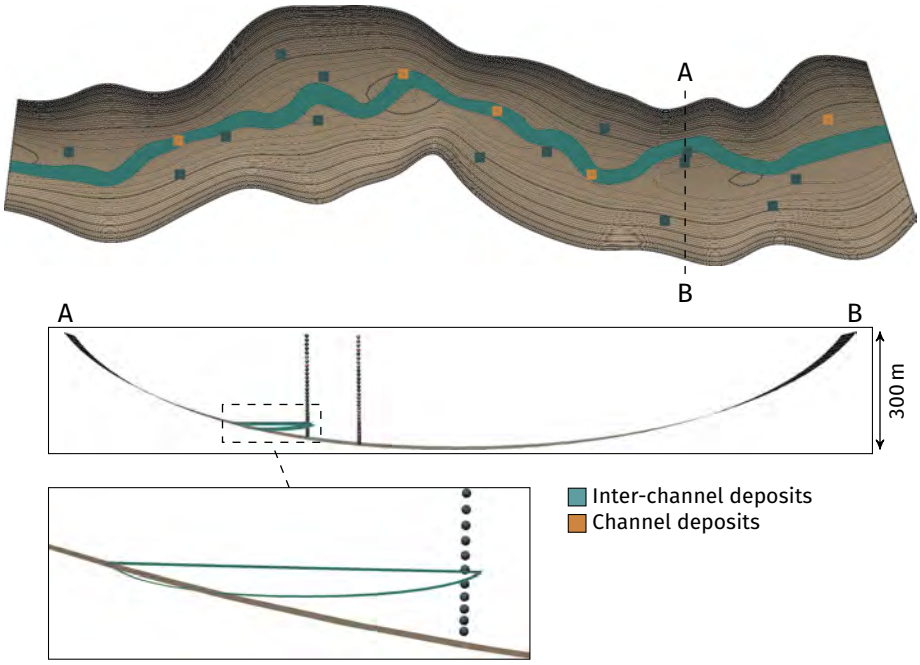

Figure 3.34 Example of incompatibility between the data and the L-system path.

for a channel to go through it, but the channel still does it. The influence of the sand probability is still noticeable (figure 3.35), with a subtle lateral development at the grid bottom due to the channel margin repulsion and a pronounced vertical trend at the grid top. The channels honor all the channel data, as the simulation process would not stop if it was not the case. But the conditioning area is based on a horizontal and a vertical criterion. Thus, this area is rectangular and not channel-shaped (figure 3.36, c). Over 234 channel data points, 15 are outside a channel and would require a post-process to strictly condition them. Similarly, some channels condition to inter-channel data: over 391 inter-channel data points, 30 are conditioned by a channel. This is either a failure of the repulsive process (figure 3.36, b), or a channel that conditions a channel data and at the end also conditions an inter-channel data (figure 3.36, a). This last case mainly arises because the simulation process is meant to favor channel data conditioning. Thus, if an inter-channel data is right below the channel data to condition, the inter-channel data is ignored.

The well data come from a realization of 40 channels. On average one realization contains 59,38 channels, with a standard deviation of 3.64. There

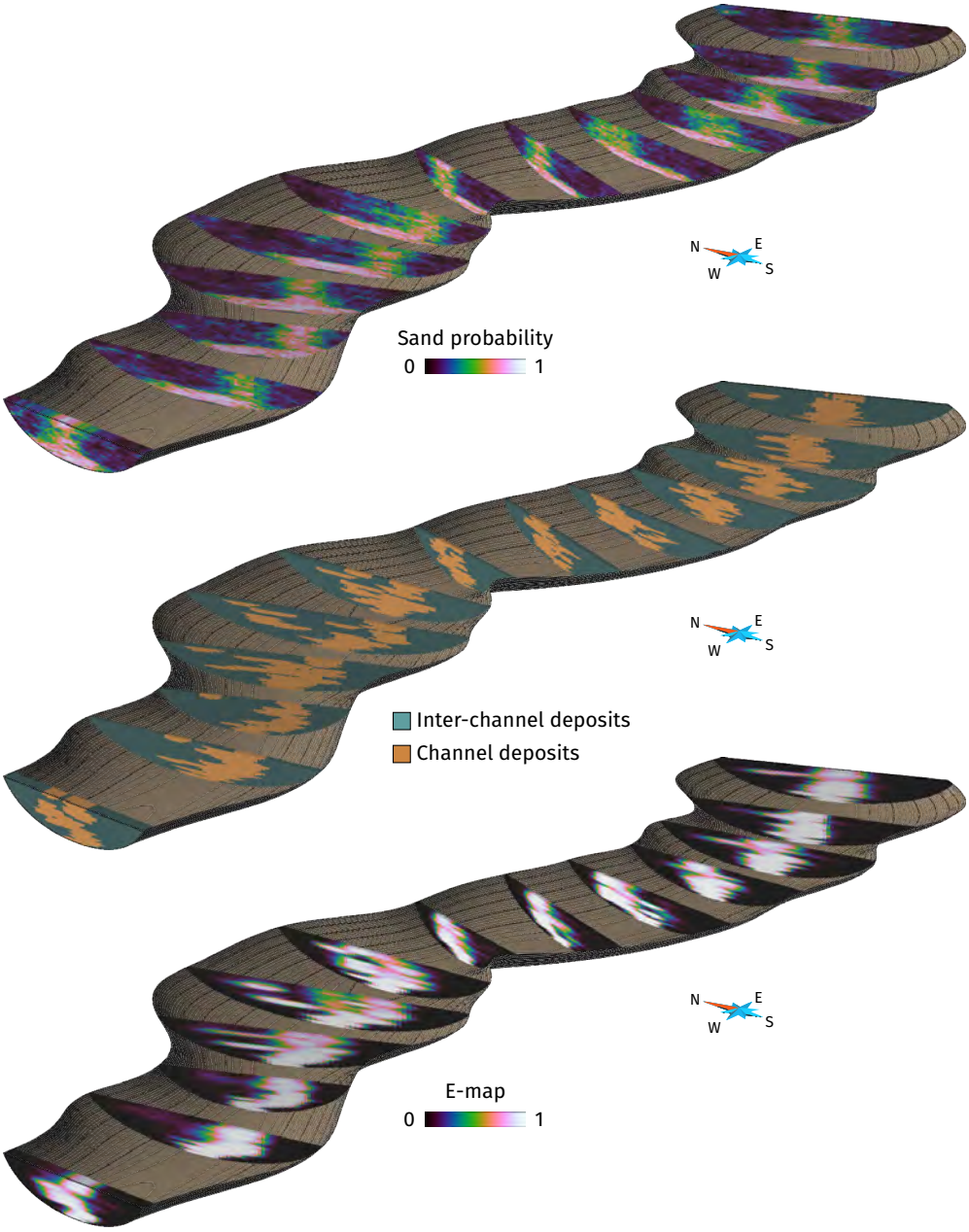

Figure 3.35 Details on the channel trend of the realization in figure 3.32 rasterized in the master channel grid. The sand property cube along the same sections is here for comparison. The E-map illustrates the mean channel distribution over the 100 unconditional realizations.

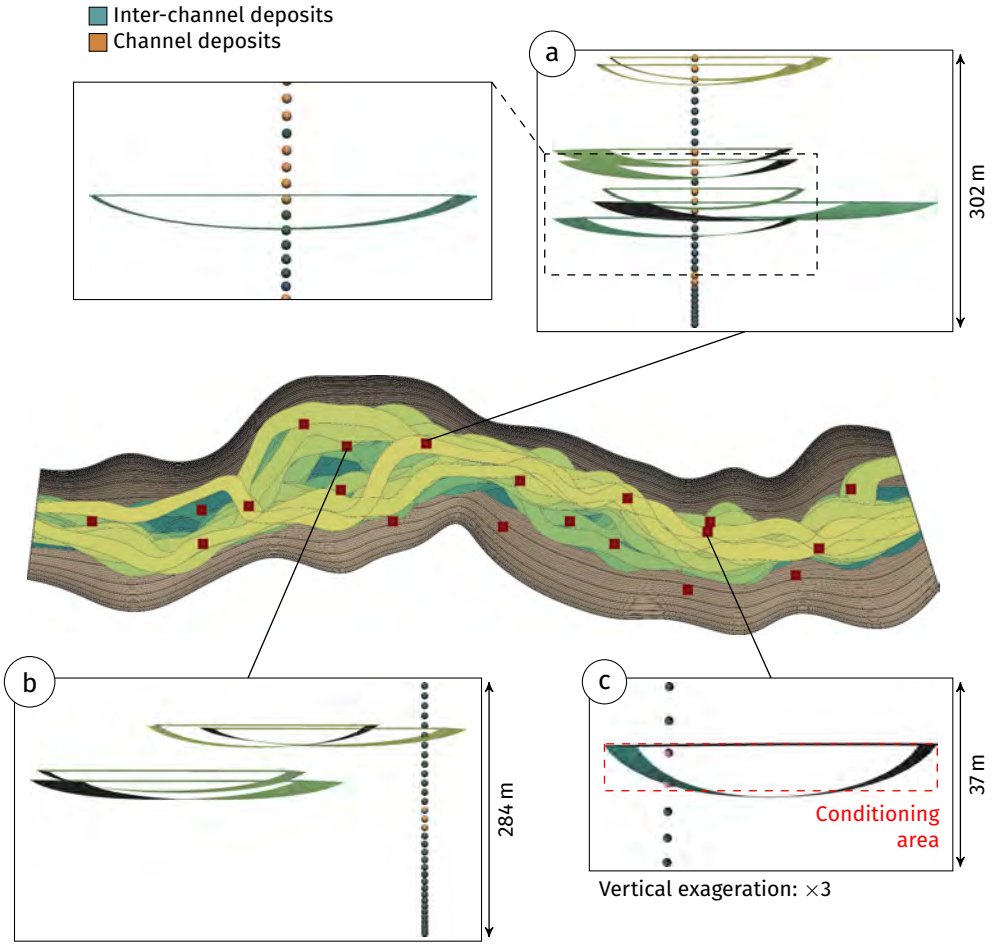

Figure 3.36 Details on the well conditioning of the realization in figure 3.32. All the channels passing at or near the wells are not showed for clarity. a. The four channels at the top of the well perfectly condition the channel data. At the middle of the well, the last channel condition both a channel data and an inter-channel data. Indeed, the process is currently not able to precisely condition the channel so that the channel data remains inside the channel and the inter-channel data remains outside. b. 5 channels are close to a set of inter-channel data along a well. One of those channels condition the inter-channel data. This case shows a failure in the repulsion process. c. The channel conditions the two channel data of the interval as defined in the simulation process. However, the channel data at the bottom is not within the channel and not conditioned *stricto sensu*.

is a clear increase due to the conditioning: none of the realizations has been able to condition all the channel data with less than 49 channels.

3.7 Discussion and perspectives

All the previous synthetic cases illustrate the method ability to simulate channels while taking into account various and numerous data. This section discusses some aspects of the simulation process.

3.7.1 About the channel morphology

With both the bend length and the curvature or the bend half-wavelength, bend amplitude and deviation angle, channel of various morphologies can be simulated, from straight to sinuous channels. The bends simulated with the current L-system rules follow a circular curve. In fluvial systems, bends are closer to a sine-generated curve than a circular curve [Langbein and Leopold, 1966], i.e., the angles between two successive segments evolve as a sine function of the channel distance, also called fattening. The bend shape also tends to be asymmetric or skewed depending on the global flow direction [e.g., Kinoshita, 1961, Brice, 1974, Carson and Lapointe, 1983]. Such asymmetry is also observable on turbiditic channels [Kolla et al., 2001] (figure 3.37). Kinoshita [1961] proposes a formula for the curvature of channel as a function of the channel distance, the bend wavelength and fattening and skewing coefficients. If necessary, the L-system rules can be easily modified to simulate bends based on a sine-generated curve or Kinoshita equation. Thanks to the L-system, the channel morphology is not a fixed feature of the method and can be changed at will.

The current process is still able to simulate asymmetric bend through two features. First when using the curvature, asymmetric can appear thanks to the stochastic process. However, such shapes do not appear at will. The channel global direction tend to skew more or less the bends depending on the global direction weight. It also tends to make the channels straighter. Here the control is more clear. However, the bends are deformed depending on the constraint direction, which are not necessarily oriented along the global flow direction. This results in one branch with bends deformed in the opposite direction than the bends of the other branch (figure 3.37). Such setting is unnatural. For now no solution has been found to control the bend asymmetry due to the global direction.

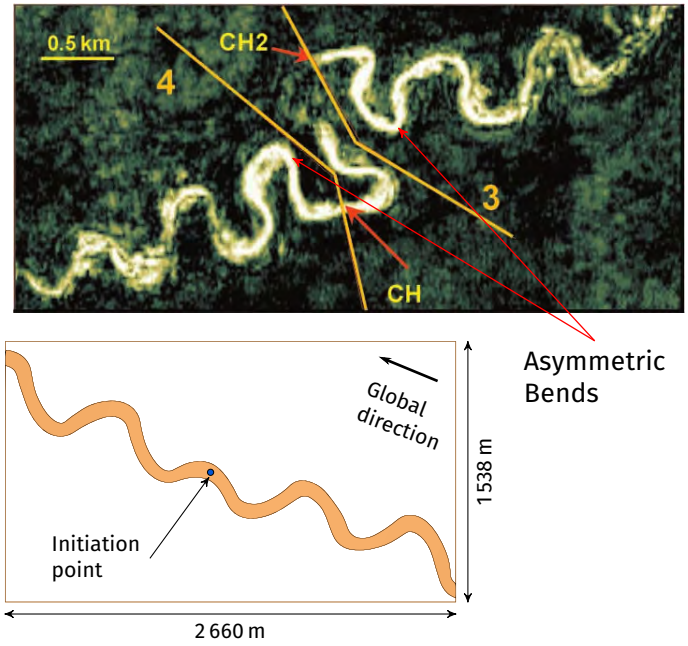

Figure 3.37 Examples of asymmetric bends on a seismic section from Angola, West Africa (modified from Kolla et al. [2001]) and below example of channel simulated with a L-system showing opposite bend asymmetries from the initiation point.

Similar issue is noticeable with the other constraints. The relative constraint setting has been developed with the idea of minimizing the deformation induced by a constraint. However when simulating channels the two most important aspects are:

- Conditioning to all the available data, as they give information about the real setting of the domain of interest.
- Preserving the channel continuity, as it has more impact on the flow than the channel sinuosity.

Currently, the method is able to satisfy both aspects. Better reproducing real channel morphology and better controlling the constraint impact still call for improvements. In this perspective, comparing the simulated morphology with real channels should give an insight on the method ability to simulate realistic bends.

When simulating channels with a high sinuosity, channel self-intersections may happen despite the global direction and the self-repulsion. The speed of

the simulation process (see section 3.7.12) makes conceivable to simply re-simulate the channel. Another solution is to suppress the loop formed by the self-intersection.

3.7.2 About constraints and conditioning

Constraints are able to handle a wide variety of constraining elements, from well data to probability cubes or seismic interpreted objects. This conditioning relies on the sum of vectors. Thus, it is a simple and fast process (see section 3.7.12). Getting the constraining vector is the only aspect that may slow down the conditioning process.

The main idea is to add as few constraints as possible, so that each constraint is expressed and taken into account at best. Adding few constraints helps to better preserve the channel morphology by limiting the deformations induced by the constraints.

A comparison with a conditioning by rejection sampling has been made to further analyze the bias introduced by the constraints on the channel morphology (figure 3.38). The rejection sampling is a simplistic conditioning process: an unconditional channel is simulated, if it fits the data it is kept, otherwise a new channel is simulated. Here the example is quite simple with two well channel data to condition. The channel parts within the inter-well area appear slightly less variable with the constraint than with the rejection sampling. It comes from the straighter morphology of the channels due to the constraint. This bias could be reduced by adapting the constraint setting, especially the magnitude, depending on the studied case.

The channel segment length has also a significant impact on the conditioning by the constraints. For a given channel length, a lower segment length means more channel segments and an easier conditioning. This is equivalent to the speed in robot motion planning: the higher the speed is, i.e., the longer the segment length is, the more the obstacle avoidance requires anticipation. This can be an issue as decreasing the channel segment length is computationally demanding. Thus, the constraint magnitudes should depend on the segment length, which is not the case for now.

Similar conditioning process is already applied in channel simulation [Lopez, 2003, Pyrcz et al., 2009] through a lateral deformation. Here the constraints are directly oriented toward the data as the channel grows. The deformation is then more easily distributed along the channel. A channel can also go straightly from one data to the other to ensure more easily the conditioning. Compared to conditioning based on a rejection procedure [e.g., Deutsch and Tran, 2002,

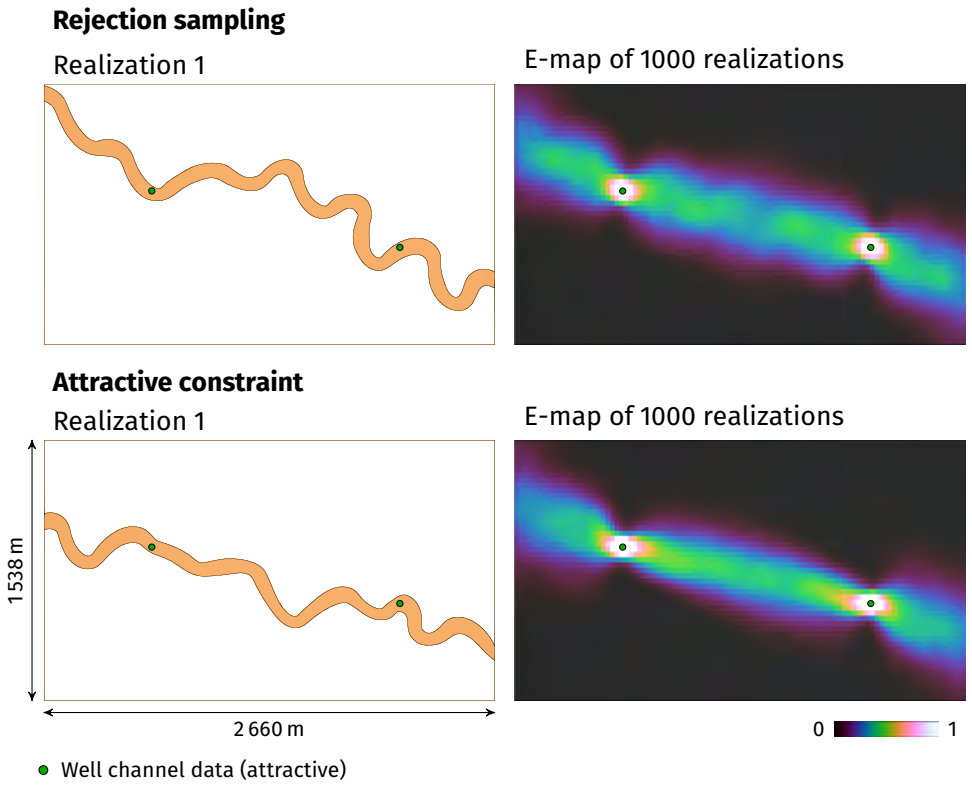

Figure 3.38 Examples of realizations conditioned to well sedimentary data using two different conditioning processes and associated E-maps of 1 000 realizations. L-system weight: 1; global direction weight: 0.2 (rejection sampling). L-system weight: 1; global direction weight: 0.2; channel data weight: 1 (attractive constraint).

Hassanpour et al., 2013], constraints are faster and more flexible, especially if the channel morphology specified as input is not consistent with the data. The conditioning of other data types than wells, e.g., property cubes, is also far easier. Compared to MPS, which can be seen as a conditioning solution for object-based simulation, constraints ensure the preservation of the channel continuity and shape.

3.7.3 Post-processing the conditioning

The L-system globally condition to the data, but a precise conditioning is difficult to achieve. For instance a L-system may not precisely condition to a

well interval with the channel shape. If some improvements are undoubtedly possible, other solutions exist to ensure the conditioning of data.

A simple solution is to suppress the channel and to re-simulate a new one. This is worth considering with significant conditioning errors, as the simulation process is fast (see section 3.7.12). However, this is not conceivable for precise conditioning at a very local scale. Another possibility is to re-simulate the channel width or thickness. This is useful if a channel goes slightly outside its confinement for instance. Finally, the last possibility is to rely on the NURBS, which are very easy to deform. Such deformation process could be useful for the conditioning of other types of data, such as channel orientation data on a well.

3.7.4 Better introducing the channel width and thickness in the conditioning

The better integration of the channel width and thickness in the constraints could be a significant improvement in the simulation process. Both the channel width and the thickness influence the conditioning through the constraint magnitude and perception area. For both features, the minimal and maximal values of the width and thickness are used. It helps to ensure the conditioning. However, it is rather strict and it would be better to use the local width and thickness of the channel.

Currently the width and the thickness are simulated at the end, when the conditioning process is already over. Nothing prevents the width and thickness to be simulated during the channel development. Due to the linear development of L-systems, the simulation path could not be random any more, but linear. This limits the stochasticity of the sequential Gaussian simulation, and could be a drawback of such process. On the other hand, it influences several aspects of the simulation process, such as the number of channels that condition to a set of channel data.

3.7.5 Conditioning to well sedimentary data

The conditioning of well channel data is done from one data to the other. Thus, a channel can condition to any number of channel data. The only restriction is to have a channel segment length lower than the inter-well space. Limiting the perception area, combined with the stochastic development of the L-system, allows to stochastically correlate the wells with some control on the resulting correlation. The main force of this process is its ability to easily ensure channel

data conditioning. Increasing the constraint weight makes the channel go straightly to the data. As demonstrated with connectivity data, the conditioning can be further forced by memorizing the data to condition until its conditioning.

Inter-channel data are more difficult to take into account. To ensure their non-conditioning, the repulsion magnitude must be high. Thus, a channel has difficulty to handle numerous inter-channel data, due to their combined repulsive action. In such cases, it is better to lower the weight related to the inter-channel data and to post-process those which are conditioned.

Here inter-channel data are considered as a homogeneous environment. In fact, it is constituted by several sedimentary bodies, for instance to levees or lobes. These data imply a channel close to them. A channel must pass at a certain distance of the data, without impinging on the sedimentary object related to that data. Modifying the magnitude by separating the inner area in two, one forbidden inner area and one outer area to condition, does not lead to satisfying results for now. Another solution is to add false channel data at a certain distance from the inter-channel data, or to rely on a NURBS deformation in post-processing.

3.7.6 Conditioning to well connectivity data

Integrating connectivity data remains for now quite simple: when two wells need to be connected, a single channel correlates them. However two wells may be connected by different channels and not just one as described. The same principle of attraction can be used, but on a previously simulated channel conditioning the well and not on the well itself. Such process requires to better handle the relationships between the channels. It also implies to preserve the connectivity of the two wells when simulating the channel fill.

The non-connectivity of the wells are only handled by repulsing the channels from the wells. It can be better handled through the repulsion of the channel that condition to the non-connected data by the channels that condition the connected data.

The simulation of the channel fill is also essential to further control both the connectivity and non-connectivity between several channels and several wells. When two wells are connected, the channel fill should ensure the preservation of the connectivity from one well to the other. Similarly, if a path of channels exist between two non-connected wells, the channel fill can ensure the non-connectivity of the wells.

When two wells are connected, the precise parts along the wells assuring the connection are not necessarily known. For now those parts are a user-defined

property. Some work could be done to explore a more automatic and stochastic process to define the parts of two well that must be connected.

3.7.7 Conditioning to a sand probability cube

An interesting aspect of the constraints is the ability given to the L-system to condition property cubes with complex variations. The method is able to influence the channels during their development, so that they follow the high probability areas. The constraint weight enables to adjust this influence of the high probability areas.

Most of the time the purpose is to have the E-map of many realizations reproducing the probability cube. Better reproducing the probability cube requires adjusting the weight for this constraint, which must not necessarily be high compared to the other constraints. The process could still be improved to better reproduce the property cube with a low weight to better preserve the channel morphology.

With the application to a sand probability, it should be remembered that it is not a channel probability. Channel filling is not homogeneous and should also be taken into account to further analyze the probability reproduction by the simulation. If channels are continuous objects, discontinuities between the high probability areas can appear in the E-map. If these discontinuities do not reproduce precisely enough the probability cube, simulating channel objects is maybe not the best option. Other solutions, such as simulating point bar packages such as proposed by Hill and Griffiths [2009] or Hassanpour et al. [2013], should be considered.

3.7.8 Integrating seismic-interpreted objects

The application of channel simulation within a master channel illustrates the constraint ability to handle a confinement. The channel centerlines never go outside the confinement. This aspect calls for a significant repulsion, which perturbs the channel distribution. Further limiting the effect of the repulsion away from the confinement should improve the uniformity of the channel distribution. Locally, the channel shape may go outside. This local miss-conditioning is pretty easy to correct by re-simulating the channel width or thickness or deforming the NURBS surfaces.

Another object that could be interpreted on seismic data are channels or channel parts. Complete channels do not require further treatment from the simulation process. Channel parts should be integrated as conditioning data.

They could be treated similarly to the well channel data. A channel part is randomly selected to initiate a channel. Two branches grow from the two extremities of the channel part. Then the extremities of the other channel parts are considered as attractive data. The deformation aptitude of the NURBS can be used to avoid an abrupt curvature transition between the simulated channel and an interpreted channel part.

3.7.9 About the parameterization

The channel section parameters are quite classical in object-based simulation of channels [e.g., Deutsch and Tran, 2002]. The width and thickness are simple parameters. The ranges and curvature weights are more complex to infer. By default, the ranges can still be chosen equal to the bend length. It is more difficult to choose a default value for the curvature weight, as both the width and thickness do not necessarily vary following the curvature.

The bend length and curvature are unusual parameters in object-based simulations of channels. The curvature is less easy to infer than a bend length, half-wavelength or amplitude. However, the resulting channel morphology varies more, with more small scale variations along a bend. The bend half-wavelength and amplitude are more common parameters, both in object-based simulations and in the geomorphological description of channels. The deviation angle is quite secondary compared to the bend half-wavelength and the bend amplitude. Its purpose is to reintroduce the bend shape variability allowed by the curvature. Nevertheless, when the deviation angle is high, it perturbs both the half-wavelength and amplitude, which does not necessarily correspond to the input values any more. Moreover, this parameter is quite complex to infer. If the half-wavelength and the amplitude are used for their inference simplicity, the deviation angle can be avoided by setting it to zero.

Compared to other object-based methods [e.g., Viseur, 2001, Deutsch and Tran, 2002, Hassanpour et al., 2013], the main difference in the parameterization comes from the constraints. These constraints call for numerous parameters. Thus asking the user to set all those parameters is not really possible, especially for several constraints. Furthermore, some parameters such as the perception area are not necessarily easy to determine. The solution proposed here is to predefined as much as possible the constraints and their parameters. However, depending on the studied case and the number of constraints, these parameters may be not compatible enough, leading to a poor conditioning. In such cases, the user can still modify the parameter values. All this requires more work to try to reduce the number of constraint parameters or, if possible,

to infer some of them automatically.

3.7.10 About the use of L-systems

One main advantage of using L-systems is the possibility for the user to change the L-system rules. Modifying the channel morphology or introducing non-stationarity along the channel path is then easy once the L-system formalism is known. This brings more flexibility in the object definition than in other object-based approaches [e.g., Viseur, 2001, Deutsch and Tran, 2002, Hassanpour et al., 2013].

Hill and Griffiths [2009] use a different kind of formal grammar to simulate channels: the plex grammar [Feder, 1971]. In the L-system formalism, a symbol in a string can have a left and a right symbol. Visually, it has two attaching points, one to the left symbol and one to the right symbol. The plex grammar generalizes this principle by enabling connections between an arbitrary number of symbols. While three-dimensional shapes are better handled by such grammar, the rules can become quickly unwieldy. Hill and Griffiths [2009] simulate channels from a training channel, similarly to MPS. Thus, the rules are automatically deduced form the training channel and the user do not manipulate them directly.

Using a training model makes possible to fully exploit analog data, if available, while limiting the parameterization. However, the training model should be large enough to capture all the channel morphology variations. While a L-system and the associated constraints call for multiple parameters, they give the possibility to simulate channels from scratch. The L-system rules to build a bend give also a more compact representation of the channel morphology. This facilitates the interaction with the user. The L-system could also get its parameter values from analog data. In this case, it does not necessarily call for a complete training model, which may be difficult to get.

To build the rules of the plex grammar, the training model is cut into smaller segments. The principle is to find the smallest set of segments describing the model. The resulting segments tend then to be as long as possible, with one or several bends corresponding to a segment. While this facilitates the rule definition, conditioning to data is less easy than with a L-system, which can use smaller segments without complicating the rules.

Table 3.10 Simulation time for a realization containing one channel. All the channels are simulated from the same location in the same domain as in section 3.5.3. The given values are the average time over 1 000 realizations and the standard deviation. The first set of realizations have no data. The second set is conditioned to the well sedimentary data of section 3.5.3. The last set is conditioned to the probability cube of section 3.5.3.

Simulation set	L-system simulation (in s)	NURBS generation (in s)
No data	0.132 ± 0.020	0.780 ± 0.107
Well data	0.144 ± 0.013	0.843 ± 0.063
Probability cube	0.141 ± 0.009	0.803 ± 0.041

3.7.11 About the simulation process

The current simulation process is able to simulate any number of channels while handling numerous data. The main source of improvement concerns the simulation stopping criterion. For now this criterion is a target number of channels. The simulation process completely ignores that target number of channels if some channel data are still not conditioned. This is worrying as the process tend to require many channels to condition all the channel data. Moreover, the number of channel data points influence the final number of channels. It could be appreciable to influence the conditioning and stay closer to the target number of channels.

Such process could give some leads to respect a channel proportion or a net-to-gross instead of a number of channels. Indeed, while the number of channels is difficult to infer, a channel proportion or a net-to-gross can be estimated from the data. Moreover, the channel proportion and the net-to-gross have a significant impact on the flow simulations. These parameters are often fitted through an iterative process in other object-based methods [e.g., Viseur, 2001, Deutsch and Tran, 2002].

3.7.12 Numerical aspects

The realizations were simulated on a 64-bit Linux system with a 2.10 GHz processor Intel® Core™ i7-3612QM and 6 GB of RAM.

The L-system process in itself is quite fast (table 3.10). Adding conditioning data does not increase much the computation time on those simple examples. Indeed, the constraints rely on the sum of vectors to condition. For the conditioning process in itself, the only aspect that increases the computation time

Table 3.11 Simulation time for a realization containing one channel with two different conditioning processes. The realizations are those illustrated by the figure 3.38. The given values are the average time over 1 000 realizations and the standard deviation.

Conditioning type	L-system simulation (in s)	NURBS generation (in s)
Rejection sampling	15.494 ± 15.489	0.834 ± 0.048
Attractive constraint	0.130 ± 0.008	0.770 ± 0.039

Table 3.12 Simulation time for a realization for each set of realizations in the master channel. The only difference between each set are the data: Set 1. Confinement only; Set 2. Confinement and probability cube ; Set 3. Confinement, probability cube and well data. The given values are the average time over 100 realizations and the standard deviation.

Simulation set	L-system simulation (in s)	NURBS generation (in s)
Set 1	3.17 ± 0.15	16.24 ± 0.22
Set 2	4.73 ± 0.10	14.57 ± 0.15
Set 3	6.64 ± 0.45	21.47 ± 1.31

is to determine those vectors. The constraints also influence the computation time as the channels tend to be straighter or need to be longer to match the data. For instance, some channels have a more tortuous aspect due to their path to escape the repulsive data. This increases the computation time. The generation of the NURBS is the most time consuming part of the process, with computation time about six times higher than the L-system simulation times.

The comparison with a simplistic rejection sampling for conditioning also highlight the significant speed of the conditioning process by constraints (table 3.11). On average, the constraint is 100 times faster than the rejection sampling. The computation times of the NURBS surfaces in the two cases illustrate the straighter channels simulated under the constraint influence.

The simulation process of several channels is also quite fast (table 3.12). Here adding a probability cube significantly increases the computation time. It is due to the perception area size, which increases with the channel segment length. In the simple cases the segment length is about 1 grid cell and in the master channel case it is about 6 grid cells. The time increase when adding well data mainly comes from the higher number of simulated channels to condition

all the channel data. The generation of the NURBS is again the most time consuming part of the process, with computation time three to five times higher than the L-system simulation times. The increase in set 3 compared to the set 1 is also due to the higher number of simulated channels. Adding a probability cube tends to form straighter channels. This decreases the computation time of the corresponding NURBS.

The conditioning process and its efficiency highly depend on the segment length. For a given channel length, smaller channel segments means more segments, which impacts the computation time. It also means heavier NURBS surfaces at the end. In such case, a re-parameterization function to use the minimal number of control points on a NURBS surface while preserving at best its shape is useful. This function is already proposed by Parquer et al. [2015] for channel modeling with NURBS.

3.8 Conclusions

This work introduces a new method for channel simulation through a formal grammar. The formal grammar, called the Lindenmayer system, simulates the channel morphology. This morphology is then wrapped with non-uniform rational B-spline surfaces to obtain the final channel object. The simulated morphologies are defined thanks to the rewriting rules of the L-system. Predefined rules are proposed to simulate straight to sinuous channels. These rules can be modified to simulate different morphologies, to add branches or to obtain non-stationary channels.

External constraints ensure the channel conditioning. They are determined from a constraining element, for instance a well data, a property cube or a seismic-interpreted object. A constraint is attractive or repulsive and is added to the L-system to influence the channel development by the related constraining element. Here some constraints related to classical conditioning data are presented: well sedimentary and connectivity data, sand probability cube and seismic interpreted sedimentary objects. As their parameterization is quite significant, most of the parameters are predefined to ensure the conditioning in most cases without much work for the user.

Object-based methods usually lack of flexibility for both well data or seismic-derived data conditioning. Here the process integrates data conditioning directly in the channel development. The conditioning then competes with the channel morphology. This induces a deformation of that morphology, and probably a statistical bias due to the conditioning. On the other side it ensures the

conditioning: if the priority is given to the data condition, the channel straightly goes to the data, or avoids it depending on the constraint type. This illustrates that when data conditioning is the focus of the simulation process, that conditioning can always be achieved, similarly to cell-based methods. Using channel objects always preserve the channel continuity, contrary to cell-based methods. The channel sinuosity can be lost, but it is less essential in flow simulation than the channel continuity.

Many improvements are still possible. First some work could be done around NURBS deformation to perfectly fit the data at a local scale. Then the conditioning process could be improved to deform less the channel morphology. This includes influencing the deformation direction of the bends so that it follows the global channel direction and not the constraint direction. It also includes a better management of different constraints with different types. From this point of view, a lot can be borrowed from robot motion planning, as the principles are pretty similar. Other sedimentary structures should be added to the process, such as lobes or levees. A NURBS parameterization already exists for those structures [Ruiu et al., 2015b]. Their development has to be integrated within the L-system rules.

Chapter 4

A geostatistical approach to the simulation of stacked channels

Abstract Turbiditic channels evolve continuously in relation to erosion-deposition events. They are often gathered into complexes and display various stacking patterns. These particular architectures have a direct impact on the connectivity of sand-rich deposits. Being able to reproduce these patterns in stochastic simulations is thus of significant importance. We propose a geometrical and descriptive approach to stochastically control the channel stacking patterns. This approach relies on the simulation of an initial channel using a Lindenmayer system. This system migrates proportionally to a migration factor through either a forward or a backward migration process. The migration factor is simulated with a sequential Gaussian simulation or a multiple-point simulation. Global avulsions are performed using a Lindenmayer system, such as the initial channel simulation. This methodology brings a control on the connectivity between the channels by adjusting the extension of the migrating areas and the migration patterns. If some aspects such as the smoothing of the migration factor or data conditioning require further work, this method furnishes encouraging results with both forward and backward migration processes.

4.1 Introduction

Facies heterogenities within a reservoir or an aquifer can have a dramatic impact on the flow. The Shiehallion field is a perfect illustration of such impact in an oil field [e.g., Gainski et al., 2010]. When the production started, its reservoir compartments appear far less inter-connected compared to the initial expectations. Sand-rich deposits within turbiditic channels form the reservoir compartments, but the channel fills are not homogeneous. Some flow barriers can appear along the channel top, sides and bottom due to mud-rich deposits, e.g., margin drapes or slumps. These elements are too small to be visible on the data, especially seismic data.

The impact of mud-rich deposits on the flow depends on the stacking pattern [Labourdette et al., 2006], i.e., how channels position themselves in relation to each others. The stacking pattern determines if a margin drape prevents any flow circulation between two channels or if it has no impact at all. This is especially important when considering turbiditic channels, as significant changes in the stacking pattern can be observed even over short distances [Mayall and O'Byrne, 2002], with a non-negligible impact on the reservoir connectivity. Thus channel stacking has to be taken into account when simulating channels for reservoir modeling. A common strategy is to simulate or mimic the processes that control the stacking.

Channel stacking is the result of the channel evolution. This evolution implies two main processes: channel migration and avulsion. The migration comes from the erosion and deposition processes due to density current circulation that forms the channel. Four main migration patterns are observed:

- A lateral channel bend migration or swing, which shifts the bend laterally and increases the channel sinuosity [Peakall et al., 2000, Posamentier, 2003] (figure 4.1).
- A downsystem channel bend migration or sweep, which shifts the bend downward [Peakall et al., 2000, Posamentier, 2003] (figure 4.1).
- A channel bend retro-migration, which decreases the channel sinuosity [Nakajima et al., 2009].
- A vertical channel migration or aggradation, which shifts the channel upward [Peakall et al., 2000] (figure 4.1).

Migration of turbiditic channels is continuous, forming accretion packages [e.g., Abreu et al., 2003, Arnott, 2007, Nakajima et al., 2009], or discrete, due to

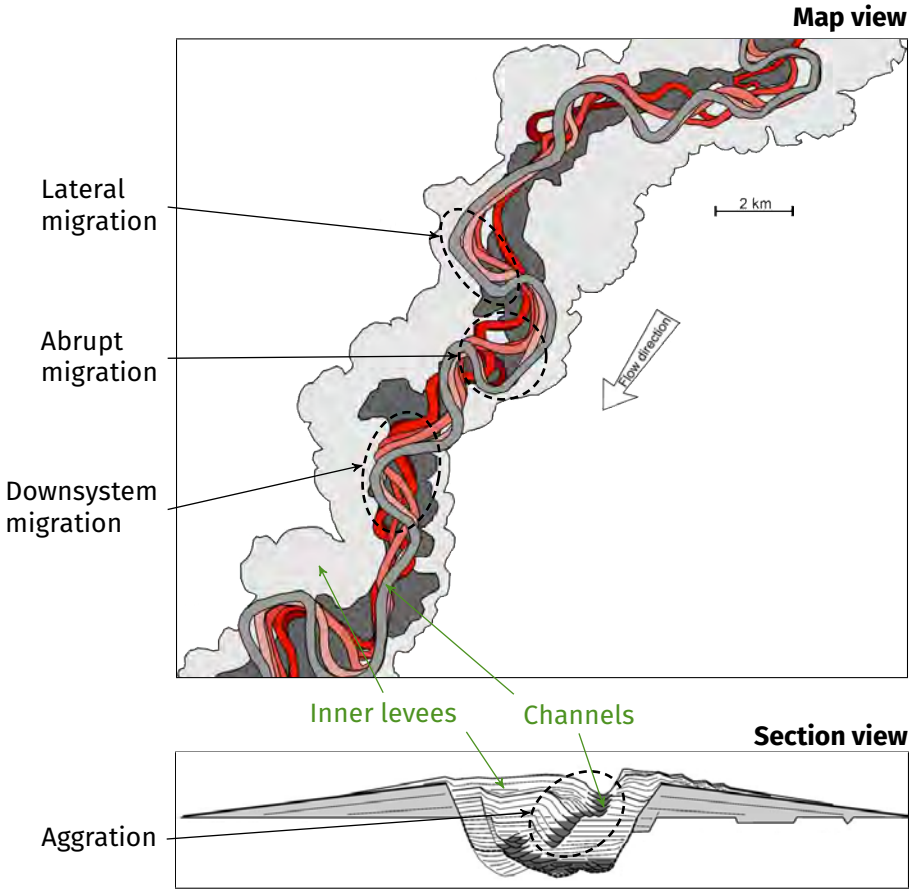

Figure 4.1 Example of migration patterns on channels interpreted on seismic data from the Benin-major channel-belt, near the Niger Delta (modified from Deptuck et al. [2003]).

abrupt migrations which correspond to local avulsion [e.g., Abreu et al., 2003, Deptuck et al., 2003]. Avulsion occurs when the currents exceed the channel capacity to contain them: the flow leaves the channel and forms another course. Contrary to abrupt migrations, regional avulsions are often a definitive abandonment of the previous course.

Mimicking migration and avulsion in stochastic simulation methods is a topical subject of study to better control the channel stacking. Whatever the method, avulsions rely on a statistical framework, due to the lack of knowledge to genetically model their initiation. Regional avulsions are handled through a

probability associated to the development of a new channel. Channel migration has been more widely studied, with numerous works attempting to develop a physical model of the migration.

In fluvial systems, the more widespread methods are two-dimensional physical simulations. They link the migration to the asymmetry in the flow field induced by the channel curvature and responsible for bank erosion [Ikeda et al., 1981]. These methods have been extended to a stochastic simulation framework by Lopez [2003] and Pyrcz et al. [2009]. If they manage to produce realistic-looking channels, such method predictions can be far from the reality depending on the simplifications introduced in the physical model [Camporeale et al., 2007]. Models with fewer simplifications call for a heavier parameterization and possibly a more important computational effort, which may not be practical in a stochastic reservoir simulation context. Data conditioning remains also a challenge.

These two-dimensional physical methods have been applied to turbiditic environments [McHargue et al., 2011]. Imran et al. [1999] even adapt them to the migration of submarine channels. However, the physical processes behind submarine channels have been, and still are, a source of controversy. The main controversy concerns the rotation direction of the secondary flow and the factors that determine this direction [e.g., Corney et al., 2006, Imran et al., 2008, Corney et al., 2008]. This aspect is a major concern because the rotation of the secondary flow controls the channel migration. Lately, Dorrell et al. [2013] argue that two-dimensional physical models are not accurate enough to capture the full three-dimensional structure of the flow field. Beside their validity, which remain questionable and questioned [e.g., Sumner et al., 2014], three-dimensional models are also computationally demanding. Thus, their convenience in a stochastic framework is doubtful. Moreover, the last channel of a system is often observable on seismic data due to its argileous fill. In such a configuration, initiating the process from this last channel, so from the youngest channel, and migrating backward to the oldest channel is more appropriate, as it starts directly from the available data [Labourdette, 2008]. Then the migration divides in two processes:

- A forward migration, which is the normal or classical migration. It starts from the oldest channel which migrates to obtain the youngest channel.
- A backward migration, which is a reverse migration. It starts from the youngest channel which migrates to obtain the oldest channel.

In the stochastic simulation of channels, most approaches are descriptive:

their goal is to directly simulate the sedimentary bodies resulting from the flow processes, not the flow processes themselves. For now, very few works have tackled the migration in a descriptive manner.

Viseur [2001] and Ruiu et al. [2015b] use a forward migration process by defining migration vectors from a weighted linear combination of vectors for lateral migration, downsystem migration, bend rotation and more recently vertical migration thanks to Parquer et al. [2015]. This method gives an important control over the migration pattern. However, the migration pattern is for now identical over the whole channel and the migration is deterministic whereas not relying on physical principles. The weights in the linear combination may also be hard to define. Concerning backward migration, Ruiu et al. [2015b] lay the foundations for process to reconstruct point bars from channels interpreted on seismic data. But this process is still at an early stage and is also purely deterministic.

In a fluvial setting, Teles et al. [1998] rely on an empirical law giving the migration displacement as a function of the curvature and the channel width. Labourdette [2008] proposes a workflow based on the occurrence of channels within a confinement, a configuration often seen in turbiditic reservoirs. Starting from the last channel of the migration process, he performs a backward migration based on empirical laws deduced from analogs to determine the distance between the channel centerline and the canyon border. However, this workflow is deterministic, limited to channels within a confinement and to the representativeness of the analog data.

We propose a different approach for channel migration, based on a descriptive stochastic simulation approach to avoid the use of too complex and incomplete physical models. The global process is similar to the principle of two-dimensional physical methods. It starts with the collection of a channel to initiate the evolution process (section 4.2). A Lindenmayer system simulates the new channel path following an avulsion. Channel migration is divided into two elements:

- The lateral and downsystem migrations and the retro-migration are the horizontal components of the migration. For the rest of this chapter, the horizontal migration is referred as migration.
- The vertical migration is the vertical component of the migration. It is referred as aggradation for the rest of this chapter.

A vertical shift of the channel simulates the aggradation. The stochastic simulation of a migration factor allows the migration. This stochastic simulation uses

either a sequential Gaussian simulation (SGS) (section 4.3) or a multiple-point simulation (MPS) method (section 4.4). With some other considerations (section 4.5), all this lays the foundations of a process to simulate both forward and backward channel migration (section 4.6). The process is applied to a synthetic case with turbiditic channels migrating within a canyon (section 4.7), which lead to some discussions and perspectives (section 4.8).

The whole method was implemented in C++ within the Gocad plug-in ConnectO. The channel envelopes with NURBS were implemented by Jérémy Ruiu within the Gocad plug-in GoNURBS [Ruiu et al., 2015b].

4.2 New channel generation

Performing either a forward or backward migration calls for a channel to initiate the process. This initiation occurs at two steps: at the beginning of the whole process and when a new channel path develops.

4.2.1 Channel initiation

Two main options are considered. When the data can not provide an initial channel, a channel path is stochastically simulated. Sometimes channels are interpretable on seismic data. These channels can initiate the process.

From L-system

L-systems offer a way to stochastically simulate the initiating channel. The simulation process is exactly that described in the previous chapter. A set of L-system rules handles the channel morphology by simulating a channel centerline. The centerline is a set of locations through which the channel passes. Each location knows the channel width, thickness and asymmetry at that location. Non Uniform Rational B-Spline (NURBS) surfaces dress the L-system to obtain the final channel shape. Data conditioning, either for well or seismic data, is done through constraints applied during the channel growth. The constraints attract or repulse the channel from the data.

This method simulates various meandering patterns, from straight channels to highly sinuous patterns (figure 4.2). It is suitable for both forward migration, which classically requires starting with a quite straight channel, and backward migration, which requires an initial channel with a high sinuosity. The parameters needed by the method, i.e., channel width, thickness and bend length,

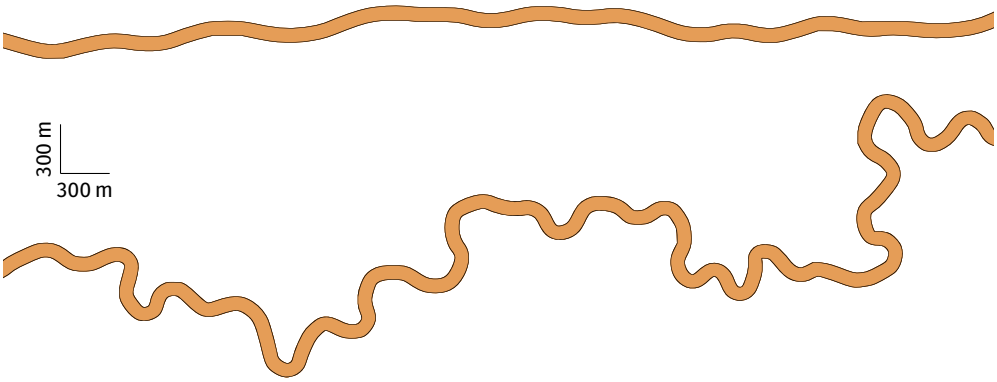

Figure 4.2 Example of a straight channel (top) and a highly sinuous channel (bottom) simulated with L-system and wrapped with NURBS. The input parameters are given in table C.1, appendix C.

curvature or half-wavelength, amplitude, can be retrieved from wells or from a seismic, if available, or on analog data coming from seismic or field studies.

From interpreted seismic data

Another way to obtain this initial channel is to interpret it directly on a seismic. Ruiu et al. [2015a] propose a method to interpret channels in a semiautomatic way. It requires to approximately arrange a channel representation based on Non-Rational Uniform B-Splines (NURBS) surfaces within a channel identified on the seismic. Then an automatic optimization fits the NURBS surfaces to the most relevant edges delimiting the channel, determined through custom edge detection. This method can be used when seismic data are available with a sufficient resolution. This is often the case in turbiditic context, where the last channel of a complex is usually filled by a highly argileous content and stands out on the seismic. It could require converting the resulting channel object into an L-system formalism depending on the implementation choices, i.e., if the migration is performed on the L-system or on the NURBS.

If channels are partially interpretable, the blanks between the interpreted channel parts can be simulated using L-systems. An extremity of a part is defined as an initiation point for the L-system, and the extremity of the following part is defined as an attractive data. Thus, the simulated system can stochastically link the two parts.

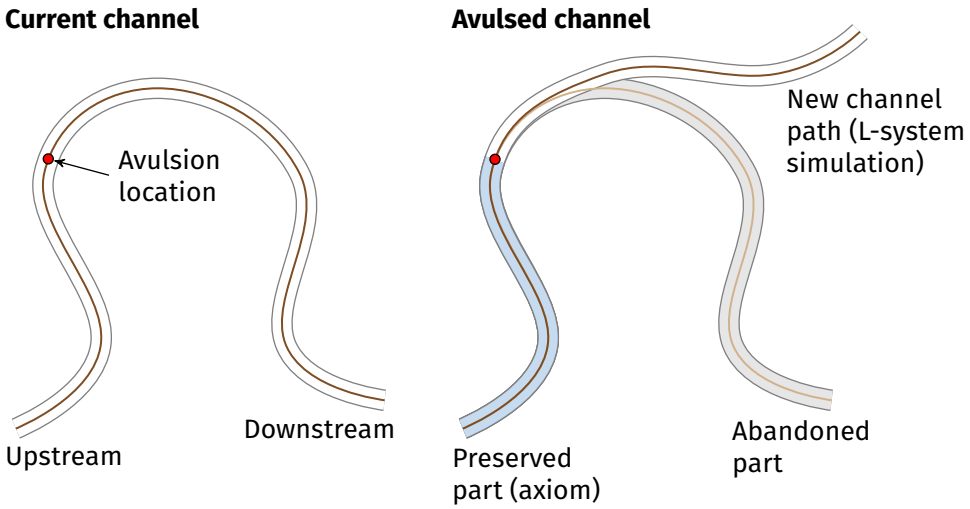

Figure 4.3 Principle of global avulsion based on L-system.

4.2.2 Regional avulsion

Regional avulsion is a key event widely observed on both fluvial and turbiditic systems. When an avulsion occurs, the channel is abruptly abandoned at a given location (figure 4.3). Upstream the flow remains in the old channel, whereas downstream a new channel is formed. However, its triggering conditions remain poorly understood due to the complexity of this process. Avulsion is so often statistically handled in simulation methods: a probability of avulsion controls the development of a new channel. This process can be influenced by the curvature, as a high curvature tends to favor an avulsion.

The approach for global avulsion is similar to the one defined by Pyrcz et al. [2009]. The avulsion starts by computing the sum of the curvatures at each channel section. A threshold is randomly drawn between zero and the sum of curvatures. The channel is then scanned from its most upstream part to the downstream part. At each section, the curvature is subtracted from the threshold. A section initiates an avulsion or not depending on two factors:

- An input probability of avulsion.
- The random curvature threshold, which should be lower than the section curvature to trigger an avulsion.

Thus the avulsion initiation at a given section is a probabilistic choice influenced by the curvature at the section location.

Then the upstream part of the L-system is isolated. The obtained string serves as axiom to simulate the new post-avulsion channel (figure 4.3). This channel is based on the same parameters as the initial channel, but different parameter values may be used. A repulsion constraint with the pre-avulsion channel can be set to avoid intersections between the two channels.

4.3 SGS for forward or backward migration

The first process we propose to simulate both forward and backward migration is based on sequential Gaussian simulation (SGS). It uses a migration factor statistically simulated by the SGS.

4.3.1 Principle

Channel migration is deeply linked to the channel curvature. Other elements come into consideration, such as soil properties or flow fluctuations. However, the physical processes behind bend evolution are complex and still not completely understood. Moreover, they differ from turbiditic to fluvial environments.

This is why we propose to rely on a more descriptive approach based on geostatistics. In physical approaches, a migration factor is computed along the nodes of a channel centerline based on fluid flow equations. Then the nodes are moved based on that factor along the normal to the centerline (figure 4.4).

We rely on a similar approach based on moving the node along the normal to the centerline to migrate a channel. Here the Euclidean distance d of displacement for a node is the length of a displacement vector $\vec{v}$:

$$d = \|\vec{v}\| \tag{4.1}$$

The displacement vector divides in two components (figure 4.5):

- A vertical component for the aggradation. Aggradation is simply done by shifting the new channel vertically by an aggradation factor ε_a, which is the same for all the channel nodes.
- An horizontal component defined by a migration factor ε_m computed using sequential Gaussian simulation.

The SGS simulates a migration factor value for each node of the centerline in a sequential manner [e.g., Deutsch and Journel, 1992]:

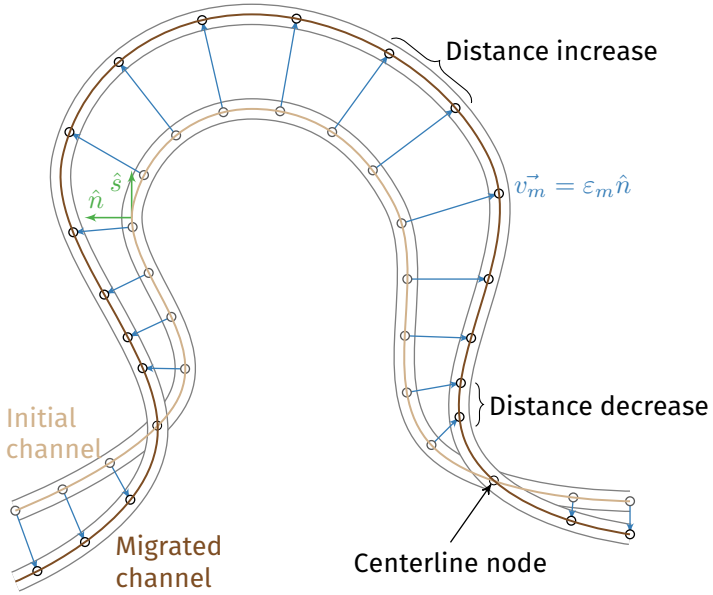

Figure 4.4 Migration principle: the centerline nodes are moved along a migration vector $\vec{v_m}$ based on the normal $\hat{n}$ to the centerline and a migration factor ε_m. $\hat{s}$ is the normalized vector along the streamwise direction.

1. A random path is defined to visit all the centerline nodes.
2. At a given node:
   a) If some nodes in a given neighborhood already have a value:
      i. A kriging system determines the Gaussian complementary cumulative distribution function (ccdf) using the data, i.e., the nodes with a value given in input, and the previously simulated nodes within the neighborhood.
      ii. A simulated value for the given node is drawn within the ccdf.
   b) Otherwise, the simulated value is drawn from an input distribution of migration factor.
3. Return to step 2 until all the nodes of the path have been visited.

The SGS requires the migration factor to be a Gaussian variable. If not, a normal score transform of the input distribution and of the data is introduced before step 1. A back transform is done at the end of the simulation process.

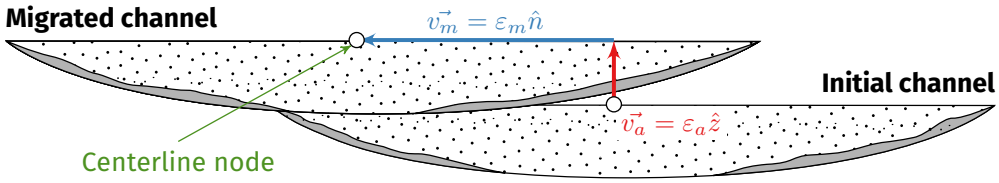

Figure 4.5 Components of the displacement vector for channel migration. $\vec{v_a}$ is the aggradation component along the vertical direction symbolized by the normalized vector $\hat{z}$. The aggradation factor ε_a determine the vertical displacement. $\vec{v_m}$ is the migration component along the normal direction to the centerline symbolized by the normalized vector $\hat{n}$. The migration factor ε_m determine the horizontal displacement.

Using directly SGS with simple kriging involves that the migrating area appears anywhere along the channel. But a migrating area is often related to a bend and is greatly influenced by the channel curvature. This aspect is taken into account by using intrinsic collocated cokriging [Babak and Deutsch, 2009] instead of simple kriging. The channel curvature is integrated as a secondary variable in the simulation process, influencing the spatial structure of the migration factor. The intrinsic collocated cokriging enables to adjust the influence of the curvature through a weight: when that weight is positive, the channel tends to migrate, when it is negative, the channel tends to retro-migrate. This weight represents the correlation between the primary variable, i.e., the migration factor, and the secondary variable, i.e., the curvature. Thus, simply by changing the curvature weight symbol the same workflow achieves both forward and backward migration processes.

4.3.2 Parameter set

Four parameters are required to perform a migration through SGS (figure 4.6): a migration factor distribution, an aggradation factor distribution, a variogram and a curvature weight.

Migration and aggradation factor distributions

Two migration factor distributions control directly the distances between two successive channels in the migration process: one for the horizontal component of the migration and one for the vertical component. These distributions can be obtained by interpreting horizontal and vertical distances between channels or point bars on seismic of field analogs for instance. They are geometrical parameters. The horizontal factor should be chosen as small as possible, as

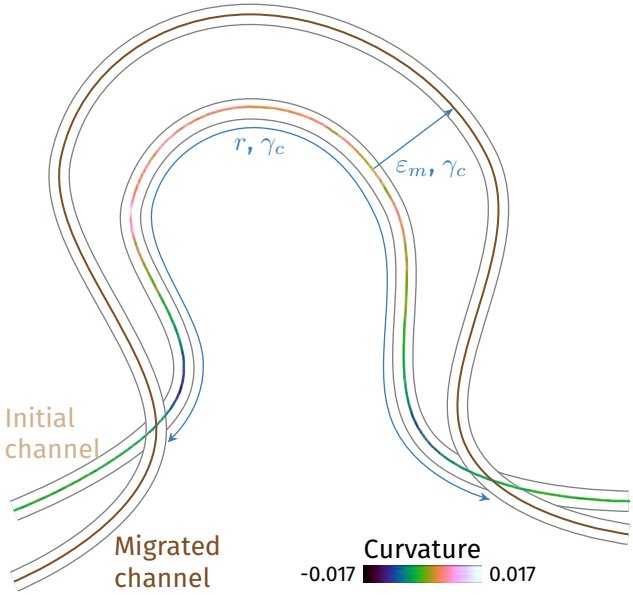

Figure 4.6 Main parameters used for horizontal bend migration with SGS. ε_m is the migration factor, r the variogram range and γ_c the curvature weight. The later perturbs the two other parameters by fitting more or less the migration spatial structure to the curvature spatial structure.

it tends to increase the impact of the small scale distance variations on the horizontal migration. The vertical factor is unique for all the modules of a given channel but may vary between channels, hence the need for a distribution.

Variogram

The variogram informs about the spatial model of a variable [e.g., Gringarten and Deutsch, 2001]. It is usually infered from the data. These data can come from the partial interpretation of migrating channels on a seismic to get migration factor values along the interpreted channel parts.

If no data is available, the migration factor is considered as a Gaussian variable. The purpose is to have a migration factor that evolves as smoothly as possible to avoid small-scale perturbations during the migration. The variogram model is then chosen Gaussian. The nugget effect adds noise to the realizations and is kept to 0. The sill is fixed to 1.

This leaves one parameter: the variogram range. This parameter represents the horizontal extension of a migration area, which can stretch over several

bends (figure 4.7). It has a main impact on the migration. By default, it must be close to the wanted bend length for the bends that develop through the process. A range smaller than the bend length leads to the development of smaller-length bends through the migration. A range larger than the bend length makes the migration occur over several bends. Thus some bends seem to migrate and other to retro-migrate.

Curvature weight

The curvature weight adjusts the curvature influence on the spatial structure of the migration factor (figure 4.7). When equals to $(-)1$, the migration factor follows strictly the curvature spatial structure, favoring lateral migration. When equals to 0, the migration factor is independent from the curvature and more various migration patterns appear: lateral migration, downsystem migration and even their counterparts in retro-migration. The curvature weight is so related to the stability of the system: when a system is unstable, channel stacking patterns are highly variable as the influence of the previous channel over the next one is weaker.

This parameter is the harder to adjust. It depends on the wanted migration patterns, which can be deduced from a seismic or from analogs. However, the lateral migration is the only pattern that can be favored in the current form of the method: having only lateral migration is possible, but having only downsystem migration is not.

4.4 MPS for forward or backward migration

Multiple-point simulation (MPS) is another approach to perform a migration. The idea is to rely on a more complete model than a variogram to define the spatial structure of the migration.

4.4.1 Principle

Simulation methods such as the SGS rely on a histogram and a variogram inferred from the data. Thus, they only catch the one- and two-point statistics and miss all the higher-order statistics. But higher-order statistics are difficult if not impossible to infer from data. Multiple-point simulation [Guardiano and Srivastava, 1993] attempts to overcome such limitation by relying on an external representation of the structures of interest, the training image. Using MPS instead of SGS in the migration process can give more realistic migrations.

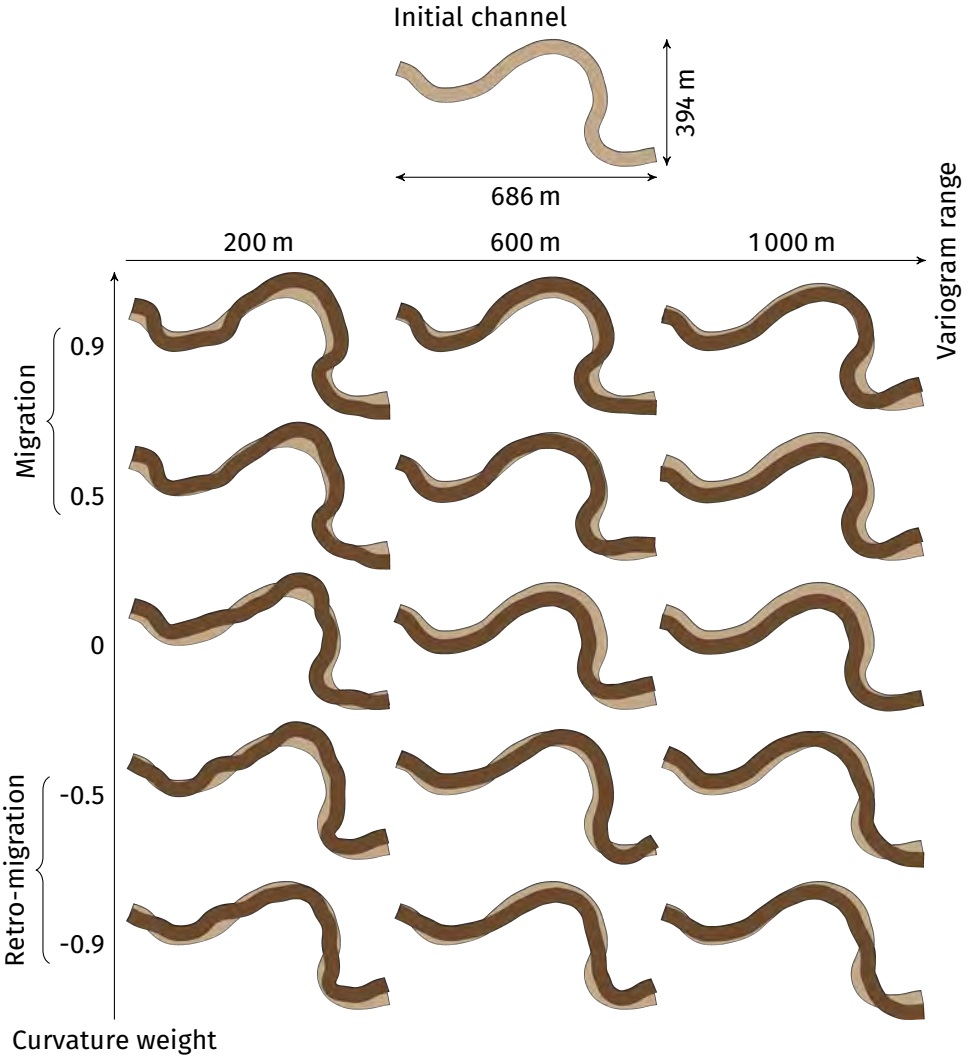

Figure 4.7 Effect of the variogram range and of the curvature weight on bend migration with SGS.

The global principle is similar to the one introduced for the SGS: each node of the channel centerline migrates following a migration factor and an aggradation factor. The values of those factors are borrowed from a training set, i.e., a set of migrating channels. This training set can come from a seismic or field analog. The migration and aggradation factors are computed all along the channels of the training set. No factors can be computed for the last channel, which is excluded from the set.

For a given channel, the aggradation factor is supposed to be the same for all the centerline nodes. A value is then randomly drawn amongst the training set and attributed to all the nodes of the channel to migrate. This channel migrates simply by shifting it vertically following the aggradation factor. The migration factor is computed using a MPS method, the Direct Sampling (DS) [Mariethoz et al., 2010]. This method has the advantage of easily handling continuous properties and secondary data. Again, the curvature serves as secondary data to influence the migration.

The whole training set is not necessary used to simulate the migration of a channel. The process relies on a training model, which can be (figure 4.8):

- Directly the whole training set. In this case, each simulated migration step is influenced by all the migration steps within the training set.
- A single migration step within the training set:
  - Drawn randomly among all the migration steps of the training set.
  - That follows the migration order of the training set. In that case, each simulated migration step corresponds to a particular migration step within the training set. With that option, the number of migration steps in the training set limits the number of simulated migration steps.

Both the migration factor and the curvature are known in the training model (figure 4.8). The migration process starts from an initial channel, whose curvature is known. The principle is then to simulate the migration factor on the initial channel based on the training model. The curvature ensures the link between the spatial variations of the migration factor in the training model and that on the simulation.

At a node to simulate, the n closest nodes with already a value form a data event N_x (figure 4.9). The principle of the DS method is to try to find these data event in the training model. A position is randomly chosen, either in the whole training set or only within a given migration step depending on the

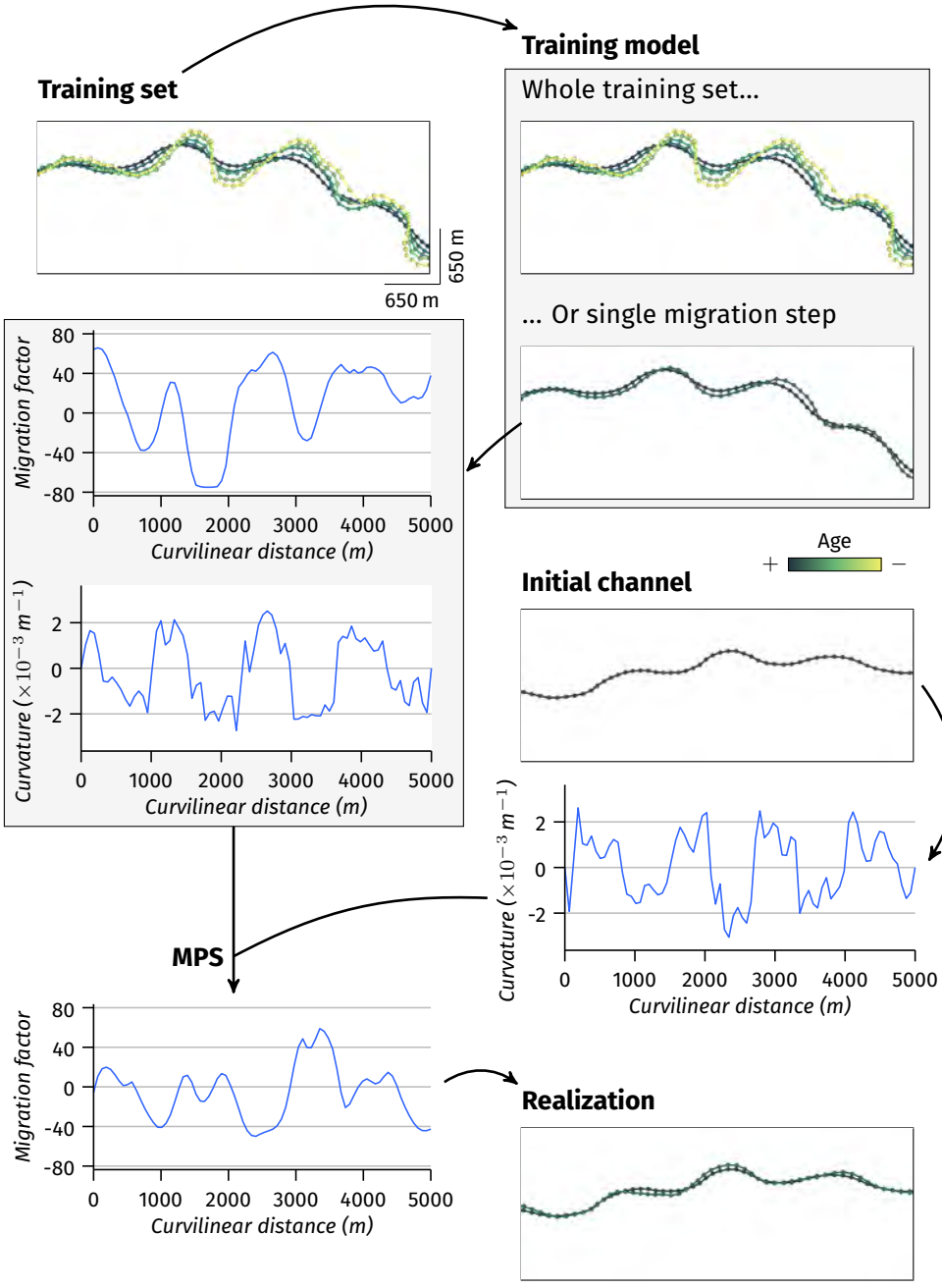

Figure 4.8 Framework for the simulation of the migration factor ε_m with MPS.

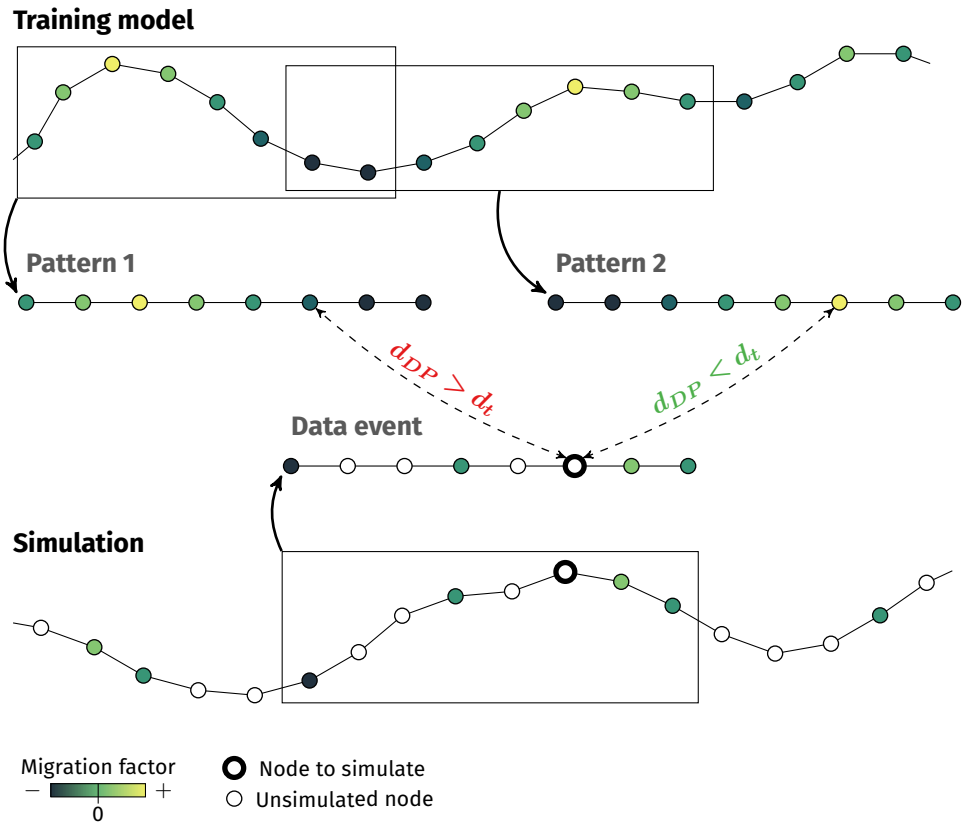

Figure 4.9 DS simulation principle: the neighboring configuration around the node to simulate, the data event, is sought within the similar configurations in the training model, the patterns. Here the neighboring configurations contains the four nodes with a known value that are the closest to the node to simulate. When the distance D_{DP} between the data event and a pattern is lower than a given threshold d_t, the process stops and the node to simulate gets the value at the same location within the pattern.

retained option. Then the process scans the training model. At each node, a distance $d_{D,P}$ is computed between the current pattern N_y and the data event N_x:

$$d_{D,P}(N_x, N_y) = \frac{1}{n} \sum_{i=1}^{n} \frac{\left|Z(x_i) - Z(y_i)\right|}{\max\limits_{y \in TS}(Z(y)) - \min\limits_{y \in TS}(Z(y))} \tag{4.2}$$

with $d_{D,P} \in [0, 1]$, n the number of nodes in the data event, Z the compared property, x a node in the data event, y a node in the training set pattern and

TS is the whole training set or just a single migration step of the training set. The process stops if the distance is lower than a given threshold. The simulated node gets the value of the central node associated to the training set pattern. During the process, the value corresponding to the lowest distance value is kept. If no distance lower than the threshold is found at the end of the scan, the simulated node gets that value.

The migration process involves two data events: one data event contains the migration factor values and another data event contains the curvature values that influence the spatial structure of the simulated migration factor. The distance computation is applied on both the migration factor and the curvature, each one with its own threshold. A value is only retained when the two distances are lower than their respective thresholds.

4.4.2 Parameter set

Besides from the training set, the DS method does not require much parameters. Most of these parameters balance the realization quality and the speed of the process. For more details about those parameters and their effect, see Meerschman et al. [2012].

4.4.3 Size parameters

Two parameters have a direct impact on the simulation speed: the maximal number of nodes in a data event and the maximal proportion of the training model to scan.

The maximal number of nodes in the data event is simply the maximal number n_{max} of nodes with a value to consider in a data event. All these nodes are the closest to the node to simulate. A low number speeds up the simulation, but it may be at the cost of the realization quality. A high number does not necessarily means a good quality. Indeed, the size of the data event limits the number of potential patterns in the training set. It is then more difficult to find a pattern similar enough to the data event.

The maximal proportion to scan determines how much of the training model to scan before stopping the process. The training model is either the whole training set, or only one migration step of that training set. This parameter stops the process when no satisfying pattern is found. It speeds up the simulation, but it may be at the cost of the realization quality.

4.4.4 Threshold parameters

The migration process based on the DS calls for two thresholds: one for the horizontal migration factor, one for the curvature. When a threshold is close to 0, the retained pattern has to be highly similar to the data event. A threshold closer to 1 authorizes more dissimilar patterns, at the cost of the realization quality.

Those parameters have two roles. First they have an impact on the simulation speed: the higher the threshold, the faster the simulation. The second role is similar to the role of the curvature weight with the SGS: it controls the impact of the curvature on the migration (figure 4.10). If the curvature threshold is far higher than the migration factor threshold, the curvature impacts less the process. If the two thresholds have similar values, the curvature influence is more noticeable. Contrary to the curvature weight of the SGS, a threshold is always positive. Thus, a threshold gives no control on migration or retro-migration trends. Only the training set controls such trends.

4.5 Numerical aspects

One key aspect of this method is shared with physical simulation methods: the horizontal migration factor has to be relatively smooth to avoid small-scale perturbations. Indeed, these perturbations tend to have a huge impact on the migration structures and can lead to inconsistencies.

4.5.1 Curvature computation

In our process, curvature values have no impact on the horizontal migration factor values themselves, only on their spatial structures. But having a curvature which evolves smoothly remains as important as in physical simulation methods. These methods usually smooth the curvature, either following a weighted average or based on cubic spline interpolation [Crosato, 2007].

Schwenk et al. [2015] underline these inaccuracies in the curvature computation and propose to use a stabler curvature formula to avoid a smoothing phase. This formula is used here to compute the channel curvature κ at a centerline node i:

$$\kappa = \frac{2(a_y b_x - a_x b_y)}{\sqrt{(a_x^2 - a_y^2)(b_x^2 - b_y^2)(c_x^2 - c_y^2)}}$$

with $a_x = x_i - x_{i-1}$, $b_x = x_{i+1} - x_{i-1}$, $c_x = x_{i+1} - x_i$ and equivalently for y.

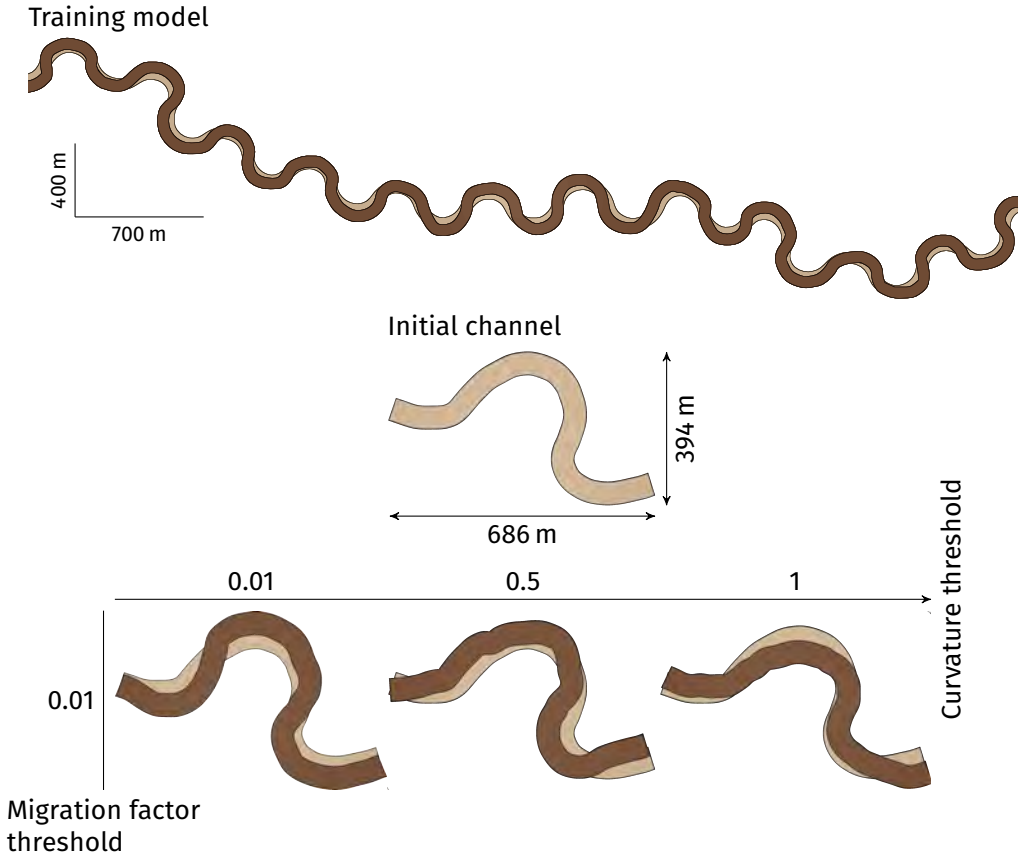

Figure 4.10 Effect of the curvature threshold on bend migration with MPS. Here lateral migration dominates the training model. When the curvature threshold decreases, the initial channel has less influence on the migration. Other migration patterns than lateral migration may appear.

4.5.2 Regridding

The regridding is a key step in channel migration. Indeed, as the bends migrate, the distance between two successive channel nodes can increase or decrease, as noticeable on figure 4.4. These variations lead to instabilities in the resulting migration. A regridding step is required to prevent too many variations of the inter-node distance.

This regridding step is the same as in physical methods [e.g., Schwenk et al., 2015]:

- If the distance between two successive nodes is higher than $\frac{4}{3}l_d$, with l_d the default channel length of the L-system, a new node is added. The parameters of this new node are deduced from the interpolation of its position. This interpolation uses a natural monotonic cubic spline interpolation of both coordinates x and y following the curvilinear coordinate.
- If the distance between two successive nodes is smaller than $\frac{1}{3}l_d$, with l_d the default channel length of the L-system, the second node is suppressed from the L-system string.

During the migration, two successive migration vectors may also cross each other, leading to an unwanted channel self-intersection. The migration vectors are so checked for intersection. If an intersection may happen, the two nodes are suppressed to eliminate the possible cycle.

4.5.3 Smoothing

If the curvature computation does not require any smoothing step, the migration factor realizations can display small-scale perturbations that have a huge, and sometimes unwanted, impact on the migration. This is especially the case when using a non-Gaussian variogram model and/or a curvature weight equals to ± 1 in the SGS. The simulated horizontal migration factor is smoothed right before the migration step. The smoothing procedure uses the weighted average defined by Crosato [2007]:

$$\varepsilon_i = \frac{\varepsilon_{i-1} + 2\varepsilon_i + \varepsilon_{i+1}}{4}$$

with ε_i the (retro-)migration factor of the module i. It can be applied several times depending on the wanted smoothness.

4.5.4 Neck cutoff determination

As the channel sinuosity increases, the two extremities of a bend come closer one to the other until the flow bypasses the bend. This is a neck cutoff, leading to the abandonment of the bypassed bend.

As done in physical simulations [e.g., Howard, 1992, Camporeale et al., 2005, Schwenk et al., 2015], neck cut-offs are simply identified when two non-successive nodes of the centerline are closer than a given threshold. The lower possible threshold is the channel width, as the margins of the two bend extremities come in contact. However, this threshold is quite restrictive and

not so realistic [Camporeale et al., 2005]. Here the threshold is set to 1.2 times the maximal channel width.

The search for cut-off starts upstream and continues to the most downstream part of the channel. The distance between a given node and another non-successive node of the centerline is compared with the threshold. When the distance is lower, those two nodes and all the nodes in-between are suppressed. The cutting path is then symbolized by two nodes. A new node is added along that path [Schwenk et al., 2015], using a cubic spline interpolation such as in the regridding.

This method of neck cutoff determination is simple but rather time-consuming. More efficient methods exist to reduce the computation time [e.g., Camporeale et al., 2005, Schwenk et al., 2015]. For now only the forward migration process handles the formation of neck cutoffs. Indeed, the cutoffs appear naturally with the sinuosity increase. In the backward process, there is no such sinuosity increase, but a sinuosity decrease. Introducing neck cutoffs in such process calls for a different method.

4.6 Simple applications

This method was implemented to make L-system strings migrate. However, the whole method is still valid for any channel representation and could be modified to be done on curves or on NURBS. L-systems have the advantage that their manipulation requires a low computational cost. This is especially useful when working with numerous and long channels composed of small channel segments.

The method was used to generate two models: one following a forward migration process (figure 4.11) and one following a backward migration process (figure 4.13). Both processes are able to reproduce various migration patterns, from lateral to downsystem migration, with even areas of retro-migration (figure 4.12 and 4.14). Some bends also evolve to complex bends constituted by several bends: this lead to the formation of new meanders(figure 4.15). These synthetic cases have been developed without any data. The variogram parameters for the migration are those predefined. The range is chosen similar to the bend length. The curvature weight is kept high, giving a dominant lateral migration. At the end few parameters are required for the migration process itself. The forward model can continue over more migration steps without any trouble: neck cutoffs tend to keep the channel within a restrained area. The backward process does not migrate much after a few steps when the channel

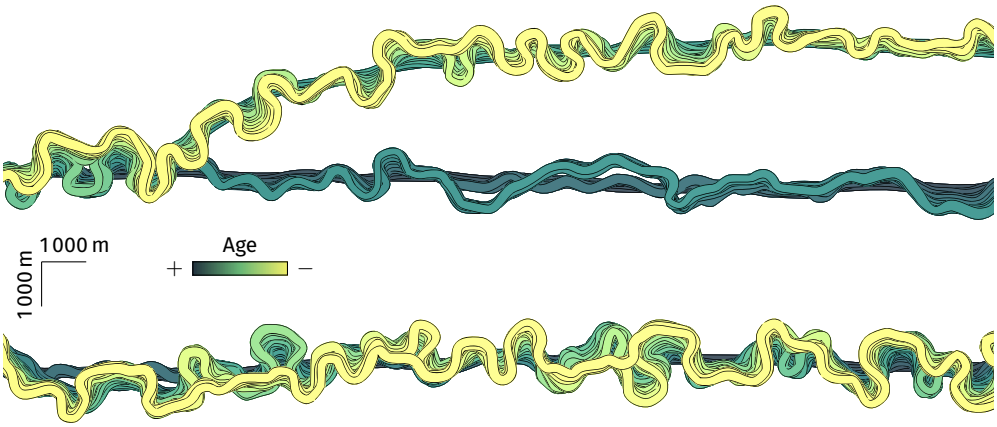

Figure 4.11 Application of a forward migration process based on SGS to two channels generated with L-system. The input parameters are given in table C.2, appendix C.

starts to miss significant bends. A regional avulsion and sometimes an abrupt migration can still revitalize the system.

Abrupt migrations are handled by introducing a second set of migration parameters. The channel centerline is scanned upstream to downstream. A probability of abrupt migration defines if an abrupt migration occurs. The appearance of an abrupt migration is also weighted by the channel curvature. When an abrupt migration occurs, an abrupt migration length is drawn from an input distribution. All the nodes along the drawn length migrate following the second set of migration parameters. Such abrupt migration process tends to introduce a spatial discontinuity with the previous channel (figure 4.12 and 4.14).

Regional avulsions momentarily stops the migration process, which starts again on the new channel. The continuity between the upstream part to the avulsion location and the newly simulated channel is finely preserved (figure 4.12 and 4.14). The use of the curvature to weight the abrupt migration and avulsion process tend to make them less appear in the backward process. This is due to the sinuosity decrease induced by such process. In this case higher probabilities are used.

Neck cutoffs appear naturally during the forward process as the sinuosity increases (figure 4.12). The backward process is unable to generate cutoffs. As the migration advances, the channel just gets straighter. It does not evolve to a complete straight line, but continuing the process does not lead to an increase

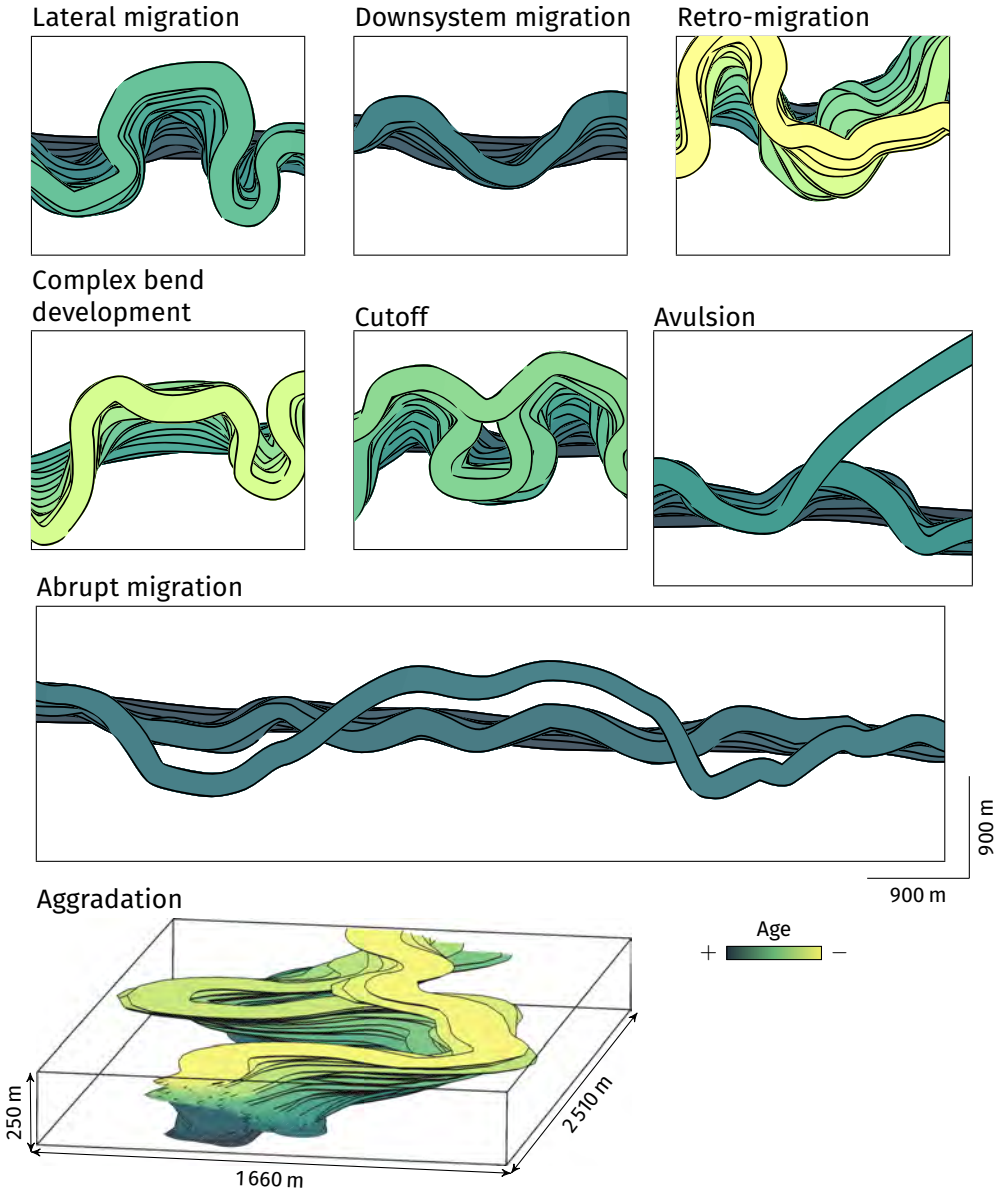

Figure 4.12 Enlargements on some areas of the channels on figure 4.11 illustrating different aspect of channel evolution reproduced by the method.

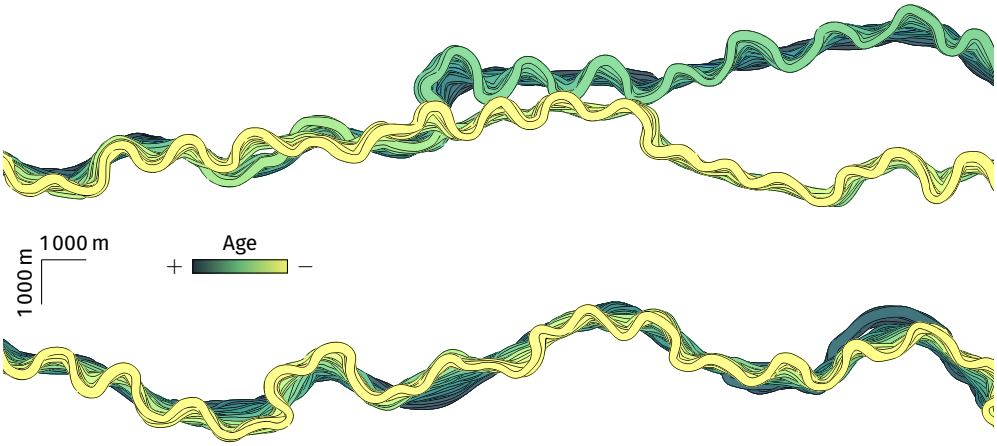

Figure 4.13 Application of a backward migration process based on SGS to two channels generated with L-system. The input parameters are given in table C.2, appendix C.

of the sinuosity: the channel remains in a steady-state.

To test the method with MPS, a training set was simulated with a SGS-based process (figure 4.16). This training set only have 9 migrating steps. Lateral migration dominates the system, with several abrupt migrations all along it. Each migration step can only look for its values in the corresponding step in the training set, and not in the whole training set. The parameters for the MPS favor the quality over the speed, with the two thresholds at zero and maximal scanned fraction of the training model of 0.75. As the simulated migration factors are quite perturbed, two smoothing iterations are added at the end of each simulation. This counterbalance the inability of the simulation process to find a pattern with a distance value consistent with the threshold.

At the end the lateral migrations is still dominant in the simulations. Abrupt migrations are also reproduced by the simulation process. However, they tend to be less frequent. They also tend to be smaller, both in length and in migration factor, than in the training set. This comes from both the inability to find the right pattern in the training set and from the smoothing.

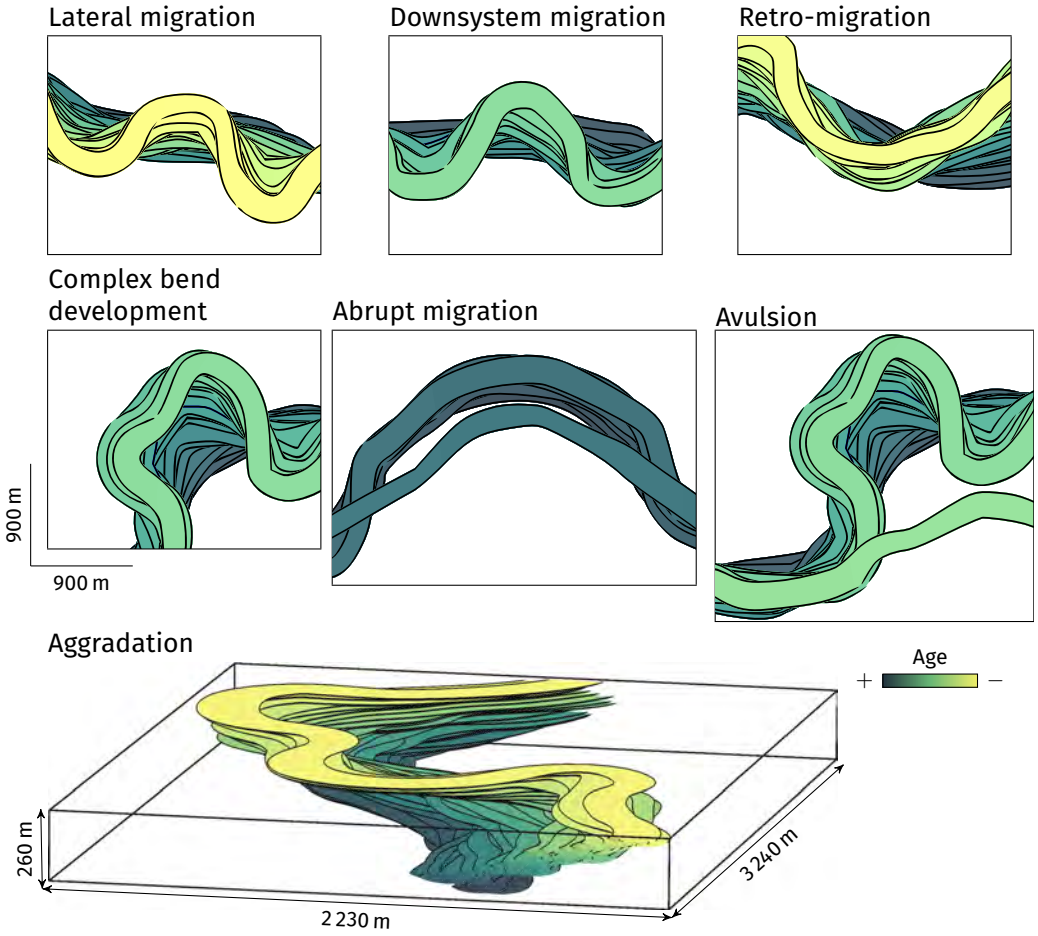

Figure 4.14 Enlargements on some areas of the channels on figure 4.13 illustrating different aspect of channel evolution reproduced by the method.

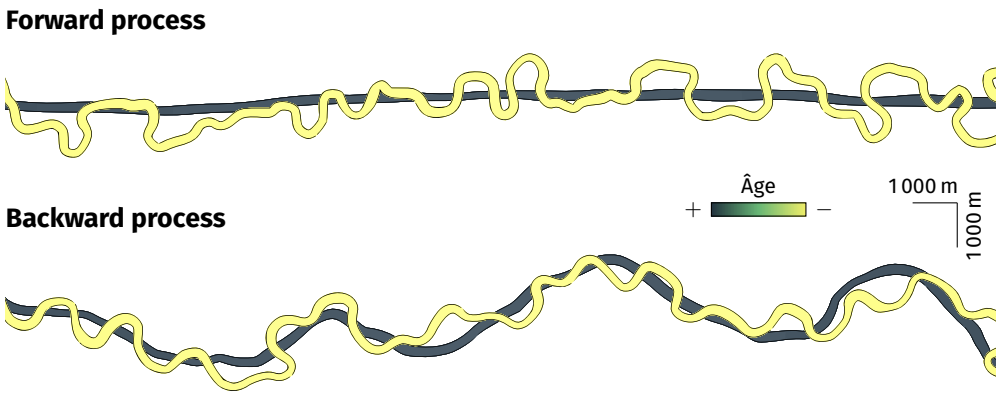

Figure 4.15 First and last channel of a forward and backward migration with SGS. The channels for the forward process come from the bottom migrating system of figure 4.11 and the initial channel is the older. The channels for the backward process come from the bottom migrating system of figure 4.13 and the initial channel is the younger. The input parameters are given in table C.2, appendix C.

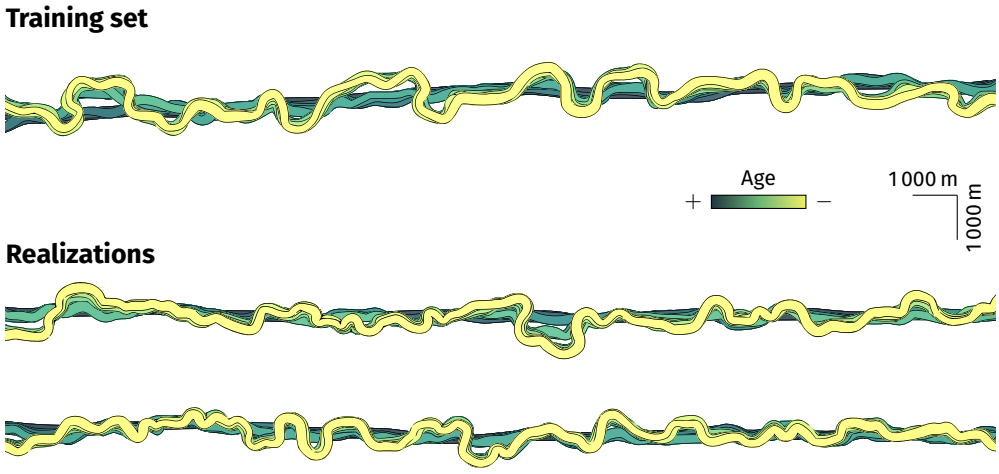

Figure 4.16 Application of a forward migration process based on MPS to two channels generated with L-system. The input parameters are given in table C.3, appendix C.

Table 4.1 Set of indicators and associated weights used for the case study. The indicator descriptions are in section 2.2, chapter 2.

Set	Subset	Indicator	Symbol	Weight
Global analysis *(measures on all the components)*		Facies proportion	p	1
		Facies adjacency proportion	p^a	1
		Facies connection probability	Γ	1
		Corrected connected component density	ϵ	1
		Unit connected component proportion	p^u	1
		Traversing connected component proportion	p^c	1
Detailed analysis *(measures on each component)*	Shape indicators	Corrected number of connected component cells	n	1
		Box ratio	β	1
		Faces/cells ratio	ζ	1
		Sphericity	ϕ	1
	Skeleton indicators	Node degree proportions	p^n	1
		Branch inverse tortuosity	t	1

4.7 Comparison of different channel stacking in terms of connectivity

The purpose of this section is to highlight the impact of the migration process on the connectivity of the simulated channels. Three sets of realizations represent different channel stacking and are compared with a focus on the connectivity.

This comparison relies on the indicators introduced in chapter 2. The table 4.1 recalls the set of indicators. The indicators are based on the connected components of the realizations. To facilitate the realization comparison, they are used to compute dissimilarity values between all the realizations by means of a heterogeneous Euclidean/Jensen-Shannon metric.

4.7.1 Case study

This case study uses that of the third chapter (section 3.6), with turbiditic channels evolving within a master channel, gradually filling the master channel.

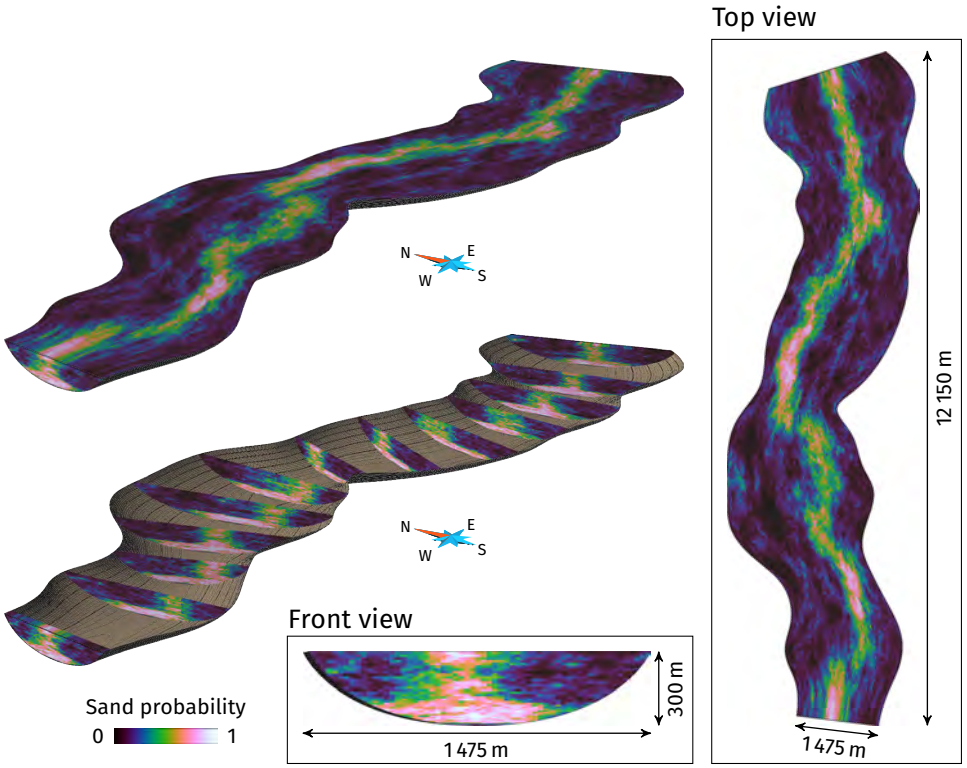

Figure 4.17 Dataset of the application: a curvilinear grid representing a master channel with a sand probability cube.

The data set includes a hexahedral grid representing the master channel (figure 4.17). This grid comes from the NURBS volume of a channel simulated by a L-system process. A sand probability cube is defined within the whole master channel. This cube informs about the channel evolution within the master channel:

- Lateral migration dominates the first phase of the master channel filling. The channels migrate within the whole master channel width, with a low aggradation and some abrupt lateral migration. This results in the deposition of sand-rich deposits over the whole bottom of the master channel.
- Aggradation dominates the second phase of the master filling. The lateral migration is less significant compared with the first phase, without any abrupt migration. This results in the deposition of sand-rich deposits in a

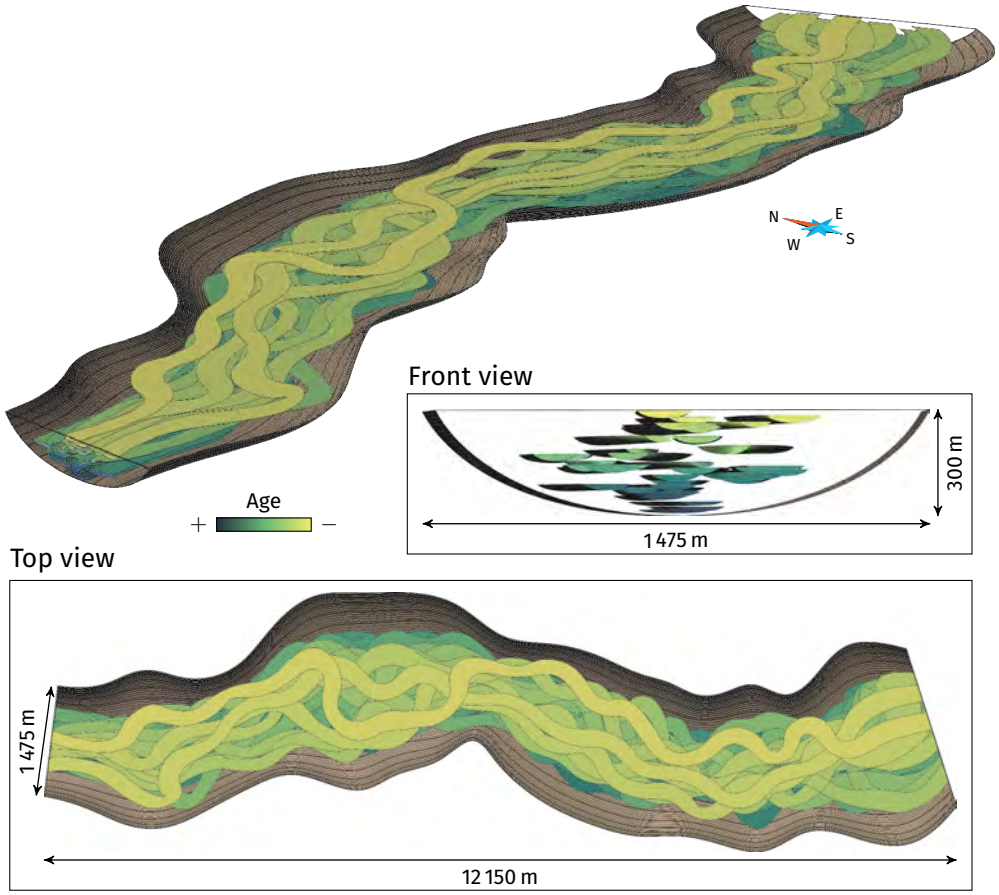

Figure 4.18 Example of a realization from the disorganized stacking set. The realization contains 40 channels within a master channel.

limited area within the top of the master channel. The rest of the master channel is filled with inter-channel deposits, in particular inner levees whose development induces the limited lateral migration.

Three set of 100 realizations are simulated within the master channel grid, with each realization containing 40 channels:

- The first set comprises L-system realizations without data except the confinement from the master channel margins (figure 4.18). The channels are randomly placed inside the grid and are free to develop in the whole canyon, without any constraint on the position of each channel relative to

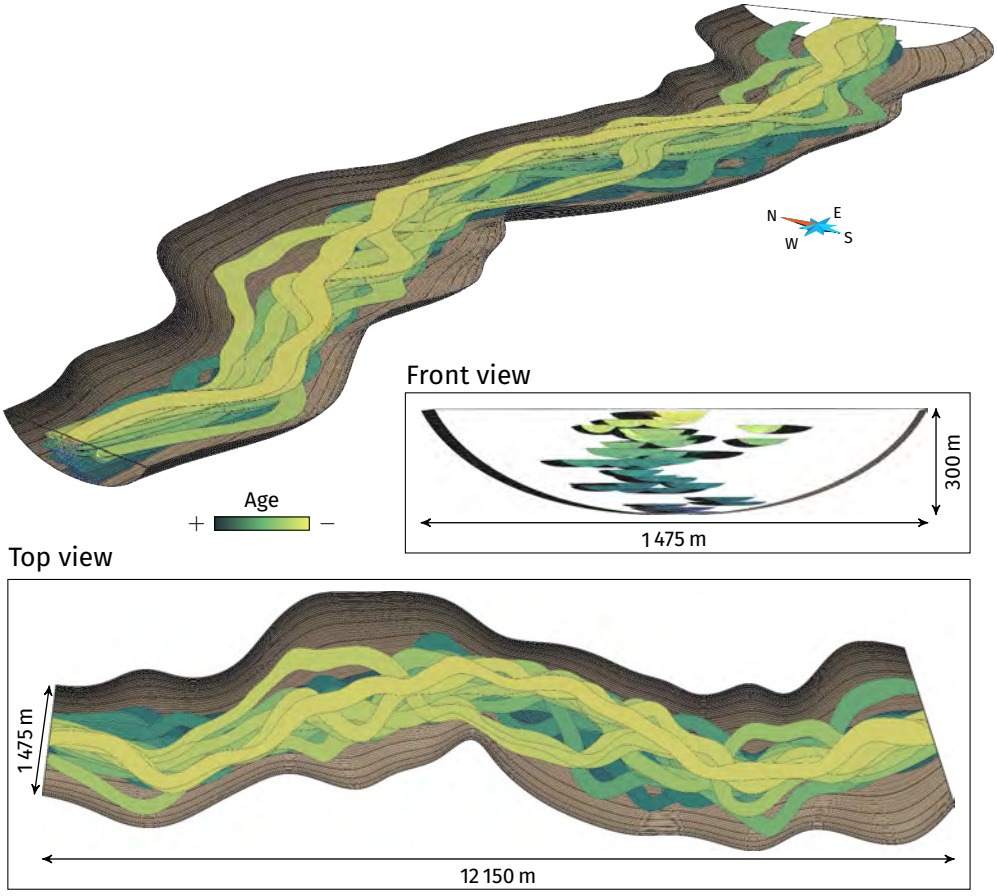

Figure 4.19 Example of a realization from the conditioned disorganized stacking set. The realization contains 40 channels conditioned to a sand probability cube within a master channel.

the others. The channels from this set have a disorganized stacking. The input parameters for this set are those of the set 1 in table B.3, appendix B.

- The second set comprises L-system realizations conditioned to the master channel margins and the sand property cube (figure 4.19). The channel random initial position and the channel development are both influenced by the sand probability cube. This influences the relative positions of the channels, but without a direct control on the channel relationships. The

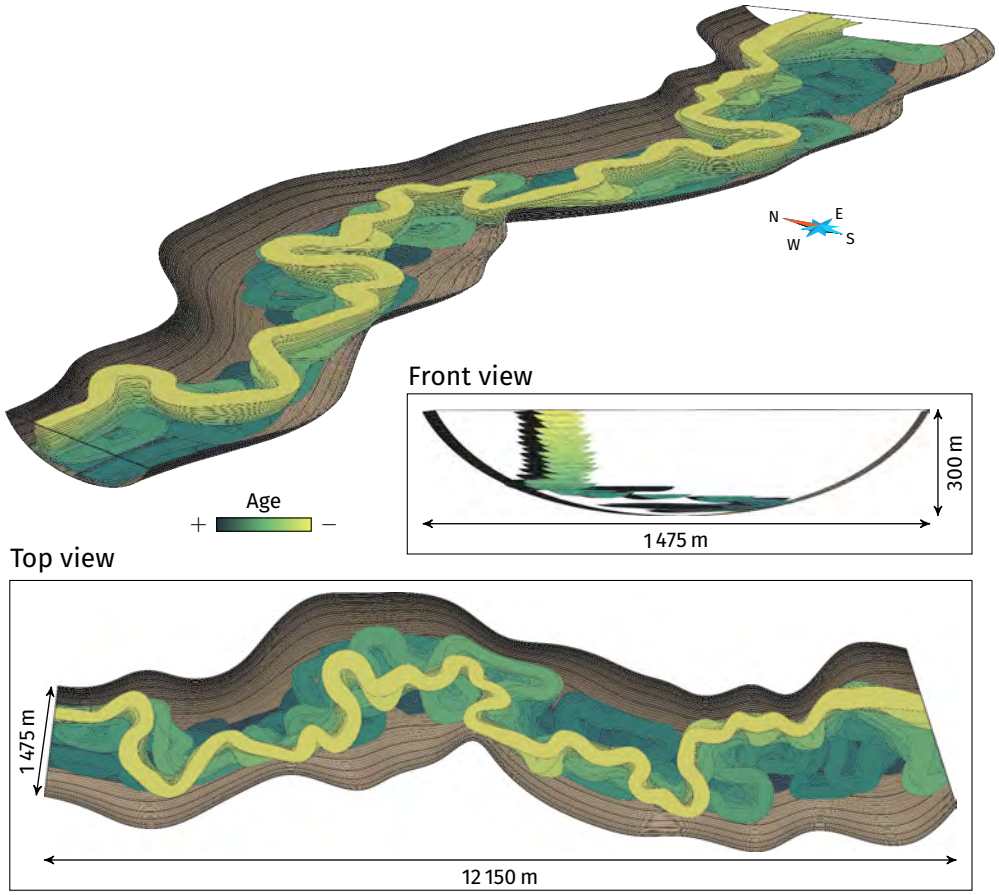

Figure 4.20 Example of a realization from the organized stacking set. The realization contains 40 channels within a master channel.

channels from this set have a conditioned disorganized stacking. The input parameters for this set are those of the set 2 in table B.3, appendix B.

- The last set comprises realizations from a forward SGS-based migration from an initial channel simulated with a L-system (figure 4.20). The initial position if the first channel is randomly drawn at a fixed vertical coordinate along the bottom of the canyon. The migration process includes two phases to reproduce the global channel evolution. A first set of parameters simulates 27 migration steps, with a high lateral migration,

some abrupt migration and few aggradation. This first phase is initiated with a channel simulated with a L-system. The next 12 steps simulate a small lateral migration with a significant aggradation. This second phase is initiated with the last channel of the first phase. If a migration will lead a channel node to go outside the master channel, the migration factor is decreased so that the channel remains within the master channel. The channels from this set have an organized stacking. The input parameters for this set are given in table C.4, appendix C.

4.7.2 Indicator results

All the indicators get the same weight of 1. Only the channels are considered, and not the inter-channel deposits within the master channel. Three indicators appear to be non-discriminant in this case study:

- The facies adjacency proportions, because the realizations only contain two facies.
- The unit connected component proportion, because the rasterized objects do not lead to any connected component of one cell.
- The traversing connected component proportion, because all the channel objects go through the entire master channel and are all traversing.

The dissimilarities are represented by a multidimensional scaling (MDS) (figure 4.21). The purpose is to represent the realizations as points, the distances between the points being as close as possible to the dissimilarities between the realizations. Here the Shepard diagram and the scree plot help to see the MDS ability to reproduce the dissimilarities. A two-dimensional representation given by the MDS is sufficient. Three dimensions would have been a bit better, but more difficult to analyze.

The dissimilarities clearly divide the realizations in two groups. The first group contains all the 100 organized stacking realizations, 47 conditioned disorganized stacking realizations and 58 disorganized realizations. The realizations of the different sets do not mix much, with three sub-groups, one per realization set. The conditioned disorganized stacking realizations are closer to the organized stacking realizations than the disorganized stacking realizations. The second group contains 53 conditioned disorganized stacking realizations and 42 disorganized stacking realizations. Compared to the first group, the realizations are a bit more mixed, with a significant variability between the realizations.

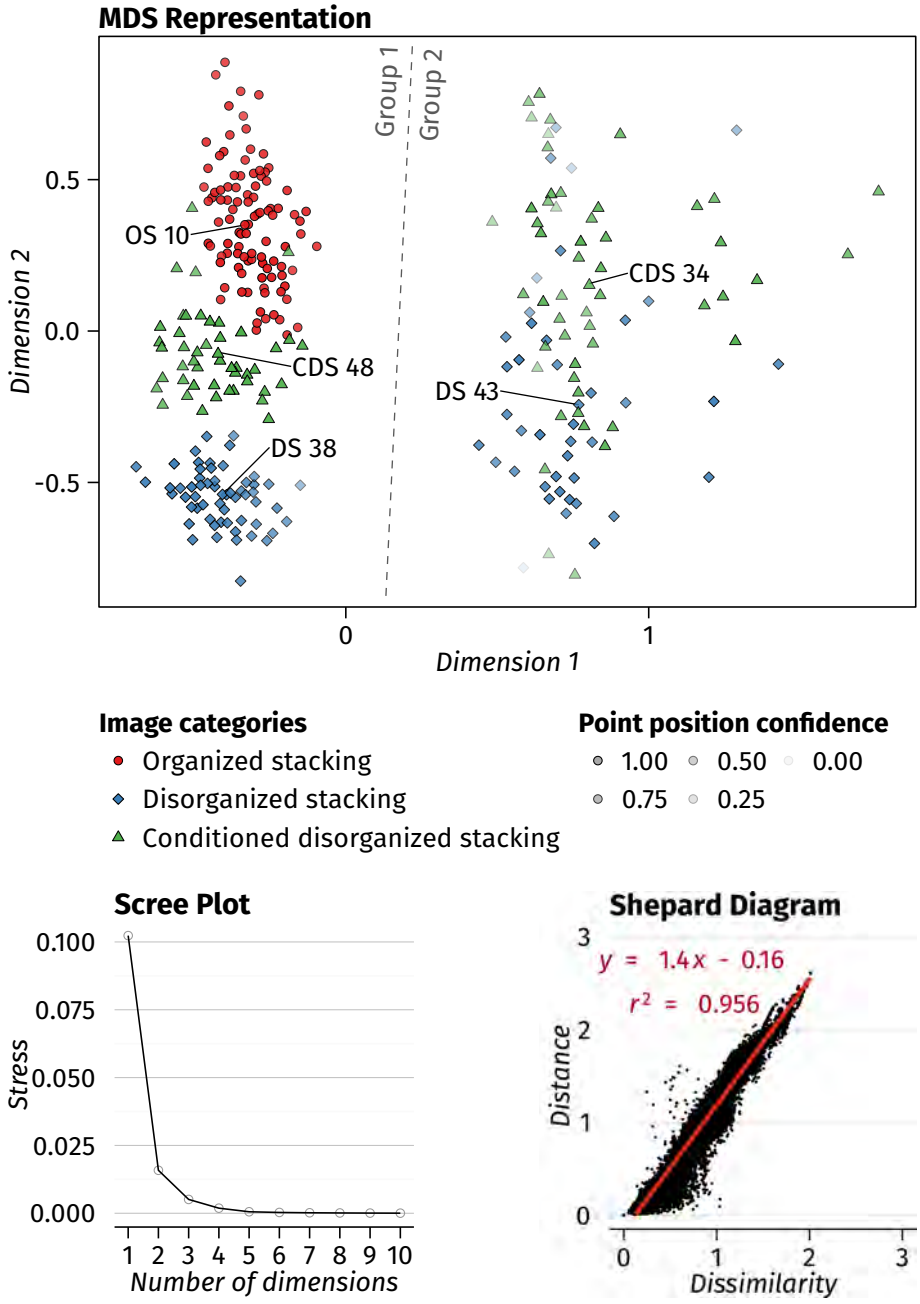

Figure 4.21 Multidimensional scaling representation comparing three set of realizations with different methods and parameters. The identified realizations are shown in figure 4.22.

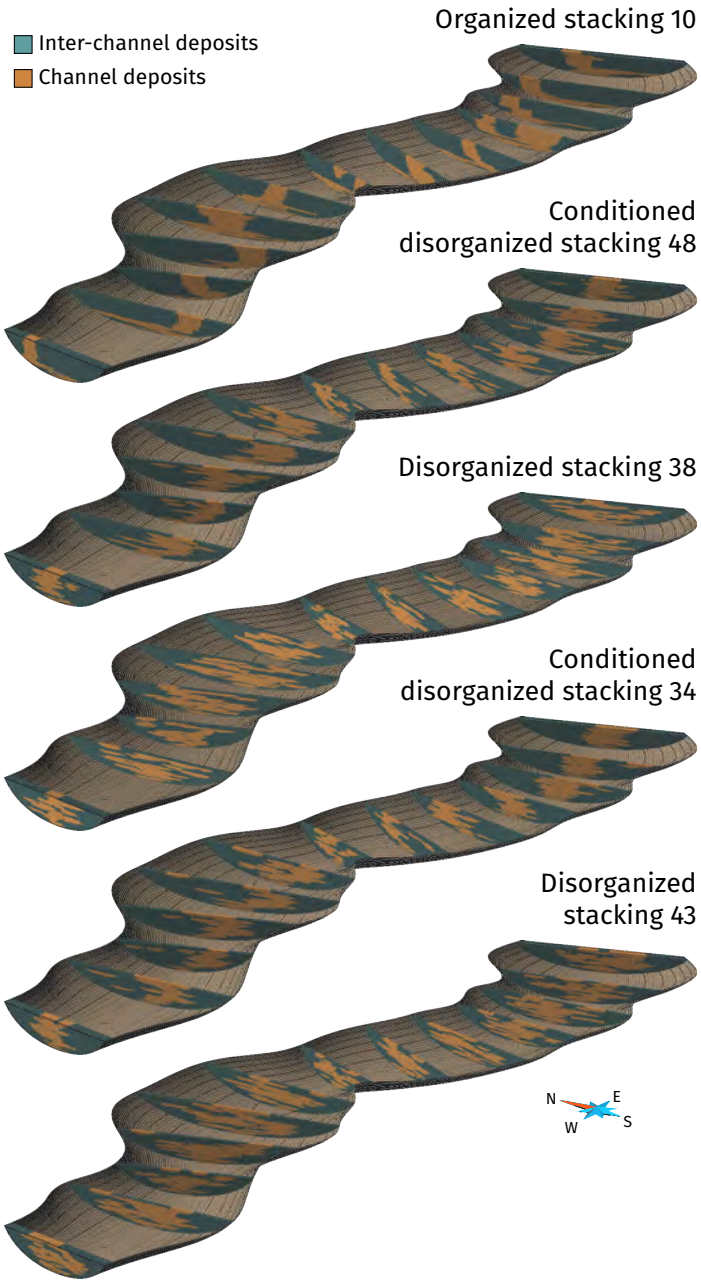

Figure 4.22 Realizations of for each set within the two groups separated by the dissimilarities. Each realization is the closest to the mean MDS point of its set and group.

Visually, the difference between the realizations of the different sets is quite clear (figure 4.22). However, examining realizations of the same set belonging to different groups does not show any significant difference.

Examining the indicators gives an explanation of the separation into two groups (figure 4.23). Realizations of the second group have lower facies connection probability, a higher component density and a lower average number of component cells than the realizations of the first group. Moreover, the realizations of the first group all have a facies connection probability of one. These realizations have channels that form a single connected component. The second group contains all the realizations with more than one connected component. This highlights the continuity of the migration process: having a non-connection between two successive channels requires an avulsion, otherwise the channels are always connected. Without migration, the control of the channel connectivity is less obvious.

Within the first group, the disorganized stacking realizations are clearly different from the other realizations. This is especially visible on the facies proportion and on the average number of component cells. Due to the disorganized stacking, the connected components of these realizations are larger than those of the other sets. On the other hand, the conditioned disorganized stacking and organized stacking realizations have similar facies proportions and average numbers of component cells. Their difference appears on the other indicators, such as the average faces/cells ratio or the average sphericity: even if the channels of the two sets occupy similar volumes within the grid, their shapes are different. The low faces/cells ratio of the organized stacking realizations highlights their organized stacking: the channels are significantly stacked over long distances, what decreases more the number of faces of the components than their number of cells. The average sphericity of these realizations is quite high compared to that of the conditioned disorganized realizations. This comes from their respect of the channel evolution: they occupy the whole width of the master channel bottom, and vertically they evolve to the top of the master channel. This also comes from the management of the channel margins: the migration is simply blocked by the channel margins, what is less constraining than the margin repulsion, especially at the bottom of the grid.

The difference between the realization sets within the first group is also visible on the skeletons (figure 4.24). The disorganized stacking realizations have higher proportions for the node degrees larger than 3 compared to the realizations of the other sets. This highlights channels that locally cross each other but are globally disconnected. This tend to generate many small branches all along the skeleton, with many loops (figures 4.26 and 4.26). The difference between

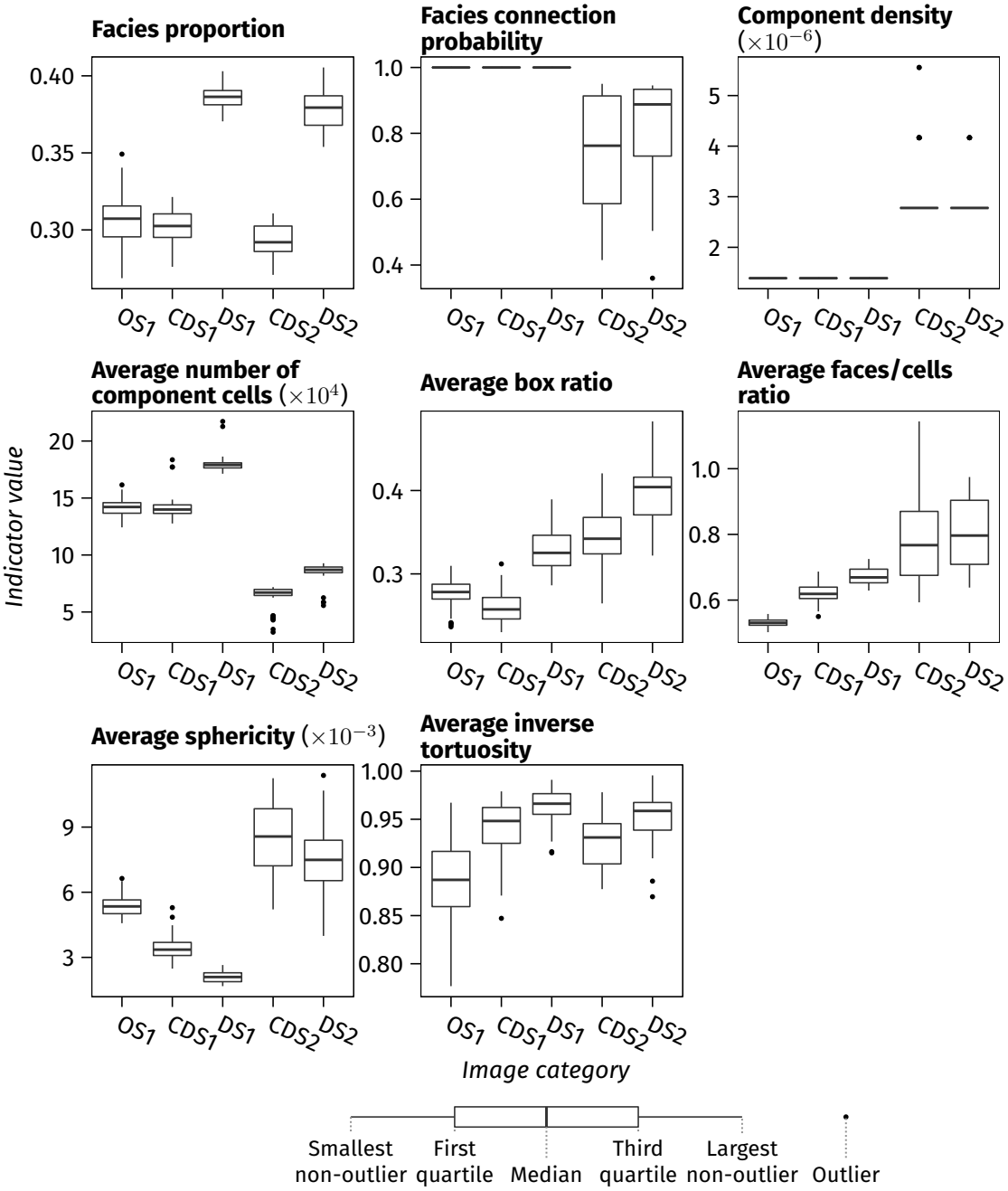

Figure 4.23 Box-plots comparing the range of indicators – except the node degree proportions – computed on three sets of realizations with different methods and parameters. *OS1*. Organized stacking realizations within the group 1; *CDS1 and CDS2*. Conditioned disorganized stacking realizations within the groups 1 and 2; *DS1 and DS2*. Disorganized stacking realizations within the groups 1 and 2;

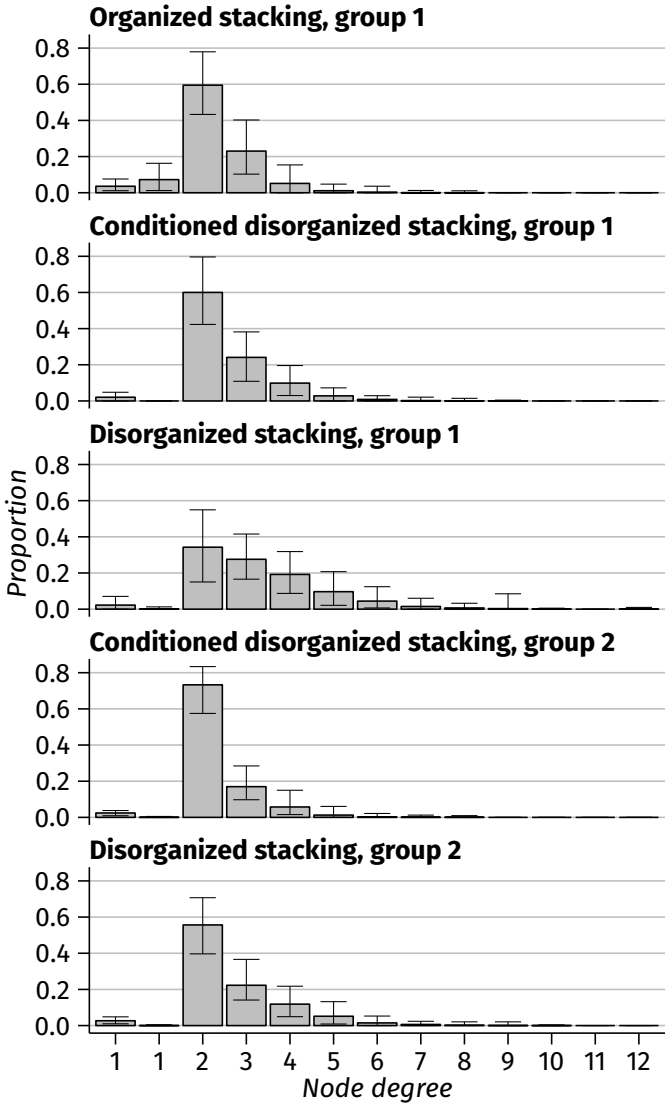

Figure 4.24 Mean node degree proportions of the levee skeletons for each set and group. The error bars display the minimum and maximum proportions. The first 1 node degree corresponds to the nodes of degree one along a grid border. The second 1 node degree corresponds to the nodes of degree one inside the grid.

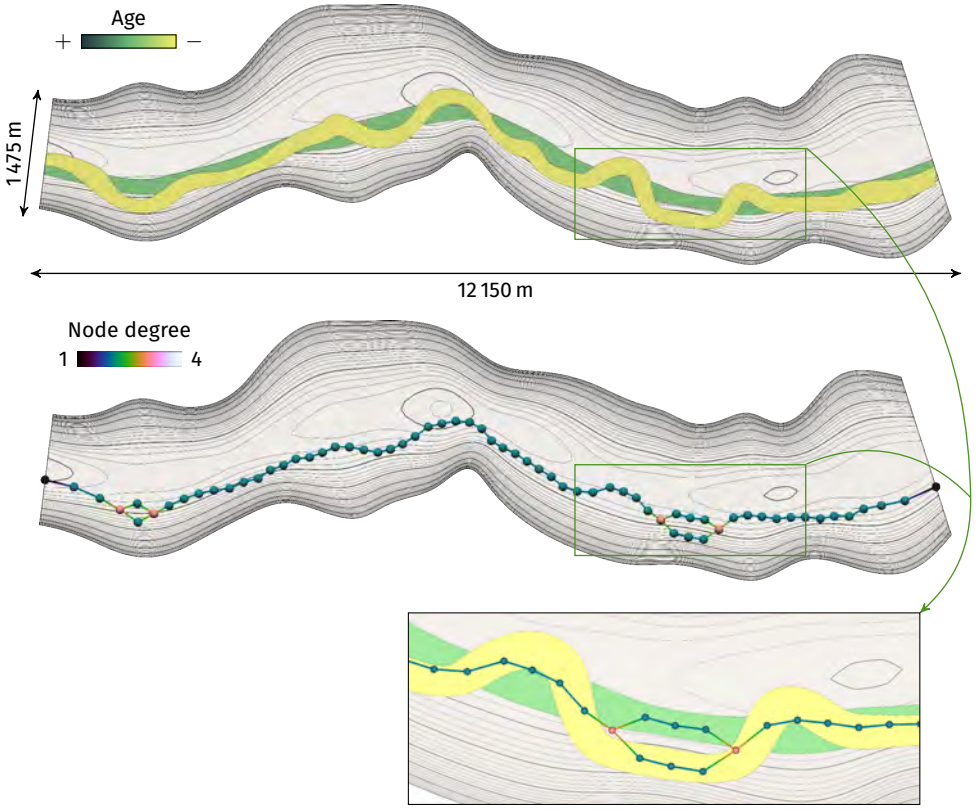

Figure 4.25 Two migrating channels with two local abrupt migrations and associated skeletons. An organized stacking of the two channels results in a single branch on the skeleton. The areas of abrupt migration, where the channels are not stacked anymore, results in a loop on the skeleton.

the conditioned disorganized stacking and the organized stacking realizations of the first group is less significant than on the other indicators. However, the conditioned disorganized stacking realizations have higher proportions for the node degrees larger than 3. Again, this highlights the tendency of their channels to cross each other without really stack within each other (figure 4.25). This is striking when visually comparing the skeletons (figure 4.26): the conditioned disorganized stacking realizations have many small branches forming loops, similarly to the disorganized stacking realizations. The organized stacking realizations have far less of those small branches. These small branches also tend to be straight, so to have a inverse tortuosity close to one. From this

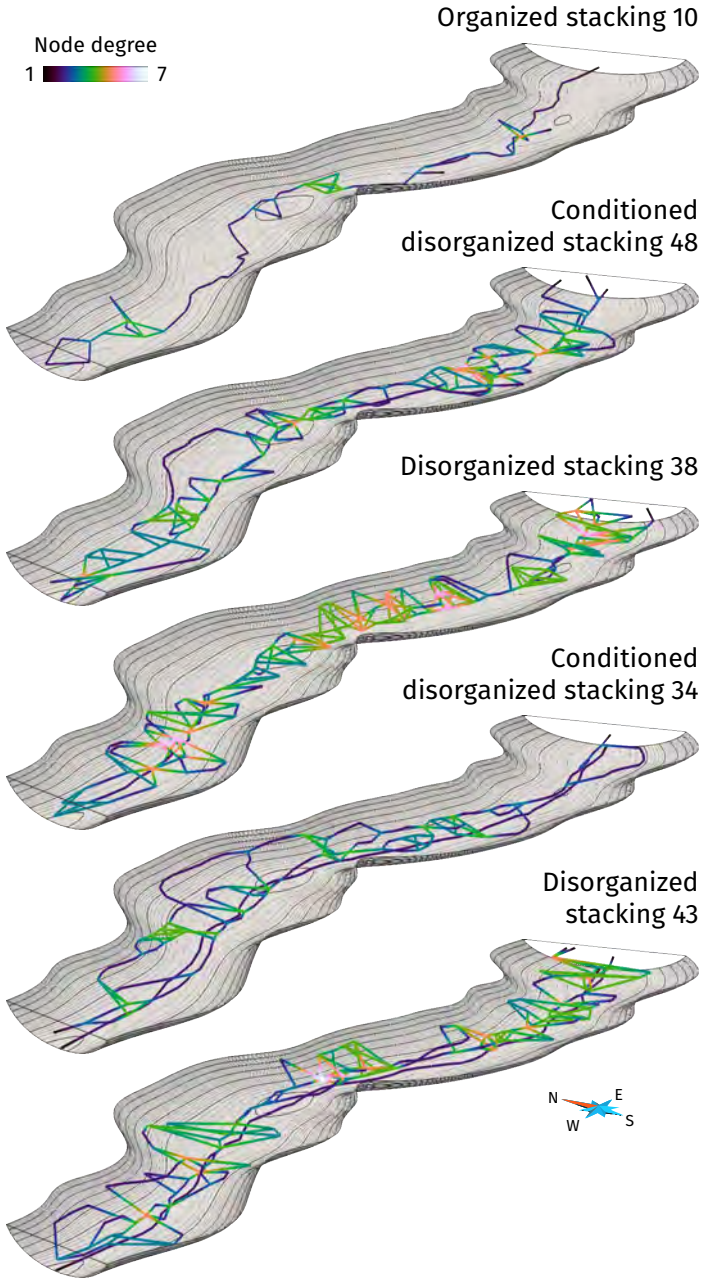

Figure 4.26 Skeletons of the channel connected components of the realizations showed in figure 4.22.

perspective, the evolution from the disorganized stacking to the conditioned disorganized stacking and the organized stacking is clear on the average inverse tortuosity: as the stacking increases, the inverse tortuosity decreases due to less straight branches.

It should be noticed that the skeletons do not capture the complete shape of the connected components in all its complexity. For instance in the organized stacking realizations, the distinction between the lateral migration at the master channel bottom and the aggradation at the top is not captured. This highlights the difficulty to determine the skeleton of an object.

Nevertheless, the differences between the three sets are clear on the indicators. The difference in stacking impacts directly the shape of the connected components and their connectivity. Adding a sand probability cube clearly helps to control the connectivity between the channels. However, the resulting channel organization is far from the clear stacking offered by the migration. Furthermore, the migration process gives a better control on the stacking and prevent non-connections if required.

4.8 Discussion and perspectives

The previous applications highlight the relevance of this approach. The next sections discuss some aspects of the method, leading to some perspectives.

4.8.1 About the migration pattern simulation

As defined, the process based on SGS leads to a dominant lateral migration through the influence of the curvature. Using a low curvature weight leads to the simulation of other patterns. However, it is not possible to choose another dominant migration pattern, such as a downsystem migration. This is not an issue for turbiditic channels, which tend to have little downsystem migration [e.g., Nakajima et al., 2009]. However, if another dominant pattern is required, the method has to be adapted. A simple solution is to modify the vector of migration by adding a downsystem component, such as done by Teles et al. [1998] or Viseur [2001]. Another solution is to change the secondary data influencing the migration. The curvature could be modified, or a different property would have to be used. From this point of view, MPS have the advantage that the training set controls the migration pattern.

Globally, the SGS remains able to reproduce various migration patterns. Most of the time, no smoothing is really required. The MPS would require more work to improve the reproduction of the migration pattern from the training set. MPS

seem to difficultly develop large bends. Several bends at a smaller scale than those in the training set tend to appear. For now smoothing steps are required to obtain satisfying results. From this point of view, the training set used in the example is not optimal as the channels have roughly the same length as in the realizations. Longer channels within the training set increase the repeatability of the patterns and improve the realization quality.

The bends should also be compared with their counterparts from real cases to assess the method ability to develop a realistic migration. When using a real case as training set, MPS should be one step ahead. But this need to be further tested. To compare the channels through the migration, statistics such as those of Howard and Hemberger [1991] can be used. But they are not directly defined to analyze the migration. Histogram and variogram of the migration factor can give a first insight, but further indicators should be developed to objectively analyze and compare migration patterns.

A comparison could then been done with physical simulation methods, especially the stochastic ones [Lopez, 2003, Pyrcz et al., 2009]. The main interrogation comes from the physical model ability to explore all the possible migrations. This questions the variety of stacking pattern that can be simulated. For instance here some retro-migrating areas can appear. These areas form outer-bank bars, which are potential reservoir areas [Nakajima et al., 2009]. Such bars have no equivalent in fluvial processes, whereas all the physical methods for the migration are developed for the fluvial environment. Thus, they may not be able to develop such migration patterns. Comparing the results of the forward and the backward migration processes would be also an interesting development.

4.8.2 About the discrete process simulation

For the SGS process, abrupt migration are introduced by a second set of migration parameters. Channels tend then to develop discontinuities from the previous channels. However, they tend to follow a similar migration pattern. Abrupt migrations and even local avulsions could also be simulated using L-systems. The initiation process would be the same as for the global avulsion. The newly simulated part would be attracted to a downstream location of the initial channel. This process is similar to the one developed by Anquez et al. [2015] to simulate anastomotic karst networks. It would possibly simulate bends completely independent from the previous channel.

MPS have shown their ability to reproduce abrupt migrations from the training set. Here again it facilitates the work for the user once a training set is

available. The only drawback is when regional avulsions or cutoffs are present in the training set. For now they are not handled, but they could be used to better simulate such processes.

The appearance of neck cutoff is not a problem in a forward process with SGS. With SGS in a backward process, neck cutoff should be simulated during the process. This would help the migration to continue whatever the number of migration steps.

4.8.3 About the parameterization

Using SGS does not call for an intensive parameterization, with only four parameters required for a simulation. The aggradation and migration factors are directly related to the vertical and horizontal distances between two successive channels. They are thus pretty easy to define. The curvature weight is a bit harder to define. A weight of 1 gives a significant influence to the curvature. By default, a weight around 0.8 gives a dominant lateral migration but lets some other migration patterns appear. Starting with a range around the wanted bend length at the end of the process gives satisfying results.

No use of data has been done yet to find the parameter values. This could be done for instance thanks to an interpretation of channels on seismic data. If all the channels are often not discernible on seismic data, some of them could give indications on the possible parameter values, for the factor distributions, the variogram parameters and even the curvature weight by comparing the channel curvature with the migration distance.

One possibility to reduce a bit more the number of parameters is to use the bend length as range. The range then varies following the channel bends and the migration step. However, the channels often tend to develop small-scale variations that perturb the bend identification and thus the bend length computation. No significant migration can be obtained with such parameterization. One possibility is to smooth the simulated migration factors or the bend lengths. A better solution would be to better identify the bends and avoid the small-scale variations. The work of O'Neill and Abrahams [1986] for instance could be a first lead.

Compared to physical methods [e.g., Ikeda et al., 1981, Parker et al., 2011, Lopez, 2003], the parameterization is far simpler when the purpose is to model the current aspect of the geology. This requires working on old channels that have been deformed. Thus the physical parameters that lead to the channel formation are difficult if not impossible to infer. Pyrcz et al. [2009] manage to reduce the number of parameters to a single maximum distance to reach by a

standardization process. The impact of such standardization on the migration process and thus on the stacking patterns is not discussed. This parameterization is easier to infer, but less flexible if the migration patterns are not satisfying. The parameters used here give a finer control to the user on the migration patterns. Furthermore, they are mainly descriptive and can be inferred from the available data.

The more processes are introduced, e.g., abrupt migration, the heavier tend to be the parameterization. The MPS approach is then pretty useful. The few parameters are more related to the ratio between the simulation quality and the simulation speed. However, the training set dictates the geological considerations, such as the presence of abrupt migrations or the dominant migration patterns. The main issue is to find a training set. The most interesting option is to find one from an analog, either seismic data such as done by Labourdette [2008] or possibly an outcrop. In a fluvial system, satellite images are interesting sources of training sets.

4.8.4 About small-scale variations and smoothing

With both SGS and MPS, the migration factor is not always completely smooth. This induces some small-scale variations that can form inflexions. Such inflexions prevent from using directly the bend length as range for the SGS, as discussed in section 4.8.3. They also tend to further develop during the migration, forming new bends at a smaller-scale than initially desired.

The emergence of such features still needs to be explored. They may come from the prior model, i.e., the variogram or the training set, as it is not necessarily smooth. The question is then if this local sharpness should affect the migration. It may also come from a failure of the simulation process, especially with MPS with too high thresholds.

The smoothing of the migration factor gives a control on the small-scale variations by eliminating their influence on the migration. However, the smoothing impact is quite significant, as discussed by Crosato [2007] on the curvature. Four to five smoothing steps can be enough to completely modify the migration structure. It should then be used carefully.

4.8.5 About the usefulness of the migration process

The comparison with object-based simulations without migration process highlights the differences in term of connectivity. This migration process gives a more important control on the stacking pattern. This is especially useful know-

ing the significant influence of the stacking pattern on the connectivity. By adding secondary data to an object-based process, it is possible to get closer to the migration results. However, the difference in terms of connectivity remains significant.

The analysis of the connectivity could be further developed by introducing the channel filling. In particular shale drapes have a significant impact on the connectivity. And in such case controlling the stacking pattern is even more important.

4.8.6 About the simulation process with migration

L-system are interesting to develop the initial channel, especially for their ability to develop channels with various sinuosity. In the MPS case, method such as the one of Mariethoz et al. [2014] could also be interesting. They simulate channel centerline based on MPS in a similar process that the one used for migration. The initial channel could then be simulated based on the first channel of the training set.

Both SGS and MPS are able to simulate a forward or a backward migration. This backward process is really useful, as the last channel of a migrating sequence is far more often interpretable on seismic data than the first one [Labourdette, 2008]. This allows initiating the process from the real data, instead starting from an unknown state and trying to condition the process to the last channel.

Some elements would be interesting to go further in the process. For now the channel width and thickness are simulated at the end of each migration step. As the width in particular has an impact on the migration, it could be interesting to simulate them earlier. With MPS, the channel width and thickness could also be simulated from the training set instead of using SGS such as done in the case studies. Other geological elements could be integrated, such as the channel filling. This is especially important due to their impact on the connectivity. Levees also need to be introduced. And when the channels migrate within a confinement such as a canyon, they can erode that confinement. Thus, they modify the confinement morphology, which could be taken into account.

4.8.7 About data conditioning

Data conditioning of the migration process has not been explored yet. Thanks to both SGS and MPS, data conditioning is pretty easy if the data are at a distance compatible with the migration factor distributions. Data can then be directly

integrated into the spatial structure of the migrated channel. To preserve the conditioning, smoothing can not be performed at the data locations.

However, the process is more difficult when the data are away from the channel: the migration can not condition the data if the channel does not come close enough. One solution is to introduce a constraint that attracts the migrating channel to the data, similarly to the initial channel conditioning or to the conditioning of Flumy [Lopez, 2003]. This implies to adjust the appearance of discrete migrations and avulsions depending on the data and their location.

It is also important to notice that the overall methodology requires an important work of data interpretation and sorting to possibly pre-attribute them to each migrating system. Conditioning to a sand probability cube is also problematic, especially to handle avulsions. This may require identifying the large-scale trends within the cube.

4.8.8 Numerical aspects

The realization were simulated on a 64-bit Linux system with a 2.10 GHz processor Intel® Core™ i7-3612QM and 6 GB of RAM.

The migration process in itself is really fast. In the master channel, it took 2.79 ± 0.20 s to simulate the initial channel and to perform the 39 steps of migrations. Here the first and last nodes of the channels are free to migrate. Thus, the initial channel length has to be chosen large enough so that the migrating channels continue to spread across the whole master channel length. Setting the migration factor to zero for the first and last nodes of the migrating channels could prevent those channel to have their extremity migrating inside the master channel. This would reduce the computation time by enabling the use of a smaller initial channel length.

The generation of the NURBS is the most time consuming part of the process, with 20.03 ± 1.17 s to materialize the 40 channels of a realization. On the migration process itself, the most time consuming parts are the regridding and the neck cutoff generation. However, more efficient solutions than the one used here exists for the neck cutoff generation [e.g., Camporeale et al., 2005, Schwenk et al., 2015].

Globally the process gives nicer results with smoother migrations as the resolution increase. Increasing the resolution means using a small element resolution and a small migration factor. This potentially induces more channels with more elements. Parquer et al. [2015] develop a re-parameterization function to use the minimal number of control points on a NURBS surface while preserving at best its shape. This can be useful to limit the weight of the NURBS

surfaces.

4.9 Conclusions

This work provides a basis for a more descriptive approach of channel migration to control channel stacking. A single approach stochastically simulates either forward or backward channel migration, starting with an initial channel simulated by L-system or directly interpreted on seismic data. The migration process is based on simulating a migration factor by SGS or MPS with the curvature as secondary data. Four parameters are required by the SGS approach to adjust the migration patterns. The MPS approach calls for four parameters related to the simulation speed and quality and a training set that controls the migration patterns. Global avulsion is done by L-system simulation, as the initial channel.

The first results are encouraging, with a significant difference in connectivity from a process with no direct control on the channel stacking. Some deeper work is required on particular points, as using the bend length as variogram range by default. Conditioning to already interpreted accretion packages is possible thanks to both SGS and MPS conditioning ability, but only if these packages are not too far from the channel. Further managing accretion packages could be done with potential fields for instance, as done for initial channel conditioning or with physical methods [e.g., Lopez, 2003]. Neck cut-offs remain to be introduced in the backward process with SGS. The training set required by MPS could be better used to take into account cutoffs and possibly avulsion, both regional or local. The channel fill should also be simulated to better assess the impact on the connectivity. If the method is introduced from the point of view of the turbiditic environment, its use of prior statistical models to migrate in a descriptive process makes the method valid for fluvial applications.

Conclusions

1 Contributions

The connectivity between sand-rich deposits is a main factor controlling flow behavior within a reservoir or an aquifer related to a channelized system. From this point of view, channels are fundamental sedimentary structures, both for their role in sediment transport and their own deposits, whose permeability enables fluid circulation. Turbiditic systems are a perfect example of how the complex architectures related to channels influence the connectivity at various scales. Based on those considerations, two strategies have been developed to better take into account the connectivity in stochastic simulations:

- A strategy to analyze the connectivity of a realization through indicators. This enables the objective comparison of realizations in terms of connectivity.
- A strategy to better model the connectivity through a better reproduction of channels while conditioning to the available data and through a better reproduction of the channel relationships.

The following sections summarize the main contributions of this thesis around those strategies.

1.1 Indicators and an analysis process to compare stochastic simulations of sedimentary bodies by focusing on the connectivity

Being able to compare realizations in terms of connectivity is of significant interest as the final purpose of these realizations is to better understand the flow behavior within the studied domain. Furthermore, geostatistical simulation

methods mostly rely on the reproduction of statistics and do not directly take into account the connectivity.

The method developed in this thesis to analyze the connectivity applies on categorical images representing sedimentary bodies. It relies on a set of indicators that further develop the use of connected components compared to previous work [e.g., Deutsch, 1998, De Iaco and Maggio, 2011]. The indicators measure for instance the component size, shape, density or the node degrees of the component skeleton. They are used to compute dissimilarities between different realizations and/or conceptual models. Such dissimilarities facilitate the analysis process by integrating all the indicators in a single value.

However, the resulting dissimilarity matrix is unreadable when dealing with hundreds of realizations, as it is usually done in stochastic modeling. Multidimensional scaling is a really powerful visualization technique which significantly facilitates the analysis process. It raises an increasing interest in the literature to compare realizations [e.g., Tahmasebi et al., 2014, Yang et al., 2016], without always enough care at the validity of the representation in a low dimensional space. Indeed, it is only a partial view of the dissimilarities which can be misleading in some circumstances. From our tests, no case has been encountered where the MDS is completely wrong in its representation of the dissimilarities, at least for a global analysis. The heat map is harder to analyze, but it represents the real dissimilarity values. It is then an interesting tool to verify the observations done on the MDS representation. In any case, going back to the indicators should be always done, at least as a precaution.

The application of the proposed method to a synthetic case results in a different ranking than the one obtained by a visual analysis. Nevertheless, a detailed analysis shows the consistency of the indicator behavior. These indicators are simple to analyze, and not computationally demanding. Using the skeletons is appealing because they capture more directly the connectivity through the topology of the connected components.

1.2 A method to stochastically simulate channelized bodies using a constrained L-system

The approach developed to stochastically simulate channels relies on a formal grammar, the Lindenmayer system. Predefined rules control the development of the channel morphology to simulate straight to sinuous channels. During that development, constraints attract or repulse the channel to condition the available data.

This approach is really fast, both for the simulation of channel and for their

conditioning. Applying the constraints gradually during the channel development appear to be flexible enough to handle numerous data simultaneously. It also gives the possibility to always condition a data. Thus, the method can simulate conditional channels even if the chosen parameter values lead to channels not conform to the data configuration. In object-based simulation, a focus is often done on well sedimentary data conditioning [e.g., Oliver, 2002, Hassanpour et al., 2013, Mariethoz et al., 2014]. Here the method is able to handle far more data types, including well connectivity data, a sand probability cube or any kind of property cube and even a confinement. Weights give further control on the impact of each constraint.

The constraints induce a deformation of the initial channel morphology, including the sinuosity. They have been developed with the purpose to keep that deformation as small as possible. However, the channel sinuosity has less impact on flow circulations than the channel continuity. This approach never degrades the continuity of the channel, contrary to cell-based methods.

1.3 A method to stochastically simulate stacked channelized bodies using a geostatistical approach

The channels simulated with a L-system are not able reproduce the complex organization of the relations between the channels as seen on outcrops or seismic images. That organization comes from migration and avulsion of the channels.

This is why the approach has been extended to include such types of controls. The proposed method relies on mimicking both migration and avulsion processes. It starts from an initial channel, either simulated with a L-system or interpreted on seismic data. Avulsion consists in simulating a new channel with a Lindenmayer system after a randomly chosen avulsion location. Migration is introduced through a geostatistical framework. This framework relies on the simulation of a migration factor with a sequential Gaussian simulation or a multiple-point simulation if a training set is available. With a training set the migration patterns can be directly borrowed from real data.

The current stochastic approaches of the migration [Lopez, 2003, Pyrcz et al., 2009] rely on physical models that are a controversial topic, especially with turbiditic systems. Here the method offers a more descriptive approach to control the stacking pattern resulting from migration and avulsion. The migration is controlled by means of a prior, which can come either from field data or from analog data. Furthermore, it is able to stochastically simulate both forward and backward migration. A backward process allows starting from the data, as the

last channel of a complex is often interpretable on seismic data but not the first channel. Thus, this approach refocuses the migration process on the data.

Three realization sets have been compared to highlight the interest of integrating a migration process within stochastic simulations of channels. The first set contains realizations without migration process, so simple L-system realizations. The second set does not integrate the migration process, but condition to a sand probability cube representing the result of the channel evolution. The last set contains realizations with migration process. Using the indicators (section 1.1) highlight the significant difference of connectivity between the different sets. It also highlights the poor control on the channel stacking without migration process. This can lead to complete – and unwanted – disconnections between some channels, so a significant impact on the connectivity.

2 Perspectives

Besides the technical improvements, several lines of research would be meaningful to further explore the integration of connectivity within stochastic simulations of channels.

2.1 Sensitivity tests and application to real data

All the methods have been tested on synthetic cases of different dimensions and settings, especially considering the types of data to take into account. Those cases have allowed exploring the possibilities offered by the methods. But the impact of the parameters on the resulting channels has only be slightly developed.

In particular, it has consequences on the conditioning of L-systems. Indeed, constraints involve many parameters, with several of them predefined to facilitate the task for the user. The ability of the predefined set to handle all, or at least most, cases has to be questioned. Sensitivity tests could also be done to explore the possible migration patterns developed thanks to the SGS or MPS. A comparison with real migrations is also a quite interesting perspective. This is especially true for the MPS-based process, which has a far higher interest when used with a training set from real data.

This aspect raises the question of the application on real data. If the synthetic cases have been developed with the idea of getting close to real cases, there are always differences with the reality. The application of all the methods proposed in this thesis on a real case would be of prime importance to either validate or further improve the chosen approaches.

2.2 Improvements of the indicators

Computing the indicators on sub-grids could be a significant development. Indeed, it would bypass the issue of comparing realizations within grids of different dimensions. This should improve the indicator efficiency to capture the connected component shape. It could also enable to capture a potential non-stationarity within the realizations.

Despite the interesting aspect of skeletons, their extraction from a component is difficult in three dimensions. Only two methods have been tested in this thesis and more exists [e.g., Cornea et al., 2007]. Using other methods could help to better capture the component topology and most importantly the component geometry.

2.3 Further use of L-systems

For now the simulation of channels is far from using the full potential of L-systems. Some examples illustrate the possibility of modifying the rules. Other possibilities include the simulation of lobes or of abandoned bends. These abandoned bends could be integrated in the backward migration process. This would complete the process, as neck cut-offs is the only missing feature compared with the forward process. Using L-systems for abrupt-migration should also improve the appearance of a disorganized stacking.

One exciting aspect of L-systems is all the developments done in numerical biology. For instance, L-systems are not only used to simulate tree morphologies, but also leaves, fruits and whole plants in three dimensions from a set of rules and the related interpretation [e.g., Prusinkiewicz et al., 2001]. Thus, the user can define its own three-dimensional objects. This aspect could be of significant interest for object-based modeling. Indeed, one limitation is to have a parameterization that defines a sedimentary object. From a user perspective, it is always annoying if that parameterization does not exist or is not satisfying. Some sedimentary objects could be then proposed by default. And if the user needs different or new objects, he would have the possibility to define them relatively easily. These developments should start by simulating the whole channel object with L-systems, and not just the channel morphology.

2.4 Better management of the data

Data conditioning is a key aspect in stochastic simulations. It could be introduced in the indicators to quantify the integration of data in the realizations. With cell-based methods, a cell with a channel value can remain without any

channel cells in its neighborhood. Thus, no channel object passes through that cell, with an impact on the connectivity. Even if the data is conditioned *stricto sensu*, such configuration should be avoided.

Within the L-system process, the preservation of the channel morphology is a main concern. That preservation significantly varies following the channel segment length. This parameter should be introduced in the constraint magnitude computation. The accuracy of conditioning by the constraints is not always good enough, even if the misfit remains at a very local scale. From this point of view, the deformation ability of NURBS is highly interesting, but still has to be tested. Conditioning to a global channel proportion or a net-to-gross would also be a significant improvement.

An interesting aspect of the constraints is their ability to take into account various types of data, including connectivity data. For now their integration is quite rough: one channel must condition a whole set of connected data. In reality, the connection may concern several channels. This just implies to better handle the relationships between the channels. For instance, a first channel conditions to a data. Another channel conditions another data, which should be connected to the first data. Then that second channel is attracted to a channel section of the first channel instead of the first data itself.

A last aspect is data conditioning in the migration process. All the methods used for avulsion and migration are able to condition. For migration, conditioning is easy at a distance less than the maximal migration distance. For larger distance, it requires another process. The bends could be attracted or repulsed, similarly as with the L-system or as done by Lopez [2003] or Pyrcz et al. [2009]. For avulsion, its triggering should be conditioned by the trend in the distance between the current channel and the data.

2.5 Introduction of the channel fill

Channel stacking is a main aspect influencing the connectivity of turbiditic systems. But the channel fill is another one. It could be highly interesting to test the indicators not on the sedimentary objects, but on the permeable deposits within those objects. The resulting shapes would be much more variable, but the analysis would be directly on the connectivity of the reservoir deposits.

For both channel and migration simulation, the use of NURBS gives access to curvilinear grids that can follow various fill geometries [Ruiu et al., 2015b]. It gives the opportunity to precisely simulate the channel fill. This simulation can relate on more classical geostatistical methods such as sequential indicator simulation. One aspect is how to combine the results from all the individual

channels. One possibility is to transfer the fill properties into a curvilinear grid including all the channels, such as done with the master canyon in the synthetic cases. This leads to lose some more or less details of the fill depending on the master grid resolution. A better solution would be to generate a hexahedral grid conform to all the channels. However, this task is currently far beyond our reach.

2.6 Link with fluvial systems

Both fluvial and turbiditic environments raise similar interests, with similar issues around fluids circulating in deposits from channelized structures. Both systems are based on a morphologically similar element: the channel. However, in terms of sedimentology, similarities between fluvial and turbiditic environments is a huge subject of controversy [e.g., Kolla, 2007, Wynn et al., 2007]. This controversy is nowadays mainly focused on the physics driving the current circulation within a channel.

If the global dimensions and architecture of fluvial and turbiditic deposits are significantly different, the methods illustrated here with turbiditic cases remains valid from a fluvial perspective. Indeed, we do not rely on the physical process underlying channelized deposits, only on the description of those deposits.

Appendix A

Simulation parameters of chapter 2

Table A.1 Parameters used to simulate the channelized environment with DeeSse.

Parameters	**Values**
Maximum number of neighbors	64
Acceptance threshold	0.05
Maximal scan fraction of the TI	0.33

Table A.2 Parameters used to simulate the channelized environment with IMPALA.

Parameters	**Values**
Number of multi-grids	4
Number of multi-grid levels in each direction	$4 \times 4 \times 1$
Search template type	Elliptic
Size of the search template (radii in m)	$7 \times 7 \times 4$
Maximal number of neighbors in the template	64

Table A.3 Parameters used to simulate the channelized environment with the object-based method of Petrel. The distributions used are all triangular.

Simulation parameters	**min**	**mode**	**max**
Channels			
Proportion (in %)	21.21	21.21	21.21
Orientation (in °)	0	0	0
Amplitude (in m)	10	15	40
Wavelength (in m)	60	70	100
Width (in m)	7	10	13
Thickness (in m)	1.5	2	4
Levees			
Proportion (in %)	8.79	8.79	8.79
Width (in m)	4	7	11
Thickness (relative to channel thickness)	0.25	0.35	0.6

Table A.4 Variogram parameters used to simulate the channelized environment with SIS.

Variogram parameters	**Channels**	**Levees**	**Mudstone environment**
Azimuth (in °)	0	0	0
Dip (in °)	0	0	0
Sill	0.145	0.109	0.210
Nugget	0	0	0
Range 1 (in m)	23	26	70
Range 2 (in m)	12	14	34
Range 3 (in m)	3	1	2.5
Type	Spherical	Exponential	Exponential

Appendix B

Simulation parameters and L-system rules of chapter 3

Table B.1 Parameters used to simulate the non-stationary channels. $\mathcal{T}$ is a triangular distribution with a minimum, a mode and a maximum.

Simulation parameters	**Decreasing sinuosity**	**Branching**
Global direction (in °)	90	90
Global direction weight	0.25	0.25
Default segment length (in m)	100	100
Channel length (in m)	20 000	30 000
Half-wavelength (in m)	$\mathcal{T}$(300,400,600)	$\mathcal{T}$(300,400,600)
Amplitude (in m)	$\mathcal{T}$(0,150,200)	$\mathcal{T}$(0,150,200)
Deviation angle (in °)	$\mathcal{T}$(0,0.057,0.57)	$\mathcal{T}$(0,0.057,0.57)
L-system weight	1	1
Channel self-repulsion weight	1	1
Channel width (in m)	$\mathcal{T}$(75,100,125)	$\mathcal{T}$(75,100,125)
Channel width range (in m)	$\mathcal{T}$(400,500,600)	$\mathcal{T}$(400,500,600)
Curvature weight	0.85	0.85
Channel thickness (in m)	$\mathcal{T}$(5,7,10)	$\mathcal{T}$(5,7,10)
Channel thickness range (in m)	$\mathcal{T}$(400,500,600)	$\mathcal{T}$(400,500,600)
Curvature weight	0.85	0.85
Asymmetry aspect ratio	0.5	0.5

Table B.2 Parameters used to simulate the channels of the figures 3.17, 3.18 and 3.23. Realizations in figures 3.21, 3.22, 3.15, 3.20 and 3.24 have the same parameters except the weights. $\mathcal{T}$ is a triangular distribution with a minimum, a mode and a maximum.

Simulation parameters	**Figure 3.17**	**Figure 3.18**	**Figure 3.23**
Global direction (in °)	70	70	70
Global direction weight	0.2	0.2	0.2
Default segment length (in cell)	1	1	1
Channel length (in cell)	–	–	–
Half-wavelength (in cell)	$\mathcal{T}$(4,7,12)	$\mathcal{T}$(4,7,12)	$\mathcal{T}$(4,7,12)
Amplitude (in cell)	$\mathcal{T}$(0,3.5,6)	$\mathcal{T}$(0,3.5,6)	$\mathcal{T}$(0,3.5,6)
Deviation angle (in °)	$\mathcal{T}$(0,0.057,0.57)	$\mathcal{T}$(0,0.057,0.57)	$\mathcal{T}$(0,0.057,0.57)
L-system weight	1	1	1
Channel self-repulsion weight	0	0	0
Channel width (in cell)	$\mathcal{T}$(2,2.75,3.5)	$\mathcal{T}$(2,2.75,3.5)	$\mathcal{T}$(2,2.75,3.5)
Channel width range (in cell)	$\mathcal{T}$(7,15,25)	$\mathcal{T}$(7,15,25)	$\mathcal{T}$(7,15,25)
Curvature weight	0.75	0.75	0.75
Channel thickness (in cell)	1	1	1
Channel thickness range (in cell)	–	–	–
Curvature weight	0.75	0.75	0.75
Asymmetry aspect ratio	0.5	0.5	0.5
Domain	Yes	Yes	Yes
Confinement weight	0	0	0
Well sedimentary data	No	Yes	No
Channel data weight	–	1	–
Channel data bandwidth (in cell)	–	1 000	–
Inter-channel data weight	–	1	–
Well connectivity data	No	No	No
Sand proportion cube	No	No	Yes
Sand proportion weight	–	–	0.2

Table B.3 Parameters used to simulate the channels within the master channel of the synthetic case. $\mathcal{T}$ is a triangular distribution with a minimum, a mode and a maximum.

Simulation parameters	**Set 1**	**Set 2**	**Set 3**
Global direction (in °)	90	90	90
Global direction weight	0.25	0.25	0.25
Default segment length (in cell)	6	6	6
Half-wavelength (in cell)	$\mathcal{T}$(10,15,25)	$\mathcal{T}$(10,15,25)	$\mathcal{T}$(10,15,25)
Amplitude (in cell)	$\mathcal{T}$(0,4,7)	$\mathcal{T}$(0,4,7)	$\mathcal{T}$(0,4,7)
Deviation angle (in °)	$\mathcal{T}$(0,0.57,5.7)	$\mathcal{T}$(0,0.57,5.7)	$\mathcal{T}$(0,0.57,5.7)
L-system weight	1	1	1
Channel self-repulsion weight	0	0	0
Channel width (in cell)	$\mathcal{T}$(5,6,8)	$\mathcal{T}$(5,6,8)	$\mathcal{T}$(5,6,8)
Channel width range (in cell)	$\mathcal{T}$(10,15,20)	$\mathcal{T}$(10,15,20)	$\mathcal{T}$(10,15,20)
Curvature weight	0.75	0.75	0.75
Channel thickness (in cell)	$\mathcal{T}$(1.5,2,2.5)	$\mathcal{T}$(1.5,2,2.5)	$\mathcal{T}$(1.5,2,2.5)
Channel thickness range (in cell)	$\mathcal{T}$(10,15,20)	$\mathcal{T}$(10,15,20)	$\mathcal{T}$(10,15,20)
Curvature weight	0.75	0.75	0.75
Asymmetry aspect ratio	0.5	0.5	0.5
Domain	Yes	Yes	Yes
Confinement weight	1	1	1
Well sedimentary data	No	No	Yes
Channel data weight	–	–	1
Channel data bandwidth (in cell)	–	–	30
Inter-channel data weight	–	–	1
Well connectivity data	No	No	No
Sand proportion cube	No	Yes	Yes
Sand proportion weight	–	1	1

Table B.4 Rules used to simulate channels with a bend length l_B from a distribution F_{l_B} and a curvature from a distribution F_c. l_d is the channel Default segment length, l_C the wanted channel length, l_c the current channel length, l_s and l_o are the distance between two channel sections, n_{s_u} are numbers of channel elements, α is the angle between two channel sections and o is the branch orientation, equal to 1 if the channel follow the global direction, -1 if the branch follow the opposite direction.

Global parameters: $l_d, l_C, F_{l_B}, F_c, l_c = 0, l_B = 0, i = 1, n_{s_o} = 0$

ω	:		T_0						
p_1	:		T_0	$\{l_B = draw(F_{l_B})\}$	: $l_c + l_B \leq l_C$	$\{n_s = \lceil l_B/l_d \rceil;$ $n_{s_1} = udraw(1, n_s - 1);$ $n_{s_2} = n_s - n_{s_1};$ $l_s = l_B/n_s\}$	$\xrightarrow{0.5}$	$[+C\{+C\}^{n_{s_1}-1}T_1] + (180) - C\{-C\}^{n_{s_2}}T_1$	Initialization
p_2	:		T_0	$\{l_B = draw(F_{l_B})\}$	: $l_c + l_B \leq l_C$	$\{n_s = \lceil l_B/l_d \rceil;$ $n_{s_1} = udraw(1, n_s - 1);$ $n_{s_2} = n_s - n_{s_1};$ $l_s = l_B/n_s\}$	$\xrightarrow{0.5}$	$[-C\{-C\}^{n_{s_1}-1}T_1] + (180) + C\{+C\}^{n_{s_2}}T_1$	
p_3	: $-C$	$<$ T_i		$\{l_B = draw(F_{l_B})\}$	: $l_c + l_B \leq l_C$	$\{n_s = \lceil l_B/l_d \rceil;$ $l_s = l_B/n_s\}$	$\longrightarrow$	$+C\{+C\}^{n_s-1}T_{i+1}$	Development
p_4	: $+C$	$<$ T_i		$\{l_B = draw(F_{l_B})\}$	: $l_c + l_B \leq l_C$	$\{n_s = \lceil l_B/l_d \rceil;$ $l_s = l_B/n_s\}$	$\longrightarrow$	$-C\{-C\}^{n_s-1}T_{i+1}$	
p_5	: $-C$	$<$ T_i			: $l_c + l_B > l_C$	$\{l_B = l_C - l_c;$ $n_s = \lceil l_B/l_d \rceil;$ $n_{s_n} = i \times udraw(0, n_s) + n_{s_o};$ $l_s = l_B/n_s\}$	$\longrightarrow$	$+C\{+C\}^{n_{s_n}-1}$ $\{n_{s_o} = n_s - n_{s_n};\ i = 0\}$	Closure
p_6	: $+C$	$<$ T_i			: $l_c + l_B > l_C$	$\{l_B = l_C - l_c;$ $n_s = \lceil l_B/l_d \rceil;$ $n_{s_n} = i \times udraw(0, n_s) + n_{s_o};$ $l_s = l_B/n_s\}$	$\longrightarrow$	$-C\{-C\}^{n_{s_n}-1}$ $\{n_{s_o} = n_s - n_{s_n};\ i = 0\}$	

Left context:	$p_1, p_2, p_3, p_4, p_5, p_6$	$\pm(\alpha, o, l_o, l_B)C(l_s, o, l_c)$
Successor	p_1, p_2	$\pm(draw(F_c) \times l_s \frac{180}{\pi} \times (\frac{n_s}{2} - n_{s_1} + 1), 1, l_s, l_B)C(l_s, 1, l_c + s)\{\pm(draw(F_c) \times l_s \frac{180}{\pi} \times (\frac{n_s}{2} - n_{s_2}), -1, l_s, l_B)C(l_s, -1, l_c + s)\}$
Successor:	p_3, p_4, p_5, p_6	$\pm(draw(F_c) \times \frac{l_s + l_o}{2} \frac{180}{\pi}, o, l_s, l_B)C(l_s, o, l_c + s)\{\pm(draw(F_c) \times l_s \frac{180}{\pi}, o, l_s, l_B)C(l_s, o, l_c + s)\}$

End condition: $l_c \geq l_C$

Appendix C

Simulation parameters of chapter 4

Table C.1 Parameters used to simulate the channels of figure 4.2. $\mathcal{T}$ is a triangular distribution with a minimum, a mode and a maximum. $\mathcal{U}$ is a uniform distribution with a minimum and a maximum.

Simulation parameters	**Straight channel**	**Sinuous channel**
Global direction (in °)	90	90
Global direction weight	0.25	0.25
Default segment length (in m)	50	50
Channel length (in m)	$\mathcal{U}(6\,000,6\,500)$	$\mathcal{U}(10\,000,10\,500)$
Bend length (in m)	$\mathcal{U}(150,500)$	$\mathcal{U}(150,500)$
Curvature (in m^{-1})	$\mathcal{T}(0,0.001,0.005)$	$\mathcal{T}(0,0.001,0.025)$
L-system weight	1	1
Channel self-repulsion weight	0	0
Channel width (in m)	80	80
Channel thickness (in m)	5	5
Asymmetry aspect ratio	0.5	0.5

Table C.2 Parameters used to simulate the SGS-based migrations in the simple cases. $\mathcal{T}$ is a triangular distribution with a minimum, a mode and a maximum. $\mathcal{U}$ is a uniform distribution with a minimum and a maximum.

Simulation parameters	Forward migration	Backward migration
Initial channel and avulsions		
Global direction (in °)	90	90
Global direction weight	0.05	0.2
Default segment length (in m)	100	100
Channel length (in m)	30 000	35 000
Bend length (in m)	$\mathcal{T}$(500,1 000,2 000)	$\mathcal{U}$(500,1 500)
Curvature (in m^{-1})	$\mathcal{T}$(0,0.0001,0.0003)	$\mathcal{T}$(0,0.002,0.007)
L-system weight	1	1
Channel self-repulsion weight	0	0
Channel width (in m)	$\mathcal{T}$(150,200,250)	$\mathcal{T}$(150,200,250)
Channel width range (in m)	$\mathcal{T}$(2 000,3 000,5 000)	$\mathcal{T}$(2 000,3 000,5 000)
Curvature weight	0.75	0.75
Channel thickness (in m)	$\mathcal{T}$(15,20,25)	$\mathcal{T}$(15,20,25)
Channel thickness range (in m)	$\mathcal{T}$(2 000,3 000,5 000)	$\mathcal{T}$(2 000,3 000,5 000)
Curvature weight	0.75	0.75
Asymmetry aspect ratio	0.5	0.5
Migrated channels		
Number of migration steps	29	29
Aggradation factor	$\mathcal{U}$(5,10)	$\mathcal{U}$(-10,-5)
Migration curvature weight	0.75	-0.75
Migration factor	$\mathcal{U}$(-75,75)	$\mathcal{U}$(-75,75)
Migration range (in m)	3 000	3 000
Abrupt migration probability	0.001	0.001
Abrupt migration length (in m)	$\mathcal{T}$(5 000,6 000,8 000)	$\mathcal{T}$(5 000,6 000,8 000)
Abrupt migration curvature weight	-0.25	0.25
Abrupt migration factor	$\mathcal{U}$(-400,400)	$\mathcal{U}$(-400,400)
Abrupt migration range (in m)	4 000	4 000
Regional avulsion probability	0.0007	0.0007

Table C.3 Parameters used to simulate the MPS-based migrations in the simple cases. $\mathcal{T}$ is a triangular distribution with a minimum, a mode and a maximum. $\mathcal{U}$ is a uniform distribution with a minimum and a maximum.

Simulation parameters	**Training set**	**Realization**
Initial channel and avulsions		
Global direction (in °)	90	90
Global direction weight	0.05	0.05
Default segment length (in m)	100	100
Channel length (in m)	30 000	30 000
Bend length (in m)	$\mathcal{T}$(500,1 000,2 000)	$\mathcal{T}$(500,1 000,2 000)
Curvature (in m^{-1})	$\mathcal{T}$(0,0.0001,0.0003)	$\mathcal{T}$(0,0.0001,0.0003)
L-system weight	1	1
Channel self-repulsion weight	0	0
Channel width (in m)	$\mathcal{T}$(150,200,250)	$\mathcal{T}$(150,200,250)
Channel width range (in m)	$\mathcal{T}$(2 000,3 000,5 000)	$\mathcal{T}$(2 000,3 000,5 000)
Curvature weight	0.75	0.75
Channel thickness (in m)	$\mathcal{T}$(15,20,25)	$\mathcal{T}$(15,20,25)
Channel thickness range (in m)	$\mathcal{T}$(2 000,3 000,5 000)	$\mathcal{T}$(2 000,3 000,5 000)
Curvature weight	0.75	0.75
Asymmetry aspect ratio	0.5	0.5
Migrated channels (SGS)		
Number of migration steps	9	–
Aggradation factor	$\mathcal{U}$(5,10)	–
Migration curvature weight	0.75	–
Migration factor	$\mathcal{U}$(-75,75)	–
Migration range (in m)	3 000	–
Abrupt migration probability	0.1	–
Abrupt migration length (in m)	$\mathcal{T}$(5 000,6 000,8 000)	–
Abrupt migration curvature weight	-0.25	–
Abrupt migration factor	$\mathcal{U}$(-400,400)	–
Abrupt migration range (in m)	3 000	–
Regional avulsion probability	0	–
Migrated channels (MPS)		
Number of migration steps	–	9
Whole training set as training model	–	No
Maximum scan fraction	–	0.75
Maximum neighbor number	–	7
Migration factor acceptance threshold	–	0
Curvature factor acceptance threshold	–	0

Table C.4 Parameters used to simulate the organized stacking realizations. $\mathcal{T}$ is a triangular distribution with a minimum, a mode and a maximum. $\mathcal{U}$ is a uniform distribution with a minimum and a maximum.

Simulation parameters	**First phase**	**Second phase**
Initial channel and avulsions		
Initial location (in cell)	$150, -, 8$	–
Global direction (in °)	90	–
Global direction weight	0.25	–
Default segment length (in cell)	6	–
Channel length (in cell)	450	–
Bend half-wavelength (in cell)	$\mathcal{T}$(15,20,30)	–
Amplitude (in cell)	$\mathcal{T}$(0,0.5,1)	–
Deviation angle (in °)	$\mathcal{T}$(0,0.57,5.7)	–
L-system weight	1	–
Channel self-repulsion weight	0	–
Channel width (in cell)	$\mathcal{T}$(5,6,8)	–
Channel width range (in cell)	$\mathcal{T}$(10,15,20)	–
Curvature weight	0.75	–
Channel thickness (in cell)	$\mathcal{T}$(1.5,2,2.5)	–
Channel thickness range (in cell)	$\mathcal{T}$(10,15,20)	–
Curvature weight	0.75	–
Asymmetry aspect ratio	0.5	–
Migrated channels		
Number of migration steps	27	12
Aggradation factor	$\mathcal{T}$(0,0.5,1)	$\mathcal{T}$(1.25,1.65,2)
Migration curvature weight	0.75	0.95
Migration factor	$\mathcal{U}$(-3,3)	$\mathcal{U}$(-0.5,0.5)
Migration range (in cell)	50	50
Abrupt migration probability	0.2	0
Abrupt migration length (in cell)	$\mathcal{T}$(60,70,80)	–
Abrupt migration curvature weight	0.75	–
Abrupt migration factor	$\mathcal{U}$(-8,8)	–
Abrupt migration range (in cell)	70	–
Regional avulsion probability	0	0

Appendix D

Karst network simulation with L-systems

Context The following proceeding article comes from the master project of Pierre Anquez, supervised during the thesis work. The project purpose was to apply the Lindenmayer system to the stochastic simulation of karst networks. It led to the definition of L-system rules integrated in a process to simulate branchwork to anastomotic karst networks.

P. Anquez, G. Rongier, P. Collon (2015) *Stochastic simulations of karst networks with Lindenmayer systems*, 35th Gocad Meeting, Nancy, France

Stochastic simulations of karst networks with Lindenmayer systems

Pierre Anquez[1], Guillaume Rongier[1,2], and Pauline Collon[1]

[1] *GeoRessources - RING, Université de Lorraine - ENSG / CNRS /CREGU. ENSG, 2 rue du Doyen Marcel Roubault, F-54518, Vandoeuvre-lès-Nancy, France*

[2] *Centre d'Hydrogéologie et de Géothermie, Université de Neuchâtel, 11 rue Emile-Argand, 2000 Neuchâtel, Switzerland*

pierre.anquez3@etu.univ-lorraine.fr ; guillaume.rongier@univ-lorraine.fr ; pauline.collon@univ-lorraine.fr

September 2015

Abstract

Some major hydrocarbon reservoirs are contained within paleokarsts and are influenced by the highly complex network geometries of the past karstic conduits. Those geometries are most of the time unknown and numerical simulations allow to better assess the uncertainty associated to those reservoirs. Several methods have been developed to simulate karstic systems but they mainly focus on branchwork karst networks. Anastomotic patterns are also observed in a significant proportion of karstic networks. Their singular connectivity implies a different response in the oil extraction process, and, thus, needs to be considered. This paper introduces a new object-based method to stochastically simulate karst networks with both branchwork and anastomotic patterns. Based on the Lindenmayer system (L-system), this method is composed of two steps. First, an intermediate karst network with only branchwork pattern is simulated. In a second time, some conduits are reconnected one by one on other conduits of the intermediate network. The very first results are two dimensional karst networks composed of some branching parts and anastomoses. This object-based method allows to generate several models reproducing the particular connectivity of complex karst networks mixing different patterns. Uncontrolled intersections between conduits sometimes appear. They could besides be limited by introducing a repulsion between the conduits. This work gives a basis for the simulation of 2.5D karst networks with possible integration of hard and soft data.

Introduction

Karstic systems are underground networks deeply related to fluid circulation as they result from the dissolution of carbonated rocks by groundwater. Some of them later constitute important hydrocarbon reservoirs. For instance, the Tarim basin and its Ordivician limestone and dolostone account for the fifth of the Chinese hydrocarbon resources [Zeng et al., 2011]. Karst development leads to very complex heterogeneities at various scales, with a huge impact on fluid flows. Predicting these heterogeneities is quite challenging but necessary to better characterize karstified reservoirs.

In order to study the flows in karstic systems, numerical models are a valuable support. Many information about karsts can be drawn from speleologist explorations. However speleology is limited to conduits that are accessible to humans: some parts of the networks can not be explored, for instance because of small or collapsed conduits. In case of shallow karsts or paleo-karsts, speleology is impossible. It leads to a lack of information which can be partially overcome with wells and seismic data. Stochastic simulations are a way to fill the remaining gaps and to better assess the uncertainties in the unexplored parts of the karst networks.

There are different approaches for karst network simulations which could be gathered in three groups:

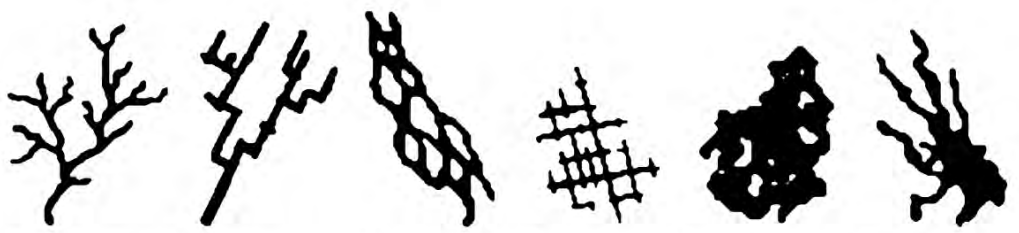

Figure 1: *Classification of patterns found in karstic networks (modified from [Palmer, 2002]).*

- *Genetic methods* compose the first group. They try to reproduce physical and chemical processes that lead to the formation of karst systems. Unfortunately those methods need long run-time and numerous parameters sometimes uneasy to define. Most of them are deterministic methods [e.g., Siemers and Dreybrodt, 1998, Bauer et al., 2000, Kaufmann and Braun, 2000], and are hard, if not impossible, to condition with available data.

- *Object-based methods* aim to describe the karst network morphology at a given time, without considering the processes at the origin of the network geometry [e.g., Pardo-Igúzquiza et al., 2012, Barthélemy and Collon-Drouaillet, 2013]. An advantage of object-based methods is the possibility to explore the uncertainties considering the data.

- *Pseudo-genetic methods* are the intersection of the previous groups: they try to preserve the strengths of both genetic and object-based methods. These methods use several models of karst morphology and karst evolution. They are based on a set of simple assumptions of the karstification physical processes that they try to honor [e.g., Jaquet et al., 2004, Borghi et al., 2012, Collon-Drouaillet et al., 2012]. They can also often take data into account in the simulation process, although this aspect remains quite limited.

To assess the heterogeneities and their impact on flow, the study of karst network connectivity at the largest scale is necessary. Palmer's classification [Palmer, 2002], based on a study on the connectivity and geometry of several karst networks, can be a source of inspiration. This classification ranges karst networks depending on recurrent patterns that can be related to speleogenetical processes (Figure 1).

A huge part of karst network simulation methods have been developed to reproduce the geometry of branchwork karsts. The anastomotic maze pattern has particular geometries composed of loops and reconnections between conduits that strongly influence fluid flows. But only few methods are able to simulate this kind of pattern [e.g., Jaquet et al., 2004, Barthélemy and Collon-Drouaillet, 2013]. Moreover, Palmer's classification remains general and a single karst network is often a mix of the various patterns. It is thus important to integrate the possibility of loop generations in a karst simulation worflow.

Lindenmayer systems, also known as L-system [Lindenmayer, 1968], are a formal grammar which consists in string rewriting from an initial string and rewriting rules. Each character of the final string can then be interpreted geometrically to obtain a simulated object. The L-system formalism has been extensively developed through the years. It is so possible to generate different final strings from a given set of rules and thus to simulate multiple objects from the same L-system.

This work is dedicated to stochastically simulate karst networks with a new object-based method based on L-systems. Different rules have been defined to simulate karst networks mixing branchwork and anastomotic patterns. This method gives multiple stochastic realisations while respecting the global topology of such networks.

1 L-system principles

A L-system is a formal grammar system based on string rewriting. A string is composed of characters, which could be letters or symbols. The set of characters used in a L-system is called the alphabet. The string can then be interpreted geometrically.

A L-system is so composed of four elements [Prezemyslaw and Lindenmayer, 1996]:

- An alphabet of characters (Table 1);
- An initial string, the axiom ω, with which the L-system starts;
- A set of production rules ($p_i, i \in [1, n]$, n being the number of rules), which are the rewriting rules of a *predecessor* by a *successor*;
- An order, the number of iterations, in other words the number of rewriting of the whole string.

1.1 Basic L-systems [Lindenmayer, 1968]

In the simplest L-systems, the production rules are only made of a predecessor and a successor:

$$predecessor \longrightarrow successor$$

For each production step i, each character is read and compared with the predecessors of the production rules. If the character matches a predecessor, it is replaced by the corresponding successor. If the current character does not match any predecessor in the production rules, the character is simply copied in the next string. For example, if a L-system is defined by the following axiom and production rules:

$$\begin{array}{lcl} \omega & : & b \\ p_1 & : & a \longrightarrow abc \\ p_2 & : & b \longrightarrow a \end{array}$$

The results for an order equal to five is:

$$\begin{array}{lcl} 0 & : & b \\ 1 & : & a \\ 2 & : & abc \\ 3 & : & abcac \\ 4 & : & abcacabcc \\ 5 & : & abcacabccabcacc \end{array}$$

These basic principles are the most simple formalism of L-system. Due to the great flexibility of this formalism, more complex rules have been added and so expand the L-system possibilities.

1.2 Geometrical interpretation of strings

The geometrical interpretation is the transcription of generated L-system strings into an image, a graph or an object. Each character of the string corresponds to a geometrical action (Table 1). Several geometrical interpretations exist but the most often used is the *turtle interpretation* [Prezemyslaw and Lindenmayer, 1996].

The principle is to translate the L-system final string, character after character, by a turtle advance. The final string is the string obtained when the number of rewriting steps are equal to the order. The turtle is represented by three unit orthogonal vectors, $\vec{H}$, $\vec{L}$ and $\vec{U}$, corresponding respectively to the direction of the turtle head, the direction of its left and the upward direction. These three vectors are updated during string interpretation.

The turtle can make two kinds of movements: turning of a given angle α around one of the three axis determined by $\vec{H}$, $\vec{L}$ and $\vec{U}$, or moving forward of a given length l_{Ci} in the direction to the

Table 1: *Classical geometrical interpretation of L-system characters*

Symbols	**Geometrical interpretation**
F	Move forward of a given length, draw a segment
f	Move forward on a given length without drawing a segment
+	Turn left by a given angle around the vector $\vec{U}$
-	Turn right by a given angle around the vector $\vec{U}$
[	Start a branch and save the position and state of the turtle
]	End a branch and replace the turtle in the latest saved position

head vector $\vec{H}$. Interpreting a L-system string consists of a suite of actions based on movements and motionless rotations (Table 1).

1.3 Stochastic L-systems

Basic L-systems are deterministic: at a given order, the resulting string of a given system is always the same. There are two ways to give stochastic results from a single L-system definition:

- By randomizing the geometrical interpretation of the final string. Only the geometry will vary, the topology remains the same.
- By defining several production rules for the same predecessor and associating a probability of application to each. Both the geometry and the topology of the final object will vary.

In the following example, when the character a is read in the string, its probability to be rewritten with abc is 75 % and its probability to be rewritten with bbb is 25 %.

$$\begin{array}{lcll} \omega & : & b & \\ p_1 & : & a & \overset{0.75}{\longrightarrow} \quad abc \\ p_2 & : & a & \overset{0.25}{\longrightarrow} \quad bbb \\ p_3 & : & b & \longrightarrow \quad a \end{array}$$

1.4 Parametric L-systems

It is possible to affect one or more parameters to a character. Parameters could be used in two different ways:

- To define some needed values in the geometrical interpretation, particularly the length of each drawn segment and the angle between two successive segments;
- To condition the application of production rules. A rule is only applied if all the conditions concerning the parameters are valid.

In the following parametric L-system, validating the condition in the production rule p_2 is necessary to apply the rule:

$$\begin{array}{lcllll} h = 0 & & & & & \\ \omega & : & b(h) & & & \\ p_1 & : & a & & \longrightarrow & ab(h+0.1) \\ p_2 & : & b(h) & : \quad h \leq 1 & \longrightarrow & a \end{array}$$

h is a global parameter, which means that it is never reset to 0 during the rewriting process. The rule p_2 is applied as long as h is lower or equal to 1. If an other production rule p_3 is defined with the

condition $h > 1$, the production rule p_2 is first applied until h reaches 1 and then the production rule p_3 is applied.

These two additional formalisms used together allow L-systems to simulate various forms and objects. Only few of the numerous L-system definitions and possibilities have been presented in this paper, for more details see Prezemyslaw and Lindenmayer [1996].

2 Karst network simulations using L-systems

We propose a new method for karst network simulation based on L-systems. Karst networks can be described by the geometry of conduits and their connections to each others. In our simulation, a conduit is the name given to a part of the karst network between two particular points, called nodes. Nodes are either bifurcation points, which are points where a conduit forks into two other conduits, or dead-end extremities. Each conduit is simulated by a succession of linear segments (Figure 2).

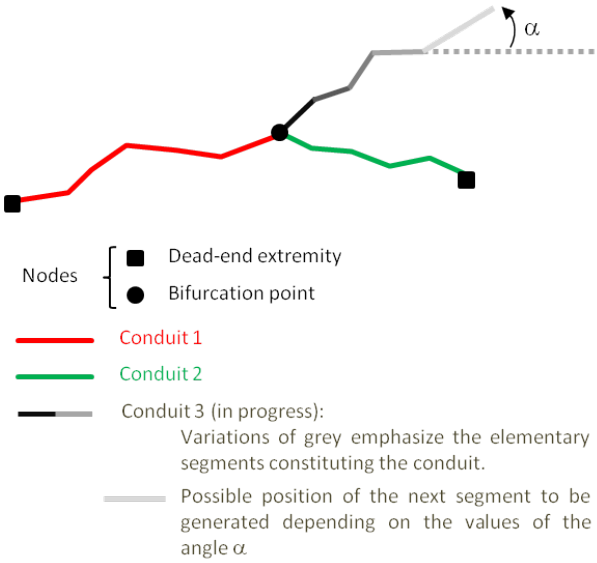

Figure 2: *Schema presenting the notions of conduits, elementary segments and nodes used for the simulation.*

If L-systems are well adaptable to rectilinear and branching objects, the formalisms presented above are not adapted to anastomotic shapes. Lindenmayer [1987] introduced another L-system formalism based on map [Nakamura et al., 1986] to simulate plant cellular tissues. Unfortunately, this formalism is more difficult to adapt to stochastic simulations. Moreover, map L-systems simulate only cyclic structures, which is not fully compatible with the simulation of karst networks, which combine loops and branching curvilinear conduits.

The method presented in this paper combines the branching pattern of classical L-system with the attraction process defined by Rongier et al. [2014b] for the simulation of channel axes. It has been coded in C++ in the ConnectO plugin of Gocad.

2.1 Input parameters

To enable some flexibility in the simulation process, several parameters are let to the user's control (Table 2). The karst outlet position $O(x, y, z)$ is the start of the simulation process, which makes the

network growths to the inlets. A global direction $\vec{d}$ controls the global orientation of the network. It is the opposite of the direction of karst natural development.

Table 2: *Input parameters for karst network simulation*

Symbols	**Parameters**
N	Number of simulations
$O(x, y, z)$	Coordinates of the karst outlet
$\vec{d}$	Global orientation of karstic network (from outlet to inlets)
L_C	Conduit lengths (probability distribution)
l_s	Elementary segment length
α	Angles between elementary segments (probability distribution)
n_l	Maximal number of loops

Conduit lengths L_C, elementary segment lengths l_s and angles between the elementary segments α provide a control on the geometry of the resulting network. Conduit lengths and angles between segments are drawn in probability distributions in order to introduce stochasticity in the resulting geometries.

Finally, the topology of the network is smoothly controlled by the parameter n_l which is the maximal number of loops that can be generated.

2.2 L-system alphabet for karst network simulation

Karst network simulation needs the definition of a L-system, with axiom, production rules and also a specific alphabet. This L-system must simulate the different karstic structures, that is to say conduits, bifurcations (points where a conduit is divided into two conduits) and dead-end passages. All of these structures are represented by symbols in the L-system alphabet; only loops can not be directly symbolized in the alphabet. Table 3 summarizes the alphabet used for karst simulations. Thus, in the L-system formalism, a conduit is a succession of modules $\{+C\}$ or $\{-C\}$, i.e. a succession of elementary segments with a rotation clockwise or counter-clockwise between each of them (Figure 2). This rotation is independent of the previous rotations and leads to various conduit geometries.

Table 3: *L-system alphabet and corresponding geometrical interpretation for karst network simulations*

Symbols	**Geometrical interpretation**
C	Move forward of a length l_s, draw a segment
T	Do nothing (represents an on-going conduit extremity)
D	Do nothing (represents a dead-end passage extremity)
W	Do nothing (represents a waiting conduit extremity)
M	Draw a segment between the previous position and the attraction point (to close loop)
$+$	Turn left by an angle α around the vector $\vec{U}$
$-$	Turn right by an angle α around the vector $\vec{U}$
[	Start a new conduit and save the position and state of the turtle
]	End the conduit and replace the turtle in the latest saved position

2.3 Simulation process

The simulation method we propose is performed in two steps. The first step consists in the simulation of an initial network with a branchwork architecture. The second step generates additional loops corresponding to the anastomotic pattern.

2.3.1 Simulation of an initial branchwork pattern network

The L-system defined for an initial branchwork network simulation uses an axiom ω and seven production rules p_1 to p_7. It is a parametric L-system (section 1.4), thus, in addition to the input parameters provided by the user (section 2.1), internal variables are used. They regroup global variables:

- n, the number of conduits that are finished, in progress or waiting;
- w, the number of waiting conduits;
- t, the number of in progress conduits, in other words the number of modules T in the whole L-system string;
- a, the number of loops (anastomoses) already simulated in the karst network ($a \leq n_l$);

and variables depending on the conduit being proceeded, used to condition the application of production rules ($T(i, l_{Ci}, L_{Ci}, e_i)$) :

- i, the index of the conduit being proceeded;
- l_{Ci}, the current length of conduit i, in other words the sum of length of already simulated segments for the conduit i;
- L_{Ci}, the conduit length to reach for stopping its growth ($l_{Ci} \leq L_{Ci}$); L_{Ci} is randomly drawn at the creation of the conduit in the probability distribution of L_C given by the user;
- e_i, an indicator of the kind of conduit extremity for the conduit i (bifurcation or dead-end passage).

L-system starts with the following axiom ω:

$$\omega \quad : \quad T(1, 0, L_{C1}, 1)$$

When there is only one conduit in progress ($t = 1$), two L-system production rules allow the growth of a conduit while the in progress length l_{Ci} is lower than the length to reach L_{Ci} :

$$\begin{array}{lcccccl} p_1 & : & T(i, l_{Ci}, L_{Ci}, e_i) & : & l_{Ci} < L_{Ci},\, t = 1 & \xrightarrow{0.5} & \{+C\}(i, l_{Ci} + l_s, L_{Ci}, rand(\alpha))T(i, l_{Ci}, L_{Ci}, e_i) \\ p_2 & : & T(i, l_{Ci}, L_{Ci}, e_i) & : & l_{Ci} < L_{Ci},\, t = 1 & \xrightarrow{0.5} & \{-C\}(i, l_{Ci} + l_s, L_{Ci}, rand(\alpha))T(i, l_{Ci}, L_{Ci}, e_i) \end{array}$$

Each addition of a segment increments the conduit length l_{Ci} by a value l_s and is followed by a rotation towards left (if module is $\{+C\}$) or right (if module is $\{-C\}$) by an angle $rand(\alpha)$ randomly drawn in the angle distribution α provided by the user. When the cumulated length l_{Ci} becomes higher than the length L_{Ci}, the conduit ends with either a bifurcation or a dead-end extremity. The choice between these two possibilities depends on the value of the parameter e_i of the last module T of the conduit (drawn in $]0, 1]$), by comparing it with the real number E defined as follows:

$$E = \begin{cases} 1 - exp\Big(- \dfrac{w}{n_l}(t-1)\Big) & if n_l > 1 \\ 1 - exp\Big(- (t-1)\Big) & otherwise \end{cases}$$

If e_i is lower than or equal to E the extremity of the conduit is a dead-end passage; on the contrary, if e_i is higher than E, the extremity is a bifurcation, beginning two new conduits. If $t = 1$, we want to exclude a dead-end passage, thus E will be equal to 0 and guarantee $e_i > E$. The ratio $\dfrac{w}{n_l}$ favours bifurcation appearance for low values of w (in that case E is closer to 0 than 1). E increases as bifurcations appear and gets closer to 1, favouring dead-end passages. This allows to approach

the wished value of loops. If n_l is equal to 0 (pure branchwork network), then bifurcation appears randomly. The production rules p_3 and p_4 express these operations:

$$
\begin{array}{lcccl}
p_3 & : & T(i, l_{Ci}, L_{Ci}, e_i) & : & l_{Ci} \geq L_{Ci},\ e_i \leq E \longrightarrow D \\
p_4 & : & T(i, l_{Ci}, L_{Ci}, e_i) & : & l_{Ci} \geq L_{Ci},\ e_i > E \longrightarrow -[\{-C\}(i, l_s, L_{Cn+1} = rand(L_C), rand[0,60]) \\
 & & & & \quad T(n+1, 0, L_{Cn+1}, rand]0,1])] \\
 & & & & \quad +[\{+C\}(i, l_s, L_{Cn+2} = rand(L_C), rand[0,60]) \\
 & & & & \quad T(n+2, 0, L_{Cn+2}, rand]0,1])]
\end{array}
$$

The application of these rules updates global parameters accordingly. If rule p_3 is applied, a conduit in progress is stopped, so t is decreased by one. If rule p_4 is applied, a conduit in progress is ended but two new conduits are in progress so t is increased by one.

In the rule p_4, the modules $+$ and $-$ represent the angles between conduit as shown in Figure 3. These angles, between the straight line bore by the last segment of the conduit coming to the bifurcation and the first segment of the conduits coming from the bifurcation, are drawn between 0 and 60 degrees. The distribution of angles given by the user is not used here in order to force the two conduits to drift away from each others. The parameters L_{Cn+1},L_{Cn+2} and e_{n+1}, e_{n+2} are randomly drawn for each new conduit: parameter L_{Ci} is drawn in the distribution of conduits lengths L_C and parameter e_i is drawn in $]0, 1]$.

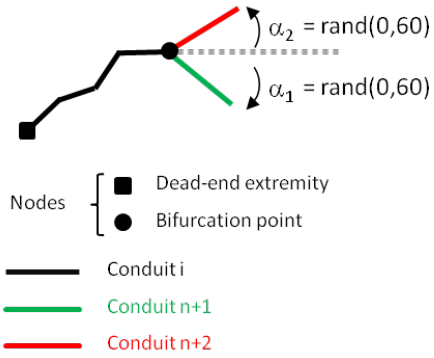

Figure 3: *At a bifurcation point, angles α_1 and α_2 are the angles between the dashed straight line and the first segment of the new conduits. α_1 and α_2 are randomly drawn between 0 and 60 degrees.*

In order to prepare the second step, which consists in generating loops, some conduits must be on standby, in other words, put in a *waiting* status. These waiting conduits, which will be the seeds of loops in the final karst network, are chosen stochastically by the apparitions of the module W as a successor of the module T. Module W apparitions need to have at least two conduits in progress, otherwise there is no remaining conduit in progress and the karst network simulation is over. Thus, p_5, p_6 and p_7 are only applied if $t > 1$. Note also that if $n_l = 0$ (pure branchwork), p_7 has a probability of 0 and p_1 and p_2 are applied independently of the value of t (the L-system is reduced to the fourth first rules).

$$
\begin{array}{lcccl}
p_5 & : & T(i, l_{Ci}, L_{Ci}, e_i) & : & l_{Ci} < L_{Ci},\ t > 1 \xrightarrow{0.48} \{+C\}(i, l_{Ci} + l_s, L_{Ci}, rand(\alpha))T(i, l_{Ci}, L_{Ci}, e_i) \\
p_6 & : & T(i, l_{Ci}, L_{Ci}, e_i) & : & l_{Ci} < L_{Ci},\ t > 1 \xrightarrow{0.48} \{-C\}(i, l_{Ci} + l_s, L_{Ci}, rand(\alpha))T(i, l_{Ci}, L_{Ci}, e_i) \\
p_7 & : & T(i, l_{Ci}, L_{Ci}, e_i) & : & l_{Ci} < L_{Ci},\ t > 1 \xrightarrow{0.04} W(i, l_{Ci}, L_{Ci}, 0)
\end{array}
$$

The rules p_5 and p_6 are almost the same as rules p_1 and p_2 described above: only the value of their application probabilities are different. If the rule p_7 is applied, the current conduit becomes a waiting

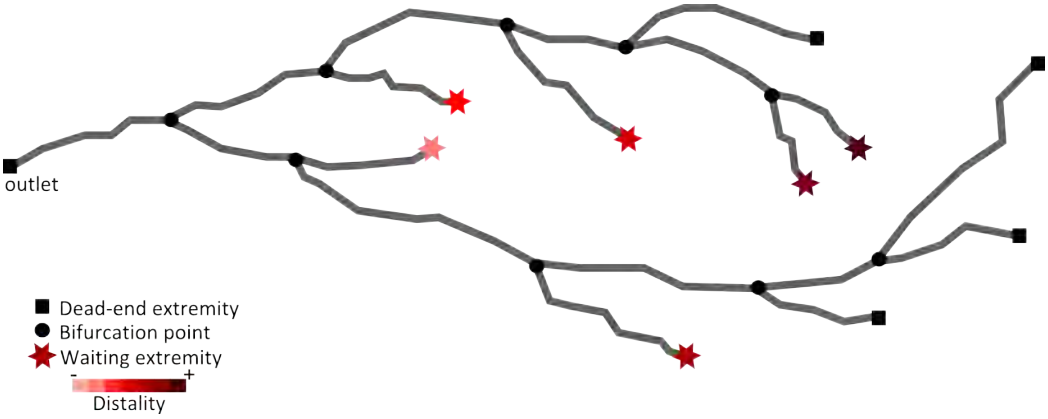

Figure 4: *A possible intermediate branchwork pattern network at the end of the first step. The* waiting *conduits are figured by stars.*

conduit because W is not replaced during the rewriting steps.

The application of rule p_7 updates two global parameters: it increases by one w, the number of waiting conduits, and it decreases by one t, the number of in progress conduits.

The seven production rules allow the simulation of an intermediate branchwork karst network with waiting conduits, which are necessary for loop simulations (Figure 4). The first step is stopped when no conduit remains in progress, i.e. when $t = 0$.

2.3.2 Simulation of loops by developing waiting conduits

The aim of this second step is to generate loops in the karst network. At the beginning of this step, the karst network has a curvilinear branchwork pattern with some waiting conduits (Figure 4). As the karstic network is simulated from outlet to inlets (in the opposite direction of natural karst development), each new conduit propagates oppositely to outlet. Thus, to avoid involuntary crossings, all the waiting extremities (points W symbolized by stars in Figure 4) are treated one by one from the most distal to the most proximal point W. The distality of a point W is defined by the scalar projection of the vector between W and the outlet onto a line along the vector of the global direction $\vec{d}$ defined by the user.

To build a loop, a point W is linked to an attraction point A representing the conduit extremity position at the end of the conduit growth. The waiting extremity is attracted towards the point A and the conduit growths until connection is achieved (Figure 5).

The main difficulty lies in the positioning of the attraction point A. In order to avoid *going back* conduits, only the network conduits that have at least one extremity with a distality higher than that of the point W are take into account (Figure 5a). Among these conduits, only those for whom the two segments between the point W and one of its two extremities do not intersect any other conduits are selected to bore the attraction point A (Figure 5b). This simplified test prevents a complete test of every elementary segments of the conduits and hence accelerates the process but it could leads to miss the detection of possible intersections. The point A is randomly chosen on one of those possible conduits (Figure 5b), i.e. in the L-system formalism, a module $\{\pm C\}$ is chosen and its geometrical position is used as attraction point.

Then, the corresponding W module in the L-system string is replaced by a T module. The global parameters are updated: w is decreased by one and t is increased by one. Consequently, the simulation of this conduit can restart. Attraction to point A follows the principle of hard data conditioning in channel simulation already developed with L-system [Rongier et al., 2014b]. Attraction is stopped when the distance between the extremity of the conduit and the point A is lower than the segment

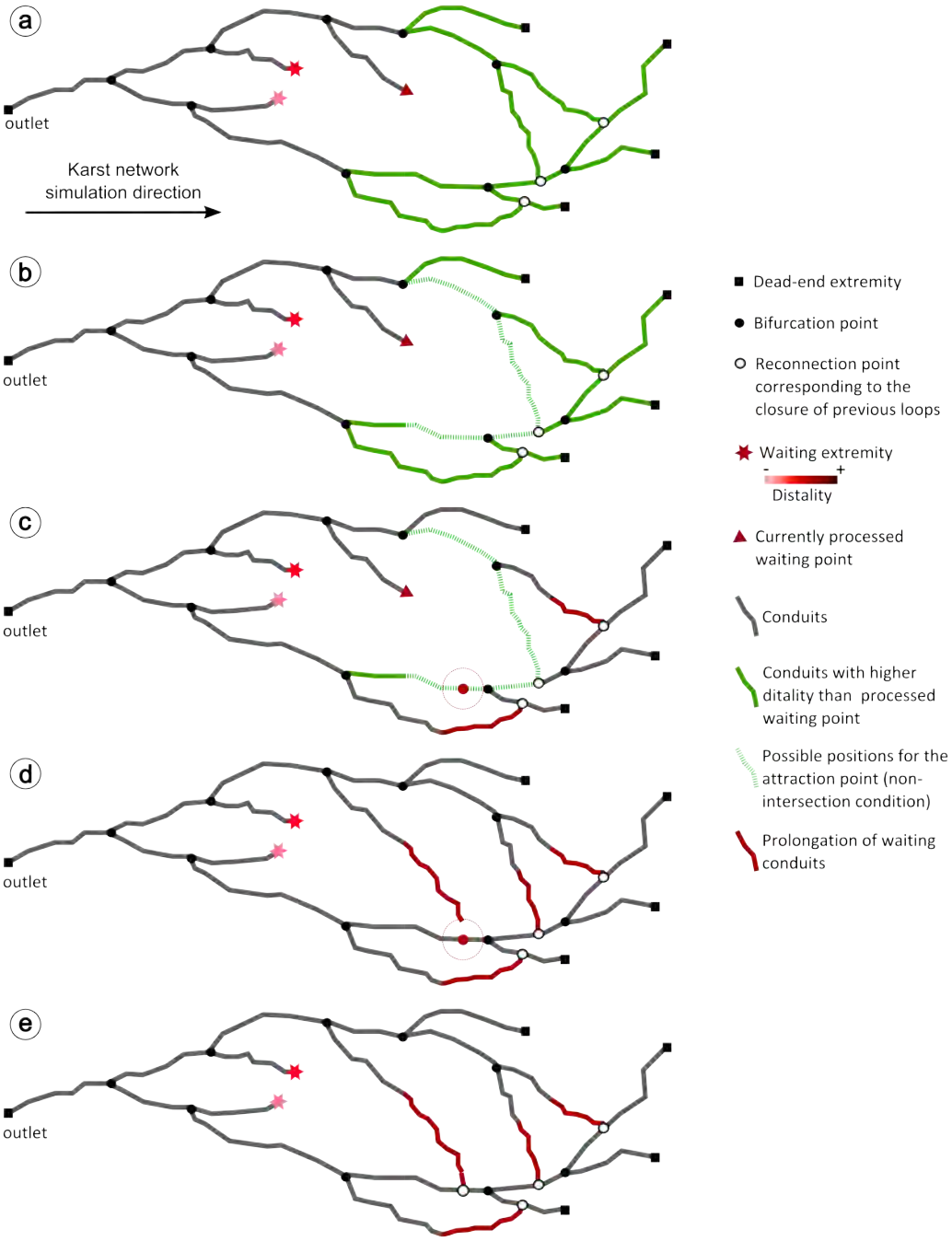

Figure 5: *Loop building. a: Selection of conduits of higher distality than currently processed waiting point. b: Selection of conduits that fulfil the simplified non-intersection condition. c: Random placement of the attraction point A. d: Growth of the processed conduit with hard data conditioning to point A until the conduit reaches the area of conditioning. e: Loop closure.*

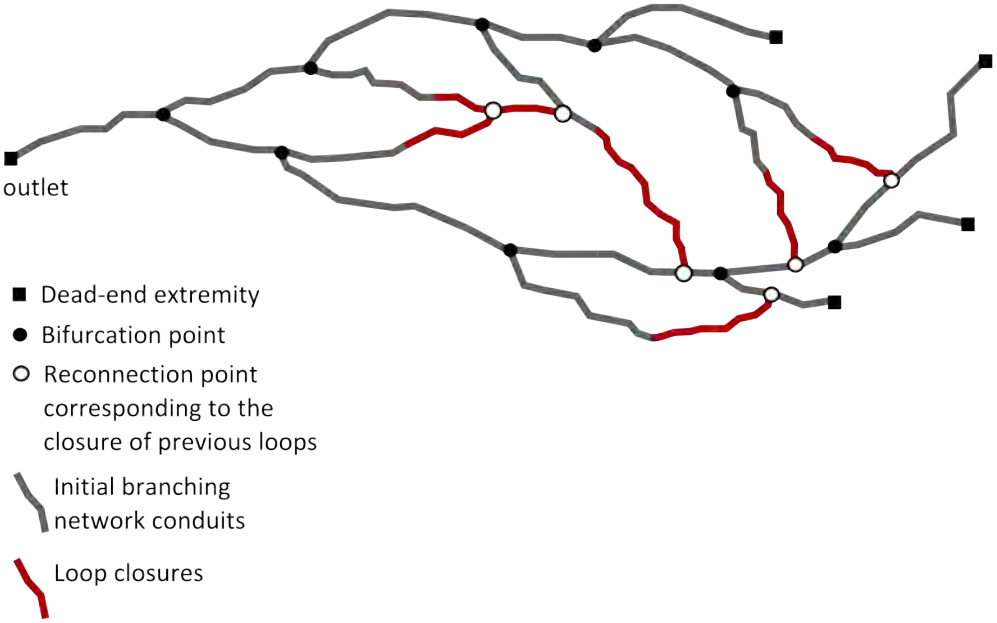

Figure 6: *Final karst network simulation with loops.*

length l_s (Figure 5c). A last segment is then traced between the extremity of the attracted conduit and point A by replacing the module T by a module M (Table 3), leading to the closure of the loop (Figure 5d).

When all the waiting conduits are treated, both parameters t and w are equal to 0. The simulation of the karst network is thus ended. The result is a karst network that can mix both branchwork and anastomotic patterns (Figure 6).

3 Results and discussion

Even if the method presented above is still at an early stage, interesting results can be shown (Figure 7). Several morphologies of karst networks have been generated. The simulated patterns stretch from pure branchwork karst networks (Figure 7a) to pure anastomotic networks (Figure 7c), with all the combinations between these two extreme poles (Figure 7, b1 and b2), as often encountered in nature [Jaquet et al., 2004].

Nevertheless, several problems appear and need improvements to be solved. In some simulations undesirable intersections between conduits are observable. Indeed, in the current state nothing prevent one conduit from growing towards another one, in particular during the first step of branchwork karst generation. Angles between conduit segments are determined by a combination of the global direction of karst simulation, a random draw in the angle distribution given by the user and the attraction vector in case of loop closure. Thus, the global direction of karst simulation does not favour crossing avoidance, as two conduits starting at the same bifurcation point will grow in the same direction without going away from each others. If it is desirable in the case of anastomoses, it generates overlapping shapes when pure branchwork patterns are wanted (Figure 8). Several solutions are currently worth considering: i) The global direction could be set perpendicular to its initial configuration just after a bifurcation, and then changed back to its initial state. ii) A repulsion constraint could be attached to existing conduits.

A second track of improvement obviously appears in the simulation parametrisation. Indeed, the

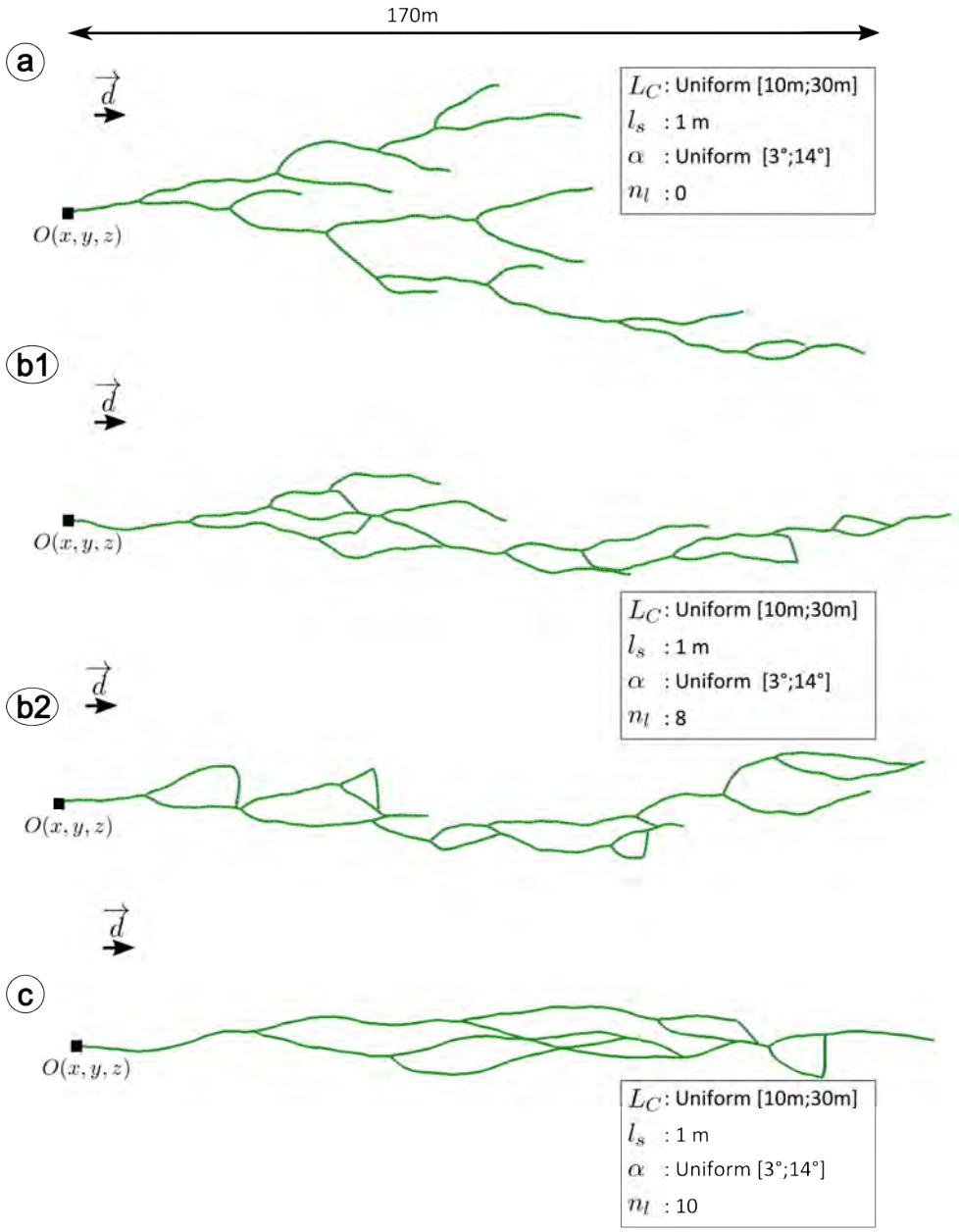

Figure 7: *Four examples of simulated networks. All the morphologies can be obtained from pure branchwork pattern network (a) to pure anastomotic pattern network (c) going through karst network composed of a combination of the two patterns (b1 and b2).*

maximal number of loops n_l alone is insufficient to clearly control the topology of the network. It would be appreciable to impose at least the total number of conduits in order to have something close to a ratio between the number of conduits and the number of loops. Howard's parameters [Howard,

Figure 8: *Karst network simulation showing uncontrollable intersections and overlappings. The grey spheres are located where the reconnections between conduits are controlled, and every conduits crossings without a sphere are uncontrolled. This uncontrollability leads sometimes to networks with bad shapes and geologic unlikelihood.*

1971] could also be used to control the global connectivity of the network [Vigouroux et al., 2010].

Finally, hard data and soft data conditioning should be incorporated in the simulator. Rongier et al. [2014b] have already integrated it in the generation of channel axis using L-systems. An adaptation is required for hard data, with a step to determine what conduit must condition a given data.

Conclusion and perspectives

This paper presents a new object-based method to simulate karst networks using L-system. The flexibility of this formalism gives the possibility to stochastically generate karst networks composed of a mix of branchwork and anastomotic patterns.

The methodology is based on the definition of a L-system that simulates the stochastic growth of branchwork conduits and on a second step of growing that uses attraction points to constrain conduits to form anastomoses. Encouraging realisations of karst networks have been obtained, going from pure branchwork patterns to pure anastomotic ones. But this work is still at an early stage and some realisations show involuntary intersections between two or more conduits. Several solutions are proposed to solve this problem and would be implemented in the near future. Improving the parametrisation of the simulation and integrating hard and soft data conditioning are also short term perspectives. The simulation of karst networks can be completed by the three dimensions modelling of conduit envelops using ODSIM (Object-Distance Simulation method) [Henrion et al., 2010, Rongier et al., 2014a].

In a long-term view, it would be interesting to adapt the L-system rules in order to simulate various patterns in a single karst network depending on the geological settings. Indeed, although the developed method is currently an object-based method, the flexibility of the L-system formalism leaves scope for the integration of a genetic dimension in the development of karst networks.

Acknowledgements

This work was performed in the frame of the RING project at Université de Lorraine. We would like to thank the industrial and academic sponsors of the Gocad Research Consortium managed by ASGA for their support. We also thank Paradigm for providing the SKUA-GOCAD software and API.

References

C. Barthélemy and P. Collon-Drouaillet. Simulation of anastomotic karst networks. In *Proc. 33rd Gocad Meeting, Nancy, France*, 2013.

S. Bauer, R. Liedl, and M. Sauter. Modelling of karst development considering conduit-matrix exchange flow. *IAHS PUBLICATION*, pages 10–15, 2000.

A. Borghi, P. Renard, and S. Jenni. A pseudo-genetic stochastic model to generate karstic networks. *Journal of Hydrology*, 414:516–529, 2012.

P. Collon-Drouaillet, V. Henrion, and J. Pellerin. An algorithm for 3d simulation of branchwork karst networks using horton parameters and A* application to a synthetic case. *Geological Society, London, Special Publications*, 370(1):295–306, 2012.

V. Henrion, G. Caumon, and N. Cherpeau. Odsim: an object-distance simulation method for conditioning complex natural structures. *Mathematical Geosciences*, 42(8):911–924, 2010.

A. D. Howard. Quantitative mesures of caves patterns. *Caves and Karst*, 13:7, 1971.

O. Jaquet, P. Siegel, G. Klubertanz, and H. Benabderrhamane. Stochastic discrete model of karstic networks. *Advances in Water Resources*, 27(7):751–760, July 2004. ISSN 03091708. doi: 10.1016/j.advwatres.2004.03.007.

G. Kaufmann and J. Braun. Karst aquifer evolution in fractured, porous rocks. *Water Resources Research*, 36(6):1381–1391, 2000. ISSN 1944-7973. doi: 10.1029/1999WR900356.

A. Lindenmayer. Mathematical models for cellular interactions in development i. filaments with one-sided inputs. *Journal of Theoretical Biology*, 18(3):280–299, Mar. 1968. ISSN 00225193. doi: 10.1016/0022-5193(68)90079-9.

A. Lindenmayer. An introduction to parallel map generating systems. In *Graph-grammars and their application to computer science*, pages 27–40. Springer, 1987.

A. Nakamura, A. Lindenmayer, and K. Aizawa. Some systems for map generation. In *The Book of L*, pages 323–332. Springer, 1986.

A. N. Palmer. Speleogenesis in carbonate rocks. *Evolution of karst: from prekarst to cessation. Postojna-Ljubljana: Zalozba ZRC*, pages 43–60, 2002.

E. Pardo-Igúzquiza, P. A. Dowd, C. Xu, and J. J. Durán-Valsero. Stochastic simulation of karst conduit networks. *Advances in Water Resources*, 35:141–150, 2012.

P. Prezemyslaw and A. Lindenmayer. The algorithmic beauty of plants, 1996.

G. Rongier, P. Collon-Drouaillet, and M. Filipponi. Simulation of 3d karst conduits with an object-distance based method integrating geological knowledge. *Geomorphology*, 217:152–164, 2014a.

G. Rongier, P. Collon-Drouaillet, and P. Renard. Channel axis simulation based on Lindenmayer systems. In *Proc. 34th Gocad Meeting, Nancy, France*, pages 1–27, 2014b.

J. Siemers and W. Dreybrodt. Early development of karst aquifers on percolation networks of fractures in limestone. *Water resources research*, 34(3):409–419, 1998.

R. Vigouroux, P. Collon-Drouaillet, and V. Henrion. New parameters for the characterization of karst geometry. In *Proceedings of th 30th Gocad Meeting, Nancy, France*, 2010.

H. Zeng, R. Loucks, X. Janson, G. Wang, Y. Xia, B. Yuan, and L. Xu. Three-dimensional seismic geomorphology and analysis of the ordovician paleokarst drainage system in the central tabei uplift, northern tarim basin, western china. *AAPG bulletin*, 95(12):2061–2083, 2011.

Appendix A L-system definition

Symbols	Parameters
	Input parameters for karst network simulation
N	Number of simulations
$O(x, y, z)$	Coordinates of the karst outlet
$\overrightarrow{d}$	Global orientation of karstic network (from outlet to inlets)
L_C	Conduit lengths (probability distribution)
l_s	Elementary segment length
α	Angles between elementary segments (probability distribution)
n_l	Maximal number of loops
	Global *internal* parameters
n	the number of conduits that are finished, in progress or waiting
w	the number of waiting conduits
t	the number of in progress conduits
a	the number of loops (anastomoses) already simulated in the karst network
	Variables depending on the conduit being proceeded
i	the index of the conduit being proceeded
l_{Ci}	the current length of conduit i
L_{Ci}	the conduit length to reach for stopping its growth
e_i	kind of conduit extremity for the conduit i (bifurcation or dead-end passage)

Global parameters values at the beginning: $n = 1, w = 0, t = 1, a = 0$

Symbols	Geometrical interpretation
C	Move forward of a length l_s, draw a segment
T	Do nothing (represents an on-going conduit extremity)
D	Do nothing (represents a dead-end passage extremity)
W	Do nothing (represents a waiting conduit extremity)
M	Draw a segment between the previous position and the attraction point (to close loop)
$+$	Turn left by an angle α around the vector $\vec{U}$
$-$	Turn right by an angle α around the vector $\vec{U}$
[	Start a new conduit and save the position and state of the turtle
]	End the conduit and replace the turtle in the latest saved position

Axiom: $\omega \quad : \quad T(1,0,L,1)$

Production rules:

$$
\begin{array}{lcccl}
p_1 & : & T(i,l_{Ci},L_{Ci},e_i) & : & l_{Ci} < L_{Ci},\ t = 1 \quad \xrightarrow{0.5} \quad \{+C\}(i,l_{Ci}+l_s,L_{Ci},rand(\alpha))T(i,l_{Ci},L_{Ci},e_i) \\
p_2 & : & T(i,l_{Ci},L_{Ci},e_i) & : & l_{Ci} < L_{Ci},\ t = 1 \quad \xrightarrow{0.5} \quad \{-C\}(i,l_{Ci}+l_s,L_{Ci},rand(\alpha))T(i,l_{Ci},L_{Ci},e_i) \\
p_3 & : & T(i,l_{Ci},L_{Ci},e_i) & : & l_{Ci} \geq L_{Ci},\ e_i \leq E \quad \longrightarrow \quad D \\
p_4 & : & T(i,l_{Ci},L_{Ci},e_i) & : & l_{Ci} \geq L_{Ci},\ e_i > E \quad \longrightarrow \quad -[\{-C\}(i,l_s,L_{Cn+1} = rand(L_C),rand[0,60]) \\
 & & & & \qquad T(n+1,0,L_{Cn+1},rand]0,1])] \\
 & & & & \quad +[\{+C\}(i,l_s,L_{Cn+2} = rand(L_C),rand[0,60]) \\
 & & & & \qquad T(n+2,0,L_{Cn+2},rand]0,1])] \\
p_5 & : & T(i,l_{Ci},L_{Ci},e_i) & : & l_{Ci} < L_{Ci},\ t > 1 \quad \xrightarrow{0.48} \quad \{+C\}(i,l_{Ci}+l_s,L_{Ci},rand(\alpha))T(i,l_{Ci},L_{Ci},e_i) \\
p_6 & : & T(i,l_{Ci},L_{Ci},e_i) & : & l_{Ci} < L_{Ci},\ t > 1 \quad \xrightarrow{0.48} \quad \{-C\}(i,l_{Ci}+l_s,L_{Ci},rand(\alpha))T(i,l_{Ci},L_{Ci},e_i) \\
p_7 & : & T(i,l_{Ci},L_{Ci},e_i) & : & l_{Ci} < L_{Ci},\ t > 1 \quad \xrightarrow{0.04} \quad W(i,l_{Ci},L_{Ci},0)
\end{array}
$$

with E defined as follows:

$$
E = \begin{cases} 1 - exp\Big(-\dfrac{w}{n_l}(t-1)\Big) & if n_l > 1 \\ 1 - exp\Big(-(t-1)\Big) & otherwise \end{cases}
$$

End conditions: $t = 0,\ w = 0$

Appendix E

Karst conduit simulation with e-ODSIM

Context The following article published in Geomorphology comes from the master work done under the supervision of Pauline Collon. The article itself was published during the thesis work. The project purpose was to stochastically simulate three-dimensional karst conduits. This method completes the network simulation method defined in the previous appendix, by simulating a conduit envelope around the network.

G. Rongier, P. Collon, M. Filipponi (2014) *Simulation of 3D karst conduits with an object-distance based method integrating geological knowledge*, Geomorphology 217, 152–164, DOI: 10.1016/j.geomorph.2014.04.024

Geomorphology 217 (2014) 152–164

Contents lists available at ScienceDirect

Geomorphology

journal homepage: www.elsevier.com/locate/geomorph

Simulation of 3D karst conduits with an object-distance based method integrating geological knowledge

Guillaume Rongier [a,*], Pauline Collon-Drouaillet [a], Marco Filipponi [b]

[a] GeoRessources UMR7359, Université de Lorraine, CNRS, CREGU, ENSG, 2 Rue du Doyen Marcel Roubault, TSA 70605, 54518 Vandœuvre-Lès-Nancy Cedex, France
[b] Bauen im Karst, Alte Spinnerei, CH-8877 Murg, Switzerland

ARTICLE INFO

Article history:
Received 4 July 2013
Received in revised form 2 April 2014
Accepted 22 April 2014
Available online 2 May 2014

Keywords:
Karst conduit
Shape
Stochastic simulation
Skeleton
Inception feature

ABSTRACT

Karst conduit shapes have a high influence on fluid flows. As these underground hidden systems are partially inaccessible, their stochastic simulation is an essential tool to assess the uncertainties related to these highly exploited water resources. The object-distance simulation method (ODSIM) is a hybrid dual-scale approach that has been recently proposed to model geological underground structures due to late processes such as dolomitized rocks, mineralized veins or karsts. Using a perturbed Euclidean distance field around a curve representing roughly the conduit centre and called a skeleton, the resulting shapes are globally cylindrical-like 3D envelopes. But at a drain scale, karstic conduits are elongated along weakness planes such as lithostratigraphic horizons, bedding planes, fractures or faults. In addition to those planes the influence of the water table is added. This work presents different improvements of ODSIM methodology for simulating more realistic shapes in the particular case of karst. Firstly, we propose using a custom distance field computed with a fast marching method. Considering the "velocity" field to be proportional to the permeability allows the resulting features to be elongated along the weakness planes. Secondly, to handle specific shapes due to the proximity of the water table, such as trenches or notches, we impose areas of higher velocity between the skeleton and the water table. Finally, we generate a custom random threshold with several variograms and/or distributions depending on the different features integrated in the "velocity" field. Applied on different models, it is shown that the resulting karst conduits have more realistic shapes than those obtained with the previous workflow, while the variability of structures which can be modelled with ODSIM is preserved.

1. Introduction

Karstic systems are underground hydrographic networks made of conduits and caves that have grown by dissolution of the surrounding rocks. They cover approximately 20% of the planet's dry ice-free land (e.g., Ford & Williams, 2007; De Waele et al., 2009) and are therefore important fluid reservoirs, providing water for probably 20 to 25% of the world's population (Ford & Williams, 2007). Development of caves is also responsible for substantial human and financial disasters by causing sinkholes in urbanized zones. These karst features can be dramatic as the surface land usually stays intact until there is insufficient support: the soil suddenly collapses, swallowing everything above (e.g., (Brinkmann et al., 2008; Frumkin et al., 2009; Parise et al., 2009)). Recent works have shown that karsts may also be a major source of paleoclimate records (e.g., Mongelli, 2002; Horvatinčić et al., 2003; Onac & Constantin, 2008; Kuo et al., 2011). Nowadays human activities are a major threat for karstic environments (e.g., De Waele et al., 2011), and furthermore climate changes may have a considerable impact on them in the future (e.g., Viles, 2003; Hartmann et al., 2012).

Despite the importance of karstic networks, their location and exact geometry remain poorly known, mainly due to the partial inaccessibility of these underground systems. These networks actually play a major role in the flow regime of most carbonate aquifers and reservoirs (e.g., Lü et al., 2008; Chaojun et al., 2010): their conduits act as preferential flow paths and concentrate the fluids. As conduit shapes result from a complex dissolution process (e.g., Ford & Williams, 2007), a straightforward modelling approach of fluid flows would represent karstic conduits as equivalent to cylindrical tubes. This approach does not take into account the shape variations like abrupt narrowings or enlargements which also greatly impact fluid flows (e.g., Field & Pinsky, 2000; Hauns et al., 2001; Goldscheider, 2008; Morales et al., 2010). Thus, knowing and modelling the shapes of these three-dimensional geological objects could be an important improvement for both water and oil and gas reservoir exploitation. The goal of this paper is to propose a tool to realize such three-dimensional modelling of karstic systems.

Two different contexts of application are examined. First, as large parts of cave systems are still unexplored, three-dimensional stochastic simulations offer a way to better assess the associated uncertainty. However, the current methods focus on the global architecture of the conduit networks (e.g., Borghi et al., 2012; Collon-Drouaillet et al.,

* Université de Lorraine - ENSG, 2 Rue du Doyen Marcel Roubault, TSA 70605, 54518 Vandœuvre-Lès-Nancy Cedex, France.
E-mail addresses: guillaume.rongier@gocad.org (G. Rongier), pauline.collon@univ-lorraine.fr (P. Collon-Drouaillet), marco.filipponi@bauen-im-karst.info (M. Filipponi).

http://dx.doi.org/10.1016/j.geomorph.2014.04.024
0169-555X/

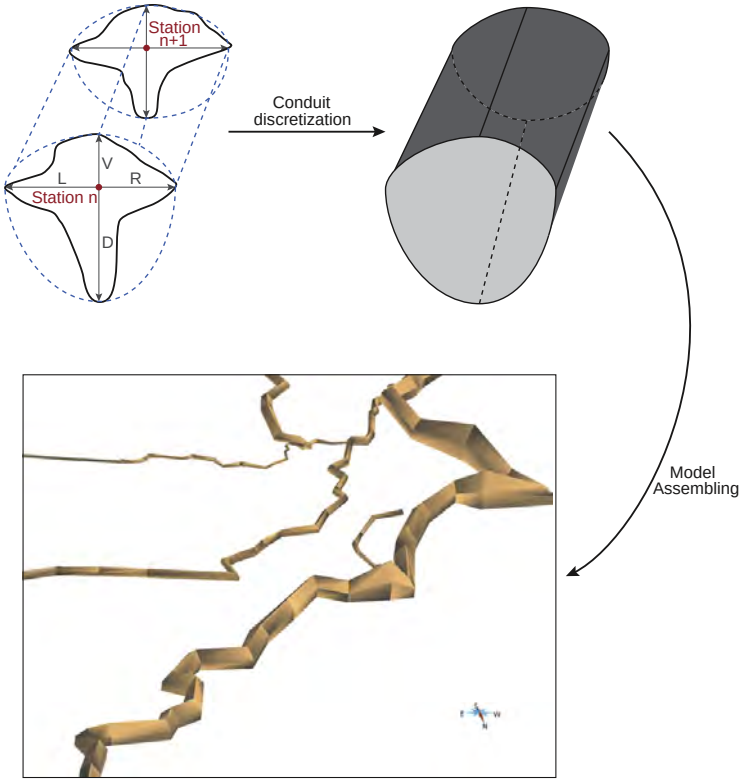

Fig. 1. Classical conduit discretization process and 3D "reconstruction" used in common speleological programs (here with GHTopo).

2012; Pardo-Igúzquiza et al., 2012). They stochastically generate several possible skeletons representing roughly the conduit centre and highlighting the uncertainties related to the conduit location. The proposed methodology is complementary to those works by providing volumetric information around those skeletons consistent with local geological settings, highlighting the uncertainties related to the conduit size and shape. Second, it provides a solution to reconstruct the three-dimensional geometry of explored and monitored cave systems. Indeed, new technologies like LiDAR have permitted precise mapping of cave conduits (e.g., Jaillet et al., 2011). But this type of acquisition is time consuming, needs specific equipment and requires a post-treatment of huge amounts of data. It is thus far more adapted to explore and model karst at the drain scale. For larger scales, there are two categories of data: i) two-dimensional maps (plan and/or profile views) which result of a projection of a three-dimensional network on a two-dimensional plane — this is the oldest and most common type of data; ii) three-dimensional information provided by "modern" cave survey. In the latter case, the underground topographic information is given by a sequence of topographic stations, located in order to fit exploration requirements: access easiness, clear sight along the cave passages, etc. At each station only distances to walls are recovered left, right, up and down (LRUD). The numerical treatment of these data leads to a discretization that represents the conduits with elliptical or rectangular section shapes (Fig. 1). Dealing with both categories of data, the 3D reconstruction remains a problem that is currently solved in common speleological programs with a linear interpolation between the various two-dimensional sections leading to more or less realistic shapes (e.g., Survex,[1] VisualTopo[2] or GHTopo[3]).

In both contexts, few works have been conducted on modelling more realistic 3D karstic conduit shapes (e.g., Labourdette et al., 2007; Henrion et al., 2010; Boggus & Crawfis, 2009). The object-distance simulation method (ODSIM) proposed by (Henrion et al., 2010) generates an envelope along a curve skeleton whose shape is irregular at fine scale but globally cylindrical at the first order. To integrate a geological constraint on the shape, e.g., for the development of hydrothermal dolomites around fractures, they use plane skeletons instead of curves. But the resulting envelope retains a round aspect at the plane extremities. Contrary to geometries generated with this simple approach, karstic shapes are more elongated along given inception features (e.g., Jameson, 1985; Filipponi, 2009) that favour karst conduit development. Thus, depending on the local geological context, the cross-section geometry of karstic conduits varies from circle to lens or "keyhole" (Section 2). These particular shapes are not reproduced by ODSIM (Section 3). In this paper, we propose a new methodology to integrate various geological features influencing conduit shapes by using a custom distance field generated with a fast marching method instead of a Euclidean distance field (Section 4). This involves the creation of a

[1] http://survex.com/.
[2] http://vtopo.free.fr/.
[3] http://siliconcavings.chez-alice.fr/.

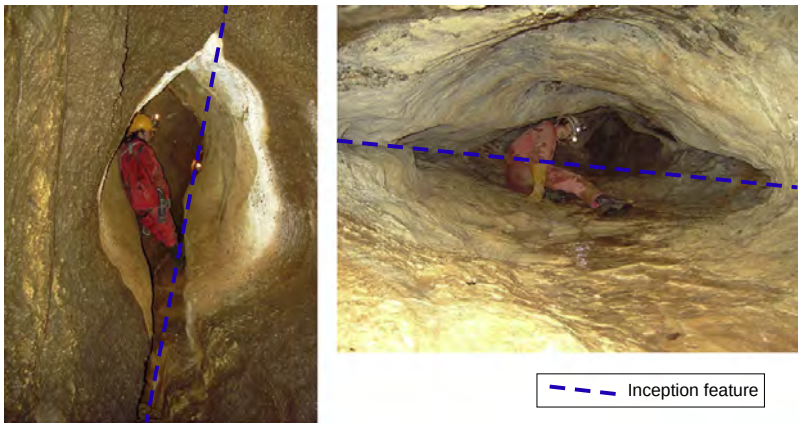

Fig. 2. Examples of karstic conduits showing shapes strongly elongated along inception features (left: Cave O80, Switzerland; right: Grottes aux fées, Switzerland).

"velocity" field that controls the front propagation of the fast marching method (Section 4). This new methodology allows us to simulate specific shapes that are realistic and consistent with geological settings and speleological knowledge of the system (Section 5).

2. Geomorphological analysis of the karstic conduits

Because karsts result from fluid circulation and dissolution capacity, the vulnerability to dissolution of the surrounding rocks plays a major role in their genesis. More particularly, karstic networks tend to develop along weakness features — either lithostratigraphic inception features, such as beds or bedding planes, or tectonic inception features, such as fractures or faults (e.g., Jameson, 1985; Lowe, 1992; Faulkner, 2006; Filipponi, 2009). These features are characterized by a strong contrast with the surrounding formations in terms of physical, lithological and/or chemical properties, such as the permeability. This contrast has a major influence on karst genesis (Filipponi, 2009; Filipponi et al., 2010): the inception features favour primary fluid circulations because of it and, thus, primary rock dissolution.

The dissolution process and the path development are not uniform in space due to the three-dimensional nature of the genesis processes and the geometrical anisotropy of the inception features. These features favour a differential dissolution, leading to an elongation of the conduits along them — often with pronounced angles — and explaining their non-cylindrical appearance in cross-section (Fig. 2). The resulting shapes are consequently more or less elliptical depending, for instance, on the dissolution capacity of the fluids or on the contrast in permeability or in carbonate content between the inception feature and the surrounding formations (Filipponi, 2009).

According to various authors, the groundwater table has a major influence on conduit development (e.g., Jameson, 1985; Ford & Williams, 2007; Farrant & Smart, 2011; Jaillet et al., 2011). In the phreatic zone, corresponding to the saturated zone below the water table, the inception features are the most influential factor upon the resulting shapes (Filipponi et al., 2009). The dissolution acts on whole conduits and in all directions. The shapes are then more or less jagged, depending on the fluids, on the surrounding rocks and on the presence of other inception features (Figs. 2, 4.1) (e.g., Jameson, 1985; Lauritzen & Lundberg, 2000; Filipponi, 2009). The vadose zone corresponds to the zone above the current water table. But the observed conduits are usually the result of a long process that has involved a past phreatic development. Keyhole passages are among the most common cross-sectional conduit geometries that are encountered (Field, 2002). They are characterized by an entrenchment, a canyon passage commonly narrower than the original passage, also called the trench. Indeed, a drop of the water table puts the original conduits in phreatic conditions. The fluids circulating in the conduits with high velocities are led by gravity, incising the floor, generating these typical cross-sectional keyhole shapes (Figs. 3, 4.2) (e.g., Jameson, 1985; Lauritzen & Lundberg, 2000; Filipponi, 2009; Jaillet et al., 2011). Horizontal dissolution notches are less common. They develop at the water table interface when conduits are partially flooded and water level variations are small enough to favour a lateral incision (e.g., Lauritzen & Lundberg, 2000; Ford & Williams, 2007; Farrant & Smart, 2011). Geometrically speaking, notches have a rounder aspect than shapes linked to inception features (Fig. 4.3).

In the following, we explain how these different observed geometries can be integrated in the ODSIM method to improve the realism of simulated karst conduits.

3. Principle of the object-distance simulation method

Henrion et al. (2010) proposed an object-distance simulation method (ODSIM) that models a three-dimensional envelope around a

Fig. 3. Example of a keyhole passage (Sieben Hengste Cave System, Switzerland).

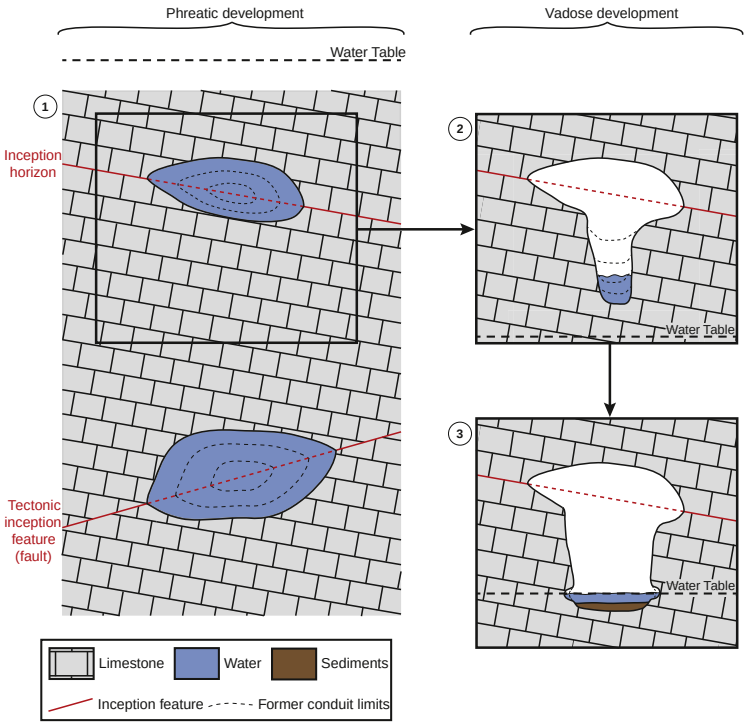

Fig. 4. Evolution of a karstic conduit depending on its position relative to the water table: 1. Genesis and growth of two conduits in the phreatic zone following different weakness planes (a lithostratigraphic horizon for the upper one, a fault for the other). 2. Following a fall of the water table, the upper conduit goes through the vadose zone which progressively generates a keyhole passage by cutting a trench. 3. Following a rise of the water table, notches grow at the trench bottom.

skeleton. For the explored parts of a karst, that skeleton can be provided by field data, such as two-dimensional maps or LRUD (Left, Right, Up and Down) data. Otherwise, stochastic simulations can be used to obtain several skeletons and take into account the uncertainties related to the conduit location (e.g., Pardo-Igúzquiza et al., 2011; Borghi et al., 2012; Collon-Drouaillet et al., 2012). The ODSIM method consists of computing a Euclidean distance field around the skeleton and perturbing it using a random threshold (Fig. 5). This threshold can be generated using a sequential Gaussian simulation (SGS) or other stochastic simulation methods (e.g., Deutsch & Journel, 1997; Goovaerts, 1997). As a stochastic simulation method, the SGS can provide an infinity of thresholds. This allows us to build several envelopes for a given skeleton, thus catching the uncertainties around the conduit shape. The perturbation is done using the following indicator function:

$$I_B(p) = \begin{cases} 1 & \text{if } D(p) \leq \varphi(p) \\ 0 & \text{else} \end{cases} \quad (1)$$

$D(p)$ is the 3D distance field computed at each point $p = [p_x p_y p_z]^T$ of a grid G and $\varphi(p)$ is the random threshold. The computed indicator property $I_B(p)$ is equal to 1 in the geological body, 0 outside. The 3D envelope corresponds to the surface at the interface between the interior and the exterior of the region corresponding to 1, or equivalently to points at a given distance of the network: $D(p) \leq \varphi(p)$. In this method, the simulated conduits can be complied with hard data conditioning (like well data or LRUD distances to walls) thanks to an iterative Gibbs sampling algorithm (Geman & Geman, 1984) with inequality constraints (Freulon & de Fouquet, 1993).

With this approach, the only way to avoid a globally cylindrical shape is to use plane skeletons instead of curves. However, the resulting envelope keeps a round aspect at the plane extremities because of the Euclidean distance. Furthermore this approach lacks flexibility when dealing with various and complex shapes, such as those seen in Section 2.

4. Integration of geomorphological information in ODSIM

The proposed methodology keeps the basic principle of ODSIM: the "distance" to an object model controls the first-order features while a random field provides the fine-scale features (Henrion et al., 2010). Our proposal is to play on these two scales. First, by using a custom distance field generated by a fast marching method and constrained to geomorphological information. This allows us to take into account simultaneously various elements involved in the conduit genesis and so influencing the conduit shapes. Second, we propose to build a random threshold by combining different variograms and/or distributions depending on the elements constraining the custom distance field (Fig. 6).

4.1. Using of a custom distance field instead of an Euclidean distance field

The fast marching method (Sethian, 1996; Sethian, 1999a; Sethian, 1999b) concerns the propagation of a front knowing its speed. The principle is to solve the Eikonal equation:

$$|\nabla T| F = 1. \quad (2)$$

T is the time field and F the velocity field. $1/F$ gives a slowness field.

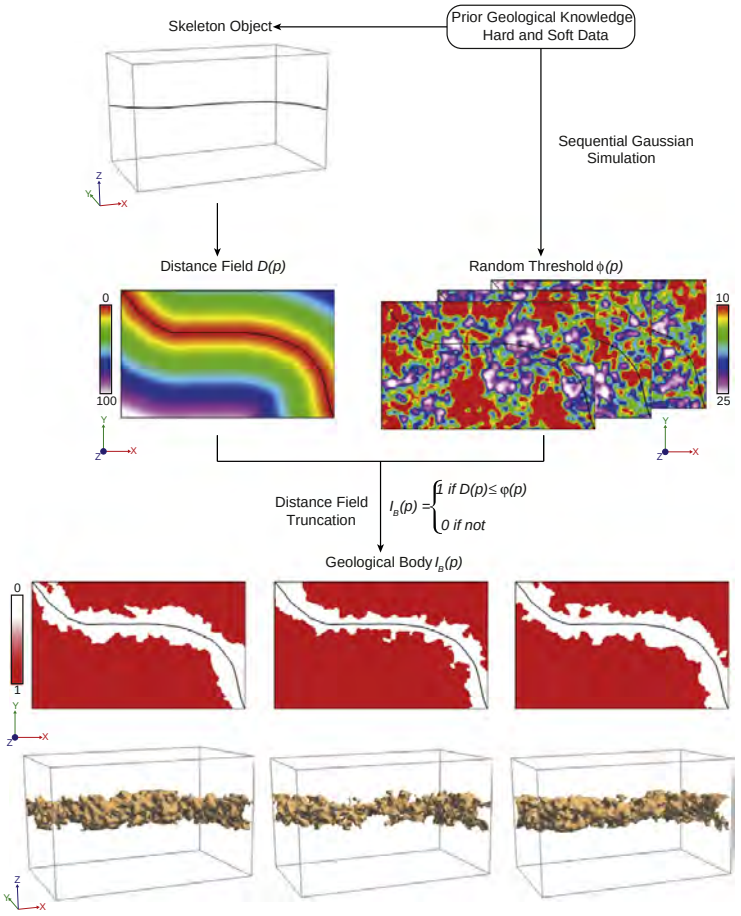

Fig. 5. ODSIM workflow (modified from Henrion et al. (2010)) applied to a karstic conduit generation. The distance field $D(p)$ is truncated with the random threshold $\varphi(p)$ giving an indicator property $I_B(p)$ of the karstic conduits and caves.

This method creates a scalar field corresponding to the arrival time $T(x, y, z)$ at which the propagation front reaches the position (x, y, z), depending on a predetermined velocity field (or equivalently a slowness field) (Fig. 7). This velocity field characterizes the speed of the front for each position (x, y, z).

In a modelling approach, a convenient aspect is that the choice of the velocity field constrains the evolution of the front and the resulting arrival time field. Putting higher values for inception features in the velocity field constrains the time field in such a way that it contains geomorphological information, providing the custom distance field (Fig. 7). Using a fast marching method gives thereby a greater flexibility to ODSIM. Nevertheless, the property used to compute the velocity field has to be thoughtfully chosen. As underlined by Borghi et al. (2012), contrasts between the values are more important than values themselves when using the fast marching method. The velocity field has to be linked with a property of the medium that respects this contrast rule.

As the notion of contrast controls both the fast marching and the karst genesis, the velocity field is built by using the permeability (or the hydraulic conductivity). This provides emphasis on the weakness planes, and moreover simplifies the choice of the property values. However, it is not sufficient to model specific structures like those encountered in the vadose zone and specific strategies need to be developed.

4.2. Building the velocity field for the vadose zone

Structures developed in vadose conditions are the result of several speleogenetic phases, corresponding to several water table positions. The goal of our method is not to reproduce each of these phases one after the other as a genetic model would do it. Instead, we propose numerical strategies to reproduce directly final conduit geometries consistent with the speleologist's observations and knowledge.

For reproducing the keyhole geometry, and more specifically the trenches appearing on the conduit floors, we propose to use an "attraction level" with high velocity values similar to those of the inception features. This attraction level may correspond to the present water table. A vertical plane between the skeleton and the attraction level is then considered as a high velocity zone by extending the attraction level values (Fig. 8). This modification constrains the front propagation which goes toward that level.

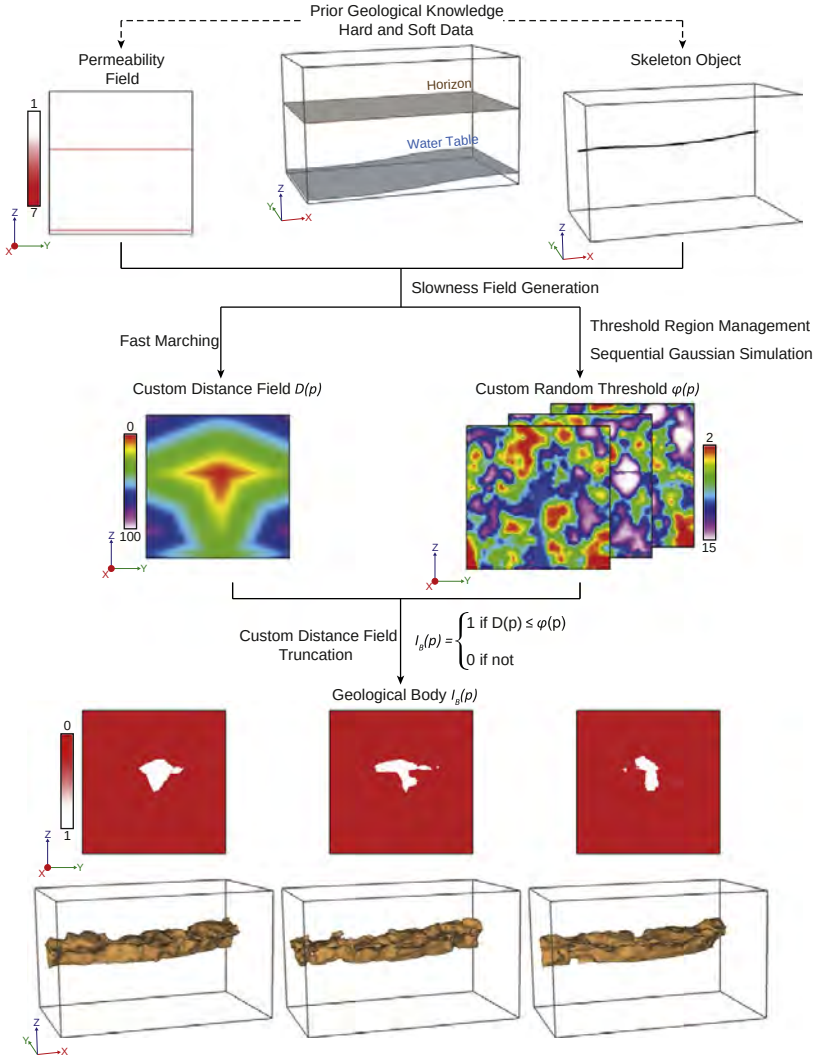

Fig. 6. New workflow for ODSIM. The original method is obtained by using a constant velocity or slowness field and the same parameters for the whole threshold. *Slowness field generation* and *fast marching* steps are further detailed in Sections 4.1 and 4.2; *threshold region management* step is detailed in Section 4.3.

To limit the effects of the attraction level on the highest conduits, a parameter representing the maximum allowed distance d_{max} between the skeleton and the attraction level is added to generate these trenches. Moreover, the distance between the skeleton and the attraction level d is used to obtain shorter depths for trenches as the conduits move away from the water table. To do that, the permeability values of the attraction level in the vertical plane building the trenches are multiplied by a factor integrating d/d_{max}, giving the vertical trench plane velocity values v:

$$v(x_s, y_s, z) = m \times \left(1 - \frac{d(x_s, y_s)}{d_{max}}\right) \times p_w(x_s, y_s, z_w) \quad (3)$$

(x_s, y_s, z_s) is a point of the skeleton, (x_w, y_w, z_w) is a point of the attraction level, z is bounded by z_s and z_w, m is a multiplication factor defined by the user, d_{max} sizes the zone of influence of the attraction level, v is the velocity value of the vertical plane at a given point (x_s, y_s, z), d is the distance between the skeleton and the attraction level at the same horizontal coordinates (x_s, y_s) and p_w is the permeability value at the attraction level at the same horizontal coordinates (x_s, y_s).

Using d causes trench depth to evolve smoothly with the distance between the skeleton and the attraction level and avoids sharp entrenchment endings on the boundaries of the influence zone (Fig. 9).

If the difference between the velocity values of the attraction level and those of the surrounding formation is not significant, the

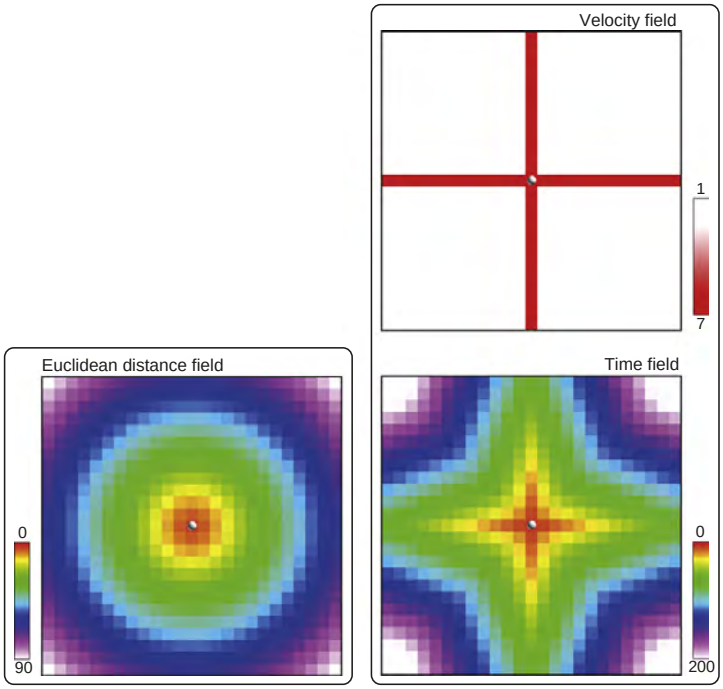

Fig. 7. Comparison between an Euclidean distance field and a field generated by fast marching. Both fields are generated from the central node of the grid, but the time field is constrained by the differences of speed given by the velocity field.

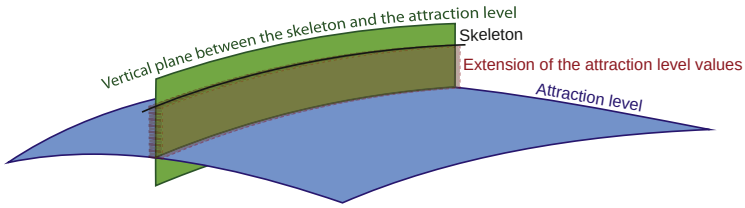

Fig. 8. Foundations for trench modelling: a vertical plane between the skeleton and the attraction level is considered. The values of the attraction level crossed by the plane are extended vertically up to the skeleton.

factor $(1 - d/d_{max})$ can invert their contrast, leading to lower velocity values for the vertical plane and so a poor front propagation. The multiplication factor m solves this issue and gives the user a control on the trench depth.

With only one column of cells representing the vertical trench plane in the grid, the resulting trenches are V-shaped and do not show vertical sides or a flat bottom. Thus, several parameters are added to give more control to the propagation of the front and be sure it gives a satisfying shape to the envelope. The main point is to extend the vertical plane sideways, using a width w and a "beginning distance" d_b to ensure straighter sides of the trenches (Fig. 10.1).

Notches are often smooth shapes created while the water table is superimposed on the conduits. These features can be easily modelled by thickening the (paleo)water table(s) in the velocity field using a factor n (Fig. 10.2). The thickening controls the smoothness and the height of the notch shape. The notch depth can be controlled by applying a multiplication factor on the velocity values around the (paleo)water table(s).

4.3. Management of the different scales of perturbations on the envelope

As said before, the velocity field controls the coarse-scale shape of the conduits, but the focus of the ODSIM approach is to combine this

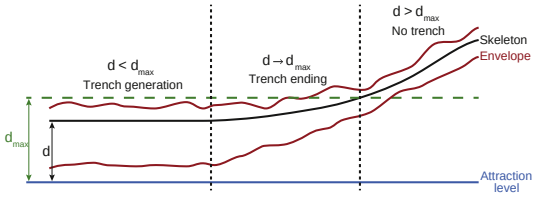

Fig. 9. Consequences on the envelope of the variations of the distance d between the skeleton and the attraction level, illustrating the impact of the formula (3). The permeability values p_w are taken from the attraction level and the distance d_{max} is defined by the user and represents the maximum allowed distance to generate a trench.

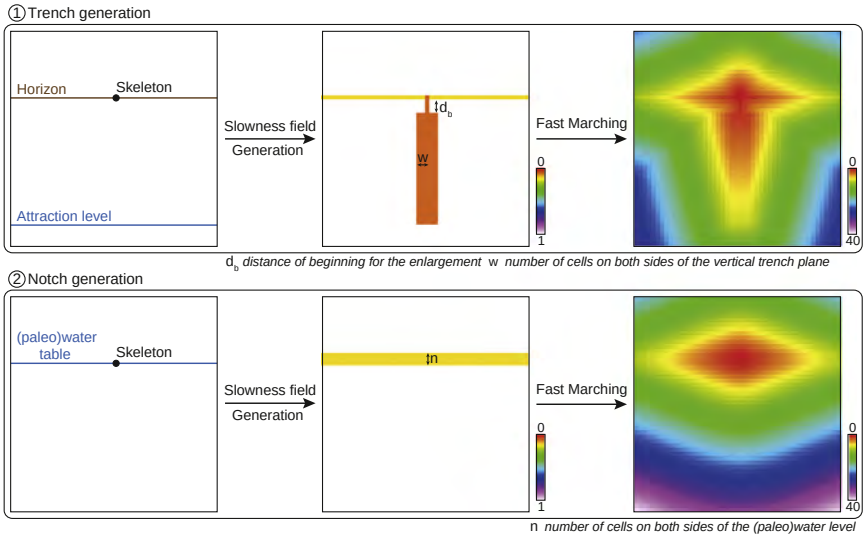

Fig. 10. Modifications of the slowness field allowing the generation of trenches and notches. The global shape of these elements is clearly visible in the field created by fast marching.

field with a random threshold that perturbs this "perfect" geometry by introducing fine-scale variability and also allows hard data conditioning. In their paper, Henrion et al. (2010) have proposed to introduce a locally variable mean into the sequential Gaussian simulation in order to accommodate a spatial trend. But this kind of modification would equally affect roof, walls and floors of the conduits by a progressive growing or narrowing.

Considering cave conduit geometries, it appears that these fine-scale variabilities are not identically affecting the roof, the walls or the floor. Due to many different factors, like breaking-down, mechanical and chemical erosion, it is common to have more variabilities along a roof than, particularly, on the bottom of a trench. Thus, conduit irregularities are not symmetrical and, moreover, their variations do not range between the same extrema (Fig. 11). Such differences between conduit ceiling, floor and/or sides can be noticed in several conduits, such as in the Abracurrie Main Chamber, Nullarbor, Australia (James et al., 2012) or in the Clearwater Cave, Gunung Mulu, Sarawak (Farrant & Smart, 2011).

Fig. 11. Example of a passage with different scales of perturbation: the top and the floor of the conduit are roughly flat whereas its sides are more wavy (Mammoth Cave, US).

To model a smooth trench floor, for instance, we propose to separate the grid in two areas: the first one contains the vertical trench planes — with eventually an extension around the planes to avoid trench side protuberances to develop below the trench floor when using very high perturbations, and the second one the rest of the grid. Then two distinct variograms and/or distributions are defined in each area. The sequential Gaussian simulation generating the random threshold has to preserve a continuous resulting field between those areas (Fig. 12).

Increasing the range of the variogram used on the trench planes smoothes their bottom while preserving small scale perturbation on the trench sides. Reducing the amplitude of the values used for the probability density function (PDF) on the trench planes avoids obtaining a large range of variation for the conduits at the bottom (Fig. 13). The same method can be applied to reduce the roughness along weakness planes. Eventually, the use of several variogram models and/or distributions for each element controlling the shape gives differential perturbations of the envelope.

5. Results and discussion

These extensions of ODSIM have been implemented as a plugin of the GOCAD geomodelling software[4] and written in C++. It should be noted that this work can be developed in another modelling software, in a numerical computing environment such as MATLAB or Scilab as well as in a stand-alone application. The methodology has been tested on two synthetic cases. By using synthetic cases, we can easily demonstrate the new possibilities (cylinder, lens, keyholes, …) offered by the method in a few examples, without falling into a controversial context. To better illustrate the independence between the skeleton simulation and the three-dimensional envelop modelling, the same karstic skeleton is used

[4] http://www.pdgm.com/products/GOCAD.

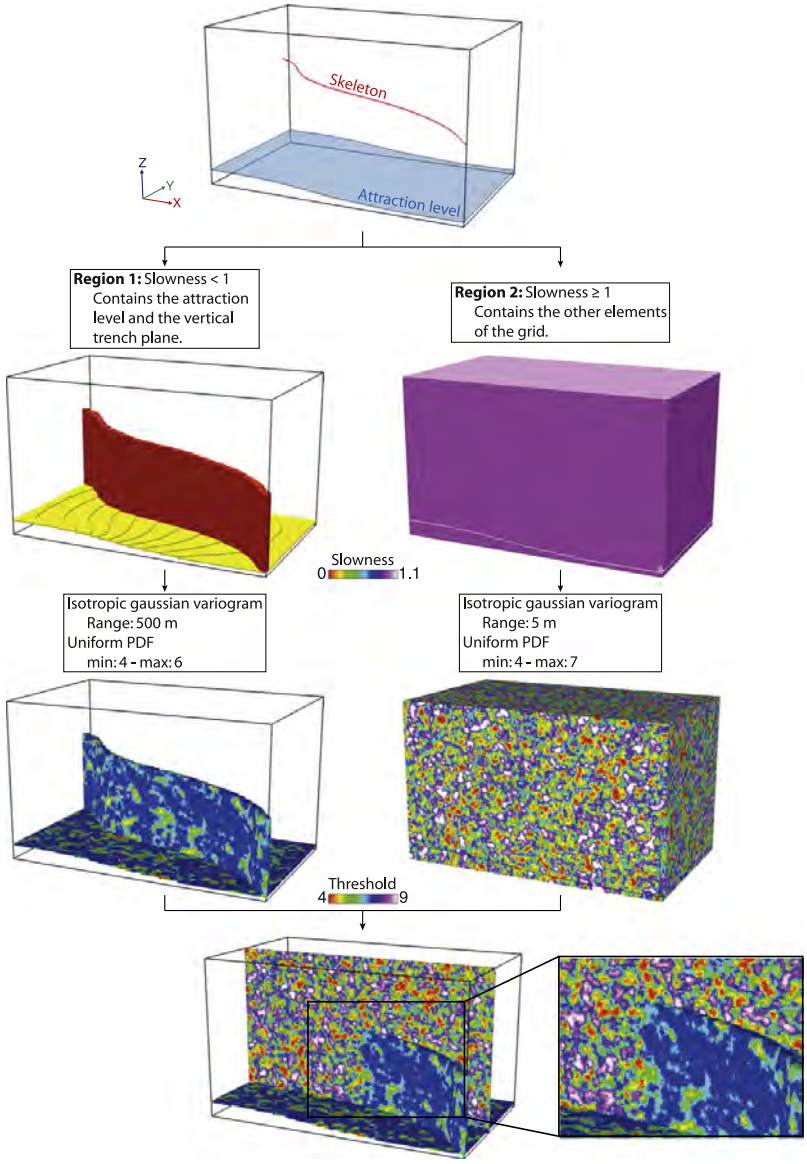

Fig. 12. Threshold generation example: the principle is to separate the structures with different perturbation types using their values in the slowness field. Here only two areas are created: the last screenshot shows the region 1 together with a section along the whole *x* axis, showing elements of the region 2. The enlargement on the right shows the continuity between the features of the two areas despite the two different distributions and variograms. This continuity is essential for obtaining good quality envelopes.

in the following examples. Inception features, water table and attraction level are modelled with triangulated surfaces. For the threshold simulations, a regular structural grid has been used. Both examples are supposed to be the expression of two genetic phases: i) an initial phreatic phase that is visible on the final shapes through an elongation along inception features; ii) and a second phase that results from a lowering of the water table. In the first example, to illustrate trench modelling capacities, an attraction level has been introduced at the water table level. The distance d_{max} has been chosen to limit entrenchments to the lowest conduit (Fig. 14). The various parameters used in this simulation are presented in Table 1 (Example 1). In the second example, we wanted to test the capacity of the method to reproduce notches (Fig. 15). A water table is thus introduced at the same altitude as the lowest conduits. It is duplicated into an attraction level to simultaneously develop trenches on the upper conduit, superposed to the inception elongation features. Detailed parameters are presented in Table 1 (Example 2).

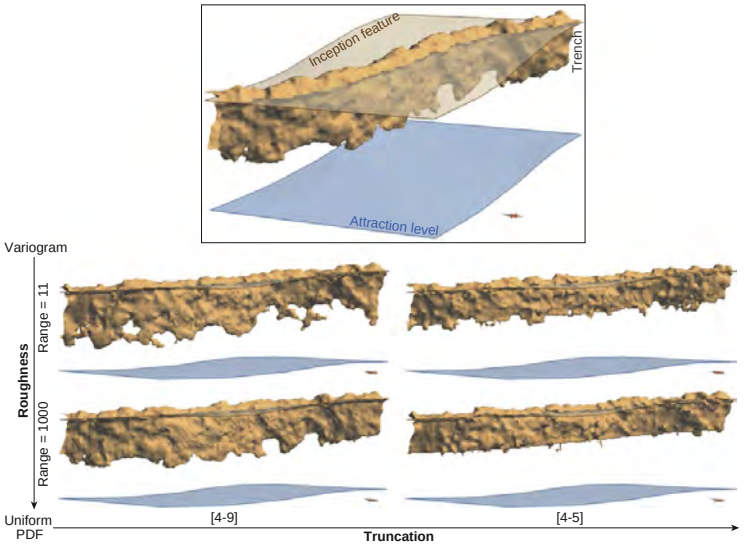

Fig. 13. Impact of the variogram and distribution used to generate the threshold: side view of the resulting envelopes. The given parameters are those of the weakness planes and the trench plane, the rest of the grid having a variogram range of 11 m and a uniform PDF of [4–9]. The velocity field values are 5 for the previous planes and 1 in the rest of the grid.

The resulting envelopes reflect the various coarse-scale karstic shapes that are now possible to model with this new methodology: i) lengthening and sharp incision along inception features (stratigraphical and tectonic); ii) realistic symmetric round shapes for the vertical conduits; iii) trenches superposed on a cylindrical or lens shape for keyhole passages; and iv) longitudinal notches. All these features can be combined. What trenches concern, depth variations follow the position of the conduits relatively to the attraction level: the further from the attraction level the conduits are, the lower is the trench depth. Their bottom is smoother than the shapes linked to the inception features thanks to the combined use of different variograms and distributions in the random threshold generation. Notch representations are more like a rounding of the lateral carving although they can be more "marked" in the caves. The result remains useful in representing large notches. Generally, the proposed methodology offers an interesting list of solutions to simulate or reconstruct realistic three-dimensional karstic conduits. In this dual-scale geostatistical simulation method, the coarse-scale features can be modelled by an adapted and modular combination of a skeleton representation of the studied object and geological/speleological constraints defined by the user.

This results in a custom velocity field representing the coarse-scale geometries. A solution is proposed for managing the different fine-scale features depending on the same geological/speleological constraints. The Gibbs sampler with inequality constraints algorithm — which is

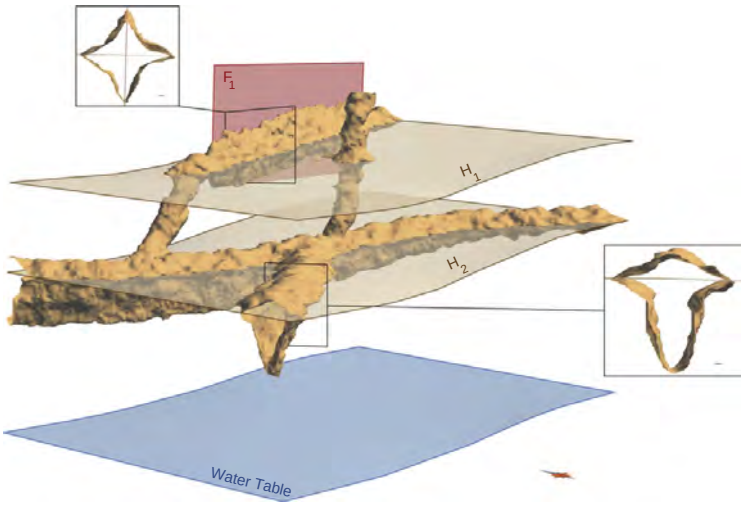

Fig. 14. Simulated envelope obtained by using two stratigraphic inception features (H_1 and H_2), one tectonic inception feature (fault F_1) and an attraction level. Complex three-dimensional karst features such as trenches or elongated shapes are successfully reproduced.

Table 1
Summary of parameters used to create the two synthetic models.

	Example 1	Example 2
GRID PARAMETERS		
Grid size (in cell)	250 × 150 × 150	250 × 150 × 150
Cell size (in m)	1 × 1 × 1	1 × 1 × 1
FAST MARCHING PARAMETERS		
Initial slowness field		
H_1 slowness value	0.2	0.2
H_2 slowness value	0.2	–
F_1 slowness value	0.2	0.2
Water table slowness value	0.2	0.2
Matrix slowness value	1	1
Trench parameters		
d_{max} (in m)	70	70
d_b (in cell)	4	4
w (in cell)	1	1
Notch parameters		
n (in cell)	–	1
THRESHOLD PARAMETERS		
Low slowness region (*Slowness* < 1)		
Variogram		
Type	Gaussian	Gaussian
Range (in m)	500	500
Distribution		
Type	Uniform	Uniform
Min–Max	4–6	4–6
High slowness region (*Slowness = 1*)		
Variogram		
Type	Gaussian	Gaussian
Range (in m)	7	7
Distribution		
Type	Uniform	Uniform
Min–Max	4–7	4–7

already available in the method (Henrion et al., 2010) — complements this toolbox by allowing hard data conditioning. Some further work is required to quantitatively validate the method capacity to reproduce realistic shapes. Several solutions could be explored:

- Compare a cave already modelled using a LiDAR survey or 2D sections and maps with several simulated conduits. Due to the stochastic nature of the process, the direct assessment of the real and simulated passage fit is worthless: a simulated conduit can be geomorphologically consistent even if it does not fit the real conduit. Some indicators have to be developed to capture the entire three-dimensional characteristics of a conduit, such as, for instance, the conduit volume or the ratio of conduit surface area to conduit volume. Those indicators are then used to compare the real conduit and the simulated ones.
- Compare the simulated shapes for the unknown parts of a network with the conditioned shapes in the known parts based on statistical or fractal-based principles such as introduced by Curl (1986) (e.g., Pardo-Iguzquiza et al., 2011).

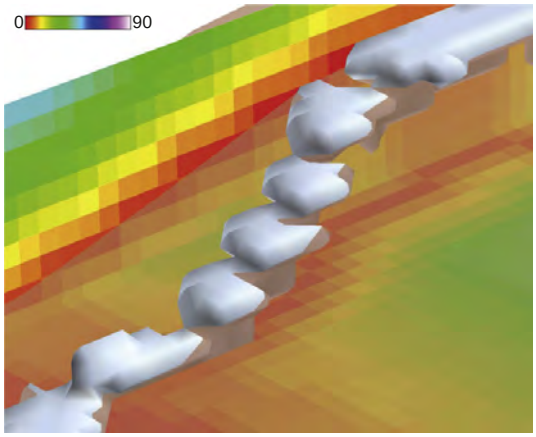

Fig. 16. Insufficient grid resolution leading to a non-continuous karstic conduit simulation. The colours correspond to the custom distance field and the transparent surface represents the weakness plane.

Despite these encouraging results, some limitations appear. First, the grid resolution can have a significant impact on the results. Indeed the introduction of the inception features in a velocity property corresponds to their rasterization in the grid. Stratigraphic inception horizons have a thickness of some centimetres to some decimetres (Filipponi, 2009), and conduits may be very stretched along them. Moreover, tectonic inception features induce very thin shapes at the intersection with the conduit. This means that shape modelling requires high grid resolutions,

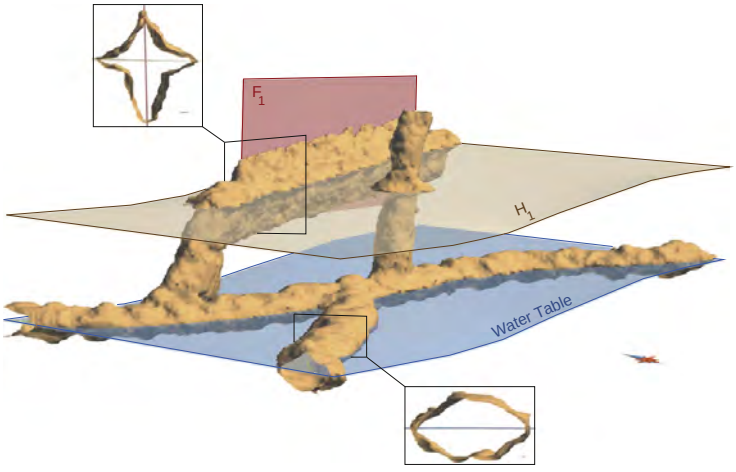

Fig. 15. Simulated envelope obtained by using one stratigraphic inception feature (H_1), one tectonic inception feature (fault F_1) and an attraction level superimposed on a water table at the same level as the lowest conduits. Complex three-dimensional karst features such as notches, trenches or elongated shapes are successfully reproduced.

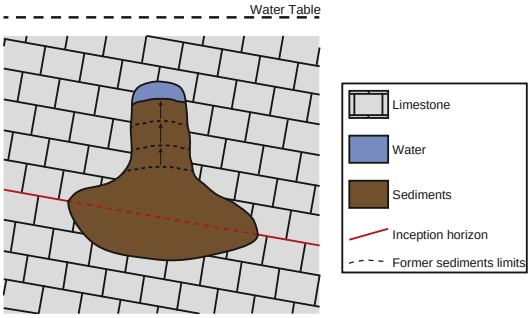

Fig. 17. Principle of the development of the paragenetic conduits: sediments progressively fill the cavity and block the downward dissolution, which favours an upward dissolution propagation.

at least to represent the global shape of the conduits in an acceptable way (Fig. 16). Another solution would be to have a non-regular grid organized along inception features. Second, the increase of the degrees of freedom in the process has a direct consequence on the increase of user choices and parameters, even if many features can be integrated directly in the custom distance field. But this last limitation is directly linked to the complexity of the studied case and difficult to avoid. Nevertheless, perhaps a new alternative could be found that avoids the use of the d_b and w parameters in the trench modelling process.

As for perspectives, a modelling method for other shapes could be studied. For instance paragenetic caves are made of conduits developed in the phreatic zone shaped like upside-down trenches, displaying an upward entrenchment of conduits (Fig. 17) (Renault, 1958; Pasini, 1967; Renault, 1968). They could probably be modelled with the same principle as trenches, but upturned. Another common geometry, partially linked to breakdowns, is strike-oriented passages (e.g., Palmer, 2012) that have a polygonal shape following horizons, with many perpendicular angles (Fig. 18). Even if various scales of variability are introduced in the simulated conduits through the threshold field, small-scale features such as scallops can still not be clearly and deliberately represented. On the other hand, larger scale features, such as conduit loops, are not linked to the conduit shape but to the network and should be introduced by the skeleton.

In a broader perspective, tests are required to assess the impact of these shapes on flow simulations. Modelling sediments could also be interesting considering their impact on fluid flows and on speleogenesis (Farrant & Smart, 2011). Finally, the entire methodology could be adapted to other underground processes, such as hydrothermal alteration, or be used to study the usefulness and applicability of the method in sinkhole prevention.

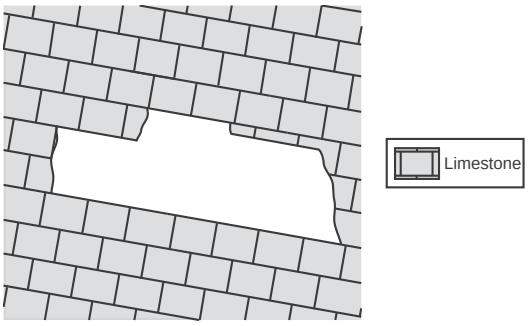

Fig. 18. A strike-oriented passage: the conduit shape follows lithostratigraphic horizons.

6. Conclusions

These improvements of ODSIM allow the stochastic generation of karst conduit envelopes around a skeleton by taking into account local geological information, especially inception features and (paleo)water table. It consequently contributes to the global workflow of stochastic karst generation, complementing the methods that stochastically generate skeletons representing the general network by introducing geomorphologically consistent conduit shapes. Various classic conduit shapes can be simulated, such as elongated or keyhole passages, while preserving the original capacities of ODSIM. Some other particular shapes still need to be taken into account to allow their simulation. Applying this method on synthetic cases gives quite satisfying results. The simulated shapes finely reproduce the most common conduit geometries while controlling the different scales and areas of shape perturbations. However, a confrontation to real data still needs to be carried out; first to validate the application to the reconstruction of explored and monitored conduits, then to validate more objectively the method's capacity to generate realistic conduits.

Acknowledgements

We would like to thank the industrial and academic members of the GOCAD Consortium,[5] especially Paradigm for providing the GOCAD Software and API, ASGA (Association Scientifique pour la Géologie et ses Applications) and the French National Scientific Research Center CNRS - GeoRessources for their support. We would also like to thank the reviewers, including Ph. Häuselmann, for constructive comments which helped improve this paper. This work was performed in the framework of the "Investissements d'avenir" Labex RESSOURCES21 (ANR-10-LABX-21).

References

Boggus, M., Crawfis, R., 2009. Explicit generation of 3D models of solution caves for virtual environments. Proceedings of the 2009 International Conference on Computer Graphics and, Virtual Reality, pp. 85–90.
Borghi, A., Renard, P., Jenni, S., 2012. A pseudo-genetic stochastic model to generate karstic networks. J. Hydrol. 414–415, 516–529.
Brinkmann, R., Parise, M., Dye, D., 2008. Sinkhole distribution in a rapidly developing urban environment: Hillsborough County, Tampa Bay area, Florida. Eng. Geol. 99, 169–184.
Chaojun, Z., Chengzao, J., Benliang, L., Xiuyu, L., Yunxiang, L., 2010. Ancient karsts and hydrocarbon accumulation in the middle and western parts of the North Tarim uplift, NW China. Pet. Explor. Dev. 37, 263–269.
Collon-Drouaillet, P., Henrion, V., Pellerin, J., 2012. An algorithm for 3D simulation of branchwork karst networks using Horton parameters and A-star. Application to a synthetic case. Geol. Soc. Lond. Spec. Publ. 370, 12. http://dx.doi.org/10.1144/SP370.3.
Curl, R.L., 1986. Fractal dimensions and geometries of caves. Math. Geol. 18, 765–783.
Deutsch, C.V., Journel, A.G., 1997. GSLIB: Geostatistical Software Library and User's Guide (Applied Geostatistics). Oxford University Press, USA.
De Waele, J., Gutiérrez, F., Parise, M., Plan, L., 2011. Geomorphology and natural hazards in karst areas: a review. Geomorphology 134, 1–8.
De Waele, J., Plan, L., Audra, P., 2009. Recent developments in surface and subsurface karst geomorphology: an introduction. Geomorphology 106, 1–8. http://dx.doi.org/10.1016/j.geomorph.2008.09.023.
Farrant, A.R., Smart, P.L., 2011. Role of sediment in speleogenesis; sedimentation and paragenesis. Geomorphology 134, 79–93.
Faulkner, T., 2006. Tectonic inception in Caledonide marbles. Acta Cardiol. 35, 7–21.
Field, M.S., 2002. A lexicon of cave and karst terminology with special reference to environmental karst hydrology. National Center for Environmental Assessment, Washington Office, Office of Research and Development, US Environmental Protection Agency.
Field, M.S., Pinsky, P.F., 2000. A two-region nonequilibrium model for solute transport in solution conduits in karstic aquifers. J. Contam. Hydrol. 44, 329–351.
Filipponi, M., 2009. Spatial Analysis of Karst Conduit Networks and Determination of Parameters Controlling the Speleogenesis along Preferential Lithostratigraphic Horizons. Ph.D. Thesis École Polytechnique Fédérale de Lausanne, Suisse.
Filipponi, M., Jeannin, P.Y., Tacher, L., 2009. Evidence of inception horizons in karst conduit networks. Geomorphology 106, 86–99.
Filipponi, M., Jeannin, P.Y., Tacher, L., 2010. Understanding cave genesis along favourable bedding planes. The role of the primary rock permeability. Z. Geomorphol. Suppl. 54, 91–114.

[5] http://www.gocad.org.

Ford, D., Williams, P., 2007. Karst Hydrogeology and Geomorphology. John Wiley and Sons, Ltd.
Freulon, X., de Fouquet, C., 1993. Conditioning a Gaussian model with inequalities. In: Soares, A. (Ed.), Geostatistics Tróia '92. Springer Netherlands. Number 5 in Quantitative Geology and Geostatistics, pp. 201–212.
Frumkin, A., Karkanas, P., Bar-Matthews, M., Barkai, R., Gopher, A., Shahack-Gross, R., Vaks, A., 2009. Gravitational deformations and fillings of aging caves: the example of Qesem karst system, Israel. Geomorphology 106, 154–164.
Geman, S., Geman, D., 1984. Stochastic relaxation, Gibbs distributions, and the Bayesian restoration of images. IEEE Transactions on Pattern Analysis and Machine Intelligence pp. 721–741.
Goldscheider, N., 2008. A new quantitative interpretation of the long-tail and plateau-like breakthrough curves from tracer tests in the artesian karst aquifer of Stuttgart, Germany. Hydrogeol. J. 16, 1311–1317.
Goovaerts, P., 1997. Geostatistics for natural resources evaluation. Applied GeostatisticsOxford University Press, New York.
Hartmann, A., Lange, J., Aguado, A.V., Mizyed, N., Smiatek, G., Kunstmann, H., 2012. A multi-model approach for improved simulations of future water availability at a large Eastern Mediterranean karst spring. J. Hydrol. 468–469, 130–138.
Hauns, M., Jeannin, P.Y., Atteia, O., 2001. Dispersion, retardation and scale effect in tracer breakthrough curves in karst conduits. J. Hydrol. 241, 177–193.
Henrion, V., Caumon, G., Cherpeau, N., 2010. ODSIM: an object-distance simulation method for conditioning complex natural structures. Math. Geosci. 42 (8), 911–924.
Horvatinčić, N., Krajcar Bronić, I., Obelić, B., 2003. Differences in the ^{14}C age, $\delta^{13}C$ and $\delta^{18}O$ of Holocene tufa and speleothem in the Dinaric karst. Palaeogeogr. Palaeoclimatol. Palaeoecol. 193, 139–157.
Jaillet, S., Sadier, B., Arnaud, J., Azéma, M., Boche, E., Cailhol, D., Filipponi, M., Roux, P.L., Varrel, E., 2011. Topographie, représentation et analyse morphologique 3D de drains, de conduits et de parois du karst. Images et modèles 3D en milieux naturels. pp. 119–130.
James, J.M., Contos, A.K., Barnes, C.M., 2012. Nullarbor caves, Australia, In: White, William B., Culver, David C. (Eds.), Encyclopedia of Caves, second edition. Elsevier Science, pp. 568–576.
Jameson, R.A., 1985. Structural segments and the analysis of flow paths in the North Canyon of Snedegar Cave, Friars Hole Cave System. Master's Thesis West Virginia University, Morgantown.
Kuo, T.S., Liu, Z.Q., Li, H.C., Wan, N.J., Shen, C.C., Ku, T.L., 2011. Climate and environmental changes during the past millennium in central western Guizhou, China as recorded by Stalagmite ZJD-21. J. Asian Earth Sci. 40, 1111–1120.
Labourdette, R., Lascu, I., Mylroie, J., Roth, M., 2007. Process-like modeling of flank-margin caves: from genesis to burial evolution. J. Sediment. Res. 77, 965–979.
Lauritzen, S.E., Lundberg, J., 2000. Solutional and erosional morphology. Speleogenesis: Evolution of Karst Aquifers: Huntsville, AlaNational Speleological Society pp. 408–426.
Lowe, D.J., 1992. The Origin of Limestone Caverns: An Inception Horizon Hypothesis. Ph.D. Thesis Manchester Polytechnic, United Kingdom.
Lü, X., Yang, N., Zhou, X., Yang, H., Li, J., 2008. Influence of Ordovician carbonate reservoir beds in Tarim Basin by faulting. Sci. China Ser. D Earth Sci. 51, 53–60.
Mongelli, G., 2002. Growth of hematite and boehmite in concretions from ancient karst bauxite: clue for past climate. Catena 50, 43–51.
Morales, T., Uriarte, J.A., Olazar, M., Antigüedad, I., Angulo, B., 2010. Solute transport modelling in karst conduits with slow zones during different hydrologic conditions. J. Hydrol. 390, 182–189.
Onac, B.P., Constantin, S. (Eds.), 2008. Archives of climate and environmental change in karst. Quaternary International, 187.
Palmer, A.N., 2012. Solution caves in regions of moderate relief, In: White, William B., Culver, David C. (Eds.), Encyclopedia of Caves, second edition. Elsevier Science, pp. 733–743.
Pardo-Igúzquiza, E., Dowd, P.A., Chaoshui, X., Durán-Valsero, J.J., 2012. Stochastic simulation of karst conduit networks. Adv. Water Resour. 35, 141–150. http://dx.doi.org/10.1016/j.advwatres.2011.09.014.
Pardo-Igúzquiza, E., Durán-Valsero, J.J., Rodríguez-Galiano, V., 2011. Morphometric analysis of three-dimensional networks of karst conduits. Geomorphology 132, 17–28.
Parise, M., De Waele, J., Gutiérrez, F., 2009. Current perspectives on the environmental impacts and hazards in karst. Environ. Geol. 58, 235–237.
Pasini, G., 1967. Nota preliminare sul ruolo speleogenetico dell'erosione "antigravitativa". Le Grotte d'Italia. . , 4 pp. 75–90.
Renault, P., 1958. Eléments de spéléomorphologie karstique. Ann. Spéliol. 13, 23–48.
Renault, P., 1968. Contribution à l'étude des actions mécaniques et sédimentologiques dans la spéléogenèse. 3e partie: les facteurs sédimentologiques. Ann. Spéliol. 23, 529–596.
Sethian, J., 1996. A fast marching level set method for monotonically advancing fronts. Proc. Natl. Acad. Sci. 93, 1591–1595.
Sethian, J., 1999a. Fast marching methods. SIAM Rev. 41, 199–235.
Sethian, J., 1999b. Level Set Methods and Fast Marching Method. Cambridge University Press, Cambridge, United Kingdom.
Viles, H.A., 2003. Conceptual modeling of the impacts of climate change on karst geomorphology in the UK and Ireland. J. Nat. Conserv. 11, 59–66.

Bibliography

S. I. Aanonsen, G. Nævdal, D. S. Oliver, A. C. Reynolds, B. Vallès, and others. The Ensemble Kalman Filter in Reservoir Engineering – A Review. *SPE Journal*, 14(03):393–412, 2009. doi: 10.2118/117274-PA. *(Cited page 35)*

J. D. Abad, O. E. Sequeiros, B. Spinewine, C. Pirmez, M. H. Garcia, and G. Parker. Secondary Current of Saline Underflow In A Highly Meandering Channel: Experiments and Theory. *Journal of Sedimentary Research*, 81(11): 787–813, 2011. doi: 10.2110/jsr.2011.61. *(Cited page 17)*

V. Abreu, M. Sullivan, C. Pirmez, and D. Mohrig. Lateral accretion packages (LAPs): an important reservoir element in deep water sinuous channels. *Marine and Petroleum Geology*, 20(6-8):631–648, 2003. doi: 10.1016/j.marpetgeo.2003.08.003. *(Cited pages xxix, 2, 20, 24, 25, 162, and 163)*

G. J. J. Aleva. Indonesian fluvial cassiterite placers and their genetic environment. *Journal of the Geological Society*, 142(5):815–836, 1985. doi: 10.1144/gsjgs.142.5.0815. *(Cited page 2)*

D. Allard and H. Group. On the Connectivity of Two Random Set Models: The Truncated Gaussian and the Boolean. In A. Soares, editor, *Geostatistics Tróia '92*, number 5 in Quantitative Geology and Geostatistics, pages 467–478. Springer Netherlands, 1993. ISBN 978-0-7923-2157-6 978-94-011-1739-5. doi: 10.1007/978-94-011-1739-5_37. *(Cited page 36)*

F. O. Alpak, M. D. Barton, and S. J. Naruk. The impact of fine-scale turbidite channel architecture on deep-water reservoir performance. *AAPG Bulletin*, 97 (2):251–284, 2013. doi: 10.1306/04021211067. *(Cited pages 12 and 14)*

Z. Anka, M. Séranne, M. Lopez, M. Scheck-Wenderoth, and B. Savoye. The long-term evolution of the Congo deep-sea fan: A basin-wide view of the interaction between a giant submarine fan and a mature passive margin

(ZaiAngo project). *Tectonophysics*, 470(1–2):42–56, 2009. doi: 10.1016/j.tecto.2008.04.009. *(Cited pages xix and 5)*

P. Anquez, G. Rongier, and P. Collon. Stochastic simulations of karst networks with Lindenmayer systems. In *Proc. 35th Gocad Meeting*, Nancy, France, 2015. *(Cited page 202)*

D. A. Armitage, T. McHargue, A. Fildani, and S. A. Graham. Postavulsion channel evolution: Niger Delta continental slope. *AAPG Bulletin*, 96(5): 823–843, 2012. doi: 10.1306/09131110189. *(Cited page 25)*

R. W. C. Arnott. Stratal architecture and origin of lateral accretion deposits (LADs) and conterminuous inner-bank levee deposits in a base-of-slope sinuous channel, lower Isaac Formation (Neoproterozoic), East-Central British Columbia, Canada. *Marine and Petroleum Geology*, 24(6-9):515–528, 2007. doi: 10.1016/j.marpetgeo.2007.01.006. *(Cited page 162)*

G. B. Arpat and J. Caers. A Multiple-scale, Pattern-based Approach to Sequential Simulation. In O. Leuangthong and C. V. Deutsch, editors, *Geostatistics Banff 2004*, number 14 in Quantitative Geology and Geostatistics, pages 255–264. Springer Netherlands, 2004. ISBN 978-1-4020-3515-9 978-1-4020-3610-1. *(Cited page 32)*

O. Babak and C. V. Deutsch. An intrinsic model of coregionalization that solves variance inflation in collocated cokriging. *Computers & Geosciences*, 35(3): 603–614, Mar. 2009. doi: 10.1016/j.cageo.2008.02.025. *(Cited page 171)*

N. Babonneau, B. Savoye, M. Cremer, and B. Klein. Morphology and architecture of the present canyon and channel system of the Zaire deep-sea fan. *Marine and Petroleum Geology*, 19(4):445–467, 2002. doi: 10.1016/S0264-8172(02)00009-0. *(Cited pages xix and 5)*

N. Babonneau, B. Savoye, M. Cremer, and M. Bez. Sedimentary Architecture in Meanders of a Submarine Channel: Detailed Study of the Present Congo Turbidite Channel (Zaiango Project). *Journal of Sedimentary Research*, 80 (10):852–866, 2010. doi: 10.2110/jsr.2010.078. *(Cited page 122)*

C. Barthélemy and P. Collon-Drouaillet. Simulation of Anastomotic Karst Networks. In *Proc. 32nd Gocad Meeting*, page 13, Nancy, 2013. *(Cited page 47)*

R. T. Beaubouef. Deep-water leveed-channel complexes of the Cerro Toro Formation, Upper Cretaceous, southern Chile. *AAPG Bulletin*, 88(11):1471–1500, 2004. doi: 10.1306/06210403130. *(Cited page 12)*

B. J. Bluck, J. D. Ward, and M. C. J. D. Wit. Diamond mega-placers: southern Africa and the Kaapvaal craton in a global context. *Geological Society, London, Special Publications*, 248(1):213–245, 2005. doi: 10.1144/GSL.SP.2005.248.01.12. *(Cited page 2)*

M. D. Blum and T. E. Törnqvist. Fluvial responses to climate and sea-level change: a review and look forward. *Sedimentology*, 47:2–48, 2000. doi: 10.1046/j.1365-3091.2000.00008.x. *(Cited page 2)*

J. B. Boisvert, M. J. Pyrcz, and C. V. Deutsch. Multiple Point Metrics to Assess Categorical Variable Models. *Natural Resources Research*, 19(3):165–175, 2010. doi: 10.1007/s11053-010-9120-2. *(Cited pages xxxi, 39, and 71)*

C. E. Bond, A. D. Gibbs, Z. K. Shipton, and S. Jones. What do you think this is?"Conceptual uncertainty" in geoscience interpretation. *GSA today*, 17(11):4, 2007. doi: 10.1130/GSAT01711A.1. *(Cited page xliv)*

A. H. Bouma. Key controls on the characteristics of turbidite systems. *Geological Society, London, Special Publications*, 222(1):9–22, 2004. doi: 10.1144/GSL.SP.2004.222.01.02. *(Cited page 4)*

A. H. Bouma, P. H. Kuenen, and F. P. Shepard. *Sedimentology of some flysch deposits: a graphic approach to facies interpretation*, volume 168. Elsevier Amsterdam, 1962. *(Cited page 7)*

A. Braathen, K. Baelum, H. H. Christiansen, T. Dahl, O. Eiken, H. Elvebakk, F. Hansen, T. H. Hanssen, M. Jochmann, T. A. Johansen, H. Johnsen, L. Larsen, T. Lie, J. Mertes, A. Mørk, M. B. Mørk, W. Nemec, S. Olaussen, V. Oye, K. Rød, G. O. Titlestad, J. Tveranger, and K. Vagle. The Longyearbyen CO2 Lab of Svalbard, Norway – Initial assessment of the geological conditions for CO2 sequestration. *Norwegian Journal of Geology*, 92:353–376, 2012. *(Cited pages xxix, xxxix, xl, and 27)*

J. W. Brandt and V. R. Algazi. Continuous skeleton computation by Voronoi diagram. *CVGIP: Image Understanding*, 55(3):329–338, 1992. doi: 10.1016/1049-9660(92)90030-7. *(Cited page 47)*

J. C. Brice. Evolution of Meander Loops. *Geological Society of America Bulletin*, 85(4):581–586, 1974. doi: 10.1130/0016-7606(1974)85<581:EOML>2.0.CO;2. *(Cited page 147)*

S. G. Buck. The Saaiplaas Quartzite Member: A Braided System of Gold- and Uranium-Bearing Channel Placers within the Proterozoic Witwatersrand Supergroup of South Africa. In J. D. Collinson and J. Lewin, editors, *Modern and Ancient Fluvial Systems*, pages 549–562. Blackwell Publishing Ltd., 1983. ISBN 978-1-4443-0377-3. *(Cited pages xxxix and 2)*

K. M. Campion, A. R. G. Sprague, and M. D. Sullivan. *Architecture and Lithofacies of the Capistrano Formation (Miocene-Pliocene), San Clemente, California*. Annual Fieldtrip Guidebook, Pacific Section SEPM, Book 100, 2005. ISBN 1-878861-93-X. *(Cited pages xix and 8)*

C. Camporeale, P. Perona, A. Porporato, and L. Ridolfi. On the long-term behavior of meandering rivers. *Water resources research*, 41(12):W12403, 2005. doi: 10.1029/2005WR004109. *(Cited pages 181, 182, and 206)*

C. Camporeale, P. Perona, A. Porporato, and L. Ridolfi. Hierarchy of models for meandering rivers and related morphodynamic processes. *Reviews of Geophysics*, 45(1):RG1001, 2007. doi: 10.1029/2005RG000185. *(Cited pages xxxv and 164)*

M. A. Carson and M. F. Lapointe. The inherent asymmetry of river meander planform. *The Journal of Geology*, pages 41–55, 1983. doi: 10.1086/628743. *(Cited page 147)*

G. Caumon, P. Collon-Drouaillet, C. Le Carlier de Veslud, S. Viseur, and J. Sausse. Surface-Based 3D Modeling of Geological Structures. *Mathematical Geosciences*, 41(8):927–945, 2009. doi: 10.1007/s11004-009-9244-2. *(Cited page xliv)*

S. Chatterjee and R. Dimitrakopoulos. Pattern-based Simulation using Self Organized Maps. In *Geomatrix'12, International Conference on Geospatial Technologies and Applications*, pages 1–3, Indian Institute of Technology Bombay (IITB), 2012. *(Cited page 32)*

A. Comunian, P. Renard, and J. Straubhaar. 3D multiple-point statistics simulation using 2D training images. *Computers & Geosciences*, 40(0):49–65, 2012. doi: 10.1016/j.cageo.2011.07.009. *(Cited page 39)*

N. D. Cornea, D. Silver, and P. Min. Curve-skeleton properties, applications, and algorithms. *Visualization and Computer Graphics, IEEE Transactions on*, 13(3):530–548, 2007. doi: 10.1109/TVCG.2007.1002. *(Cited pages 47 and 213)*

R. K. Corney, J. Peakall, D. R. Parsons, L. Elliott, J. L. Best, R. E. Thomas, G. M. Keevil, D. B. Ingham, and K. J. Amos. Reply to discussion of Imran et al. on "The orientation of helical flow in curved channels" by Corney et al., Sedimentology, 53, 249–257. *Sedimentology*, 55(1):241–247, 2008. doi: 10.1111/j.1365-3091.2007.00925.x. *(Cited pages 17, 34, and 164)*

R. K. T. Corney, J. Peakall, D. R. Parsons, L. Elliott, K. J. Amos, J. L. Best, G. M. Keevil, and D. B. Ingham. The orientation of helical flow in curved channels. *Sedimentology*, 53(2):249–257, 2006. doi: 10.1111/j.1365-3091.2006.00771.x. *(Cited pages 17, 34, and 164)*

T. F. Cox and M. A. Cox. *Multidimensional scaling*. Chapman and Hall, London, 1994. ISBN 978-1-58488-094-3. *(Cited pages xxxii, 54, 55, and 56)*

B. T. Cronin, A. Hurst, H. Celik, and I. Türkmen. Superb exposure of a channel, levee and overbank complex in an ancient deep-water slope environment. *Sedimentary Geology*, 132(3-4):205–216, May 2000. doi: 10.1016/S0037-0738(00)00008-7. *(Cited page 12)*

A. Crosato. Effects of smoothing and regridding in numerical meander migration models. *Water Resources Research*, 43(1):W01401, 2007. doi: 10.1029/2006WR005087. *(Cited pages 179, 181, and 204)*

S. De Iaco. On the use of different metrics for assessing complex pattern reproductions. *Journal of Applied Statistics*, 40(4):808–822, 2013. doi: 10.1080/02664763.2012.754853. *(Cited pages xxxi and 39)*

S. De Iaco and S. Maggio. Validation Techniques for Geological Patterns Simulations Based on Variogram and Multiple-Point Statistics. *Mathematical Geosciences*, 43(4):483–500, 2011. doi: 10.1007/s11004-011-9326-9. *(Cited pages 39 and 210)*

J. De Leeuw. Applications of convex analysis to multidimensional scaling. In *Recent Developments in Statistics*, pages 133–146. J.R. Barra, F. Brodeau, G. Romier and B. Van Cutsem, Amsterdam, north holland publishing company edition, 1977. *(Cited page 56)*

J. De Leeuw and W. J. Heiser. Convergence of correction matrix algorithms for multidimensional scaling. *Geometric representations of relational data*, pages 735–752, 1977. *(Cited page 56)*

J. De Leeuw and W. J. Heiser. Multidimensional scaling with restrictions on the configuration. *Multivariate analysis*, 5:501–522, 1980. *(Cited page 56)*

J. De Leeuw and P. Mair. Multidimensional scaling using majorization: SMACOF in R. *Journal of Statistical Software*, 31(3):1–30, 2009. *(Cited page 58)*

M. E. Deptuck, G. S. Steffens, M. Barton, and C. Pirmez. Architecture and evolution of upper fan channel-belts on the Niger Delta slope and in the Arabian Sea. *Marine and Petroleum Geology*, 20(6-8):649–676, 2003. doi: 10.1016/j.marpetgeo.2003.01.004. *(Cited pages xix, xxiii, 9, 24, and 163)*

M. E. Deptuck, Z. Sylvester, C. Pirmez, and C. O'Byrne. Migration-aggradation history and 3-D seismic geomorphology of submarine channels in the Pleistocene Benin-major Canyon, western Niger Delta slope. *Marine and Petroleum Geology*, 24(6-9):406–433, 2007. doi: 10.1016/j.marpetgeo.2007.01.005. *(Cited pages 13 and 35)*

C. Deutsch and T. Tran. FLUVSIM: a program for object-based stochastic modeling of fluvial depositional systems. *Computers & Geosciences*, 28(4):525–535, 2002. doi: 10.1016/S0098-3004(01)00075-9. *(Cited pages xx, 31, 38, 86, 149, 154, 155, and 156)*

C. V. Deutsch. Fortran programs for calculating connectivity of three-dimensional numerical models and for ranking multiple realizations. *Computers & Geosciences*, 24(1):69–76, 1998. doi: 10.1016/S0098-3004(97)00085-X. *(Cited pages xx, xxxi, 39, 41, 46, and 210)*

C. V. Deutsch and T. A. Hewett. Challenges in reservoir forecasting. *Mathematical Geology*, 28(7):829–842, 1996. doi: 10.1007/BF02066003. *(Cited page 38)*

C. V. Deutsch and A. G. Journel. *GSLIB: Geostatistical Software Library and User's Guide*. Oxford University Press, New York, 1992. ISBN 978-0-19-510015-0. *(Cited pages xx, xlvi, 28, 29, 38, 86, and 169)*

C. V. Deutsch and L. Wang. Hierarchical object-based stochastic modeling of fluvial reservoirs. *Mathematical Geology*, 28(7):857–880, 1996. doi: 10.1007/BF02066005. *(Cited pages 30 and 33)*

R. M. Dorrell, S. E. Darby, J. Peakall, E. J. Sumner, D. R. Parsons, and R. B. Wynn. Superelevation and overspill control secondary flow dynamics in submarine channels. *Journal of Geophysical Research: Oceans*, 118(8):3895–3915, 2013. doi: 10.1002/jgrc.20277. *(Cited pages 20, 34, and 164)*

L. Droz, T. Marsset, H. Ondréas, M. Lopez, B. Savoye, and F.-L. Spy-Anderson. Architecture of an active mud-rich turbidite system: The Zaire Fan (Congo–Angola margin southeast Atlantic) Results from ZaïAngo 1 and 2 cruises. *AAPG Bulletin*, 87(7):1145–1168, 2003. doi: 10.1306/03070300013. *(Cited pages xix and 5)*

L. Droz, T. Marsset, B. Dennielou, N. Babonneau, B. Savoye, and M. Bez. Avulsion phenomenon: process and consequences on fan evolution. A new perspective from the Zaire (Congo) Turbidite System (ZaiAngo Project, Ifremer/Total). In *10th International Congress of the Brazilian Geophysical Society*, 2007. doi: 10.1190/sbgf2007-450. *(Cited pages 10 and 25)*

A. Einstein. The Cause of the Formation of Meanders in the Courses of Rivers and of the So-Called Baer's Law. *Die Naturwissenschaften*, 14:223–224, 1926. *(Cited page 16)*

D. J. Evans and R. A. Chadwick. *Underground Gas Storage: Worldwide Experiences and Future Development in the UK and Europe*. Geological Society of London, 2009. ISBN 978-1-86239-272-4. *(Cited page xxxix)*

J. Feder. Plex languages. *Information Sciences*, 3(3):225–241, July 1971. doi: 10.1016/S0020-0255(71)80008-7. *(Cited page 155)*

D. V. Fitterman, C. M. Menges, A. M. Al Kamali, and F. Essa Jama. Electromagnetic mapping of buried paleochannels in eastern Abu Dhabi Emirate, U.A.E. *Geoexploration*, 27(1-2):111–133, 1991. doi: 10.1016/0016-7142(91)90018-8. *(Cited pages xxix, xxxix, and 2)*

R. D. Flood and J. E. Damuth. Quantitative characteristics of sinuous distributary channels on the Amazon Deep-Sea Fan. *Geological Society of America Bulletin*, 98(6):728–738, 1987. doi: 10.1130/0016-7606(1987)98<728:QCOSDC>2.0.CO;2. *(Cited page 6)*

M. Gainski, A. G. MacGregor, P. J. Freeman, and H. F. Nieuwland. Turbidite reservoir compartmentalization and well targeting with 4D seismic and production data: Schiehallion Field, UK. *Geological Society, London, Special Publications*, 347(1):89–102, 2010. doi: 10.1144/SP347.7. *(Cited pages xix, xli, xlii, 14, 35, and 162)*

A. Galli, H. Beucher, G. L. Loc'h, B. Doligez, and H. Group. The Pros and Cons of the Truncated Gaussian Method. In M. Armstrong and P. A. Dowd, editors, *Geostatistical Simulations*, number 7 in Quantitative Geology and

Geostatistics, pages 217–233. Springer Netherlands, 1994. ISBN 978-90-481-4372-6 978-94-015-8267-4. doi: 10.1007/978-94-015-8267-4_18. *(Cited pages 28, 38, and 86)*

W. E. Galloway. Siliciclastic slope and base-of-slope depositional systems: component facies, stratigraphic architecture, and classification. *AAPG bulletin*, 82(4):569–595, 1998. doi: 10.1306/1D9BC5BB-172D-11D7-8645000102C1865D. *(Cited page 10)*

A. García-Gil, E. Vázquez-Suñe, M. M. Alcaraz, A. S. Juan, J. Á. Sánchez-Navarro, M. Montlleó, G. Rodríguez, and J. Lao. GIS-supported mapping of low-temperature geothermal potential taking groundwater flow into account. *Renewable Energy*, 77:268–278, 2015. doi: 10.1016/j.renene.2014.11.096. *(Cited page xxxix)*

R. Gaujoux and C. Seoighe. A flexible R package for nonnegative matrix factorization. *BMC Bioinformatics*, 11(1):367, 2010. doi: 10.1186/1471-2105-11-367. *(Cited page 58)*

M. Gennesseaux, A. Mauffret, and G. Pautot. Les glissements sous-marins de la pente continentale niçoise et la rupture de câbles en mer Ligure (Méditerranée occidentale). *Comptes Rendus de l'Académie des Sciences de Paris*, 290 (14):959–962, Jan. 1980. *(Cited page 3)*

F. Giorgio Serchi, J. Peakall, D. B. Ingham, and A. D. Burns. A unifying computational fluid dynamics investigation on the river-like to river-reversed secondary circulation in submarine channel bends. *Journal of Geophysical Research: Oceans*, 116(C6):C06012, 2011. doi: 10.1029/2010JC006361. *(Cited page 17)*

J. Gómez-Hernández and X.-H. Wen. To be or not to be multi-Gaussian? A reflection on stochastic hydrogeology. *Advances in Water Resources*, 21(1): 47–61, 1998. doi: 10.1016/S0309-1708(96)00031-0. *(Cited page 38)*

J. C. Gower. Some distance properties of latent root and vector methods used in multivariate analysis. *Biometrika*, 53(3-4):325–338, 1966. doi: 10.1093/biomet/53.3-4.325. *(Cited page 55)*

E. Gringarten and C. V. Deutsch. Teacher's Aide Variogram Interpretation and Modeling. *Mathematical Geology*, 33(4):507–534, 2001. doi: 10.1023/A:1011093014141. *(Cited page 172)*

S.-A. Grundvåg, E. P. Johannessen, W. Helland-Hansen, and P. Plink-Björklund. Depositional architecture and evolution of progradationally stacked lobe complexes in the Eocene Central Basin of Spitsbergen. *Sedimentology*, 61(2): 535–569, 2014. doi: 10.1111/sed.12067. *(Cited pages xix and xl)*

F. B. Guardiano and R. M. Srivastava. Multivariate Geostatistics: Beyond Bivariate Moments. In A. Soares, editor, *Geostatistics Tróia '92*, number 5 in Quantitative Geology and Geostatistics, pages 133–144. Springer Netherlands, 1993. ISBN 978-0-7923-2157-6 978-94-011-1739-5. *(Cited pages 30, 38, and 173)*

M. C. Hanna, D. Uffen, S. Emsley, and T. Inks. Reliable Geophysics. *CSEG recorder*, April 2015:53–59, 2015. *(Cited pages xix and xliii)*

M. M. Hassanpour, M. J. Pyrcz, and C. V. Deutsch. Improved geostatistical models of inclined heterolithic strata for McMurray Formation, Alberta, Canada. *AAPG Bulletin*, 97(7):1209–1224, 2013. doi: 10.1306/01021312054. *(Cited pages 31, 150, 153, 154, 155, and 211)*

J. C. Hernández Del Pozo, I. Ocete, R. García, and R. Carmona. Locating hidden river courses via geo-technical investigation? Application in the city of Granada, Spain. *Natural Hazards and Earth System Science*, 5(6):911–923, 2005. doi: 10.5194/nhess-5-911-2005. *(Cited page 2)*

E. J. Hill and C. M. Griffiths. Describing and generating facies models for reservoir characterisation: 2D map view. *Marine and Petroleum Geology*, 26(8):1554–1563, 2009. doi: 10.1016/j.marpetgeo.2008.09.004. *(Cited pages 87, 153, and 155)*

A. D. Howard. Modeling channel migration and floodplain sedimentation in meandering streams. *Lowland floodplain rivers: geomorphological perspectives*, pages 1–41, 1992. *(Cited page 181)*

A. D. Howard and A. T. Hemberger. Multivariate characterization of meandering. *Geomorphology*, 4(3-4):161–186, 1991. doi: 10.1016/0169-555X(91)90002-R. *(Cited pages 104 and 202)*

S. Ikeda, G. Parker, and K. Sawai. Bend theory of river meanders. Part 1. Linear development. *Journal of Fluid Mechanics*, 112:363–377, 1981. doi: 10.1017/S0022112081000451. *(Cited pages 16, 34, 164, and 203)*

J. Imran, G. Parker, and C. Pirmez. A nonlinear model of flow in meandering submarine and subaerial channels. *Journal of Fluid Mechanics*, 400:295–331, Dec. 1999. doi: 10.1017/S0022112099006515. *(Cited pages 16, 34, and 164)*

J. Imran, M. A. Islam, H. Huang, A. Kassem, J. Dickerson, C. Pirmez, and G. Parker. Helical flow couplets in submarine gravity underflows. *Geology*, 35(7):659–662, 2007. doi: 10.1130/G23780A.1. *(Cited page 17)*

J. Imran, M. A. Islam, and A. Kassem. "The orientation of helical flow in curved channels" by Corney et al., Sedimentology, Vol. 53, pp. 249–257 – discussion. *Sedimentology*, 55(1):235–239, 2008. doi: 10.1111/j.1365-3091.2007.00924.x. *(Cited pages 17, 34, and 164)*

M. A. Islam, J. Imran, C. Pirmez, and A. Cantelli. Flow splitting modifies the helical motion in submarine channels. *Geophysical Research Letters*, 35(22), 2008. doi: 10.1029/2008GL034995. *(Cited page 17)*

A. K. Jain. *Fundamentals of digital image processing*, volume 3. Prentice-Hall Englewood Cliffs, 1989. ISBN 978-0-13-336165-0. *(Cited page 47)*

M. Janocko, M. B. J. Cartigny, W. Nemec, and E. W. M. Hansen. Turbidity current hydraulics and sediment deposition in erodible sinuous channels: Laboratory experiments and numerical simulations. *Marine and Petroleum Geology*, 41:222–249, 2013a. doi: 10.1016/j.marpetgeo.2012.08.012. *(Cited pages xx, 17, 19, 20, and 22)*

M. Janocko, W. Nemec, S. Henriksen, and M. Warchoł. The diversity of deep-water sinuous channel belts and slope valley-fill complexes. *Marine and Petroleum Geology*, 41:7–34, 2013b. doi: 10.1016/j.marpetgeo.2012.06.012. *(Cited pages 2, 7, and 9)*

E. Johannessen, T. Henningsen, N. Bakke, T. Johansen, B. Ruud, P. Riste, H. Elvebakk, M. Jochmann, G. Elvebakk, and M. Woldengen. Palaeogene clinoform succession on Svalbard expressed in outcrops, seismic data, logs and cores. *First Break*, 29(1768), 2011. doi: 10.3997/1365-2397.2011004. *(Cited pages xix and xl)*

E. P. Johannessen and R. J. Steel. Shelf-margin clinoforms and prediction of deepwater sands. *Basin Research*, 17(4):521–550, 2005. doi: 10.1111/j.1365-2117.2005.00278.x. *(Cited pages xix and xl)*

H. Johannesson and G. Parker. Secondary Flow in Mildly Sinuous Channel. *Journal of Hydraulic Engineering*, 115(3):289–308, 1989. doi: 10.1061/(ASCE)0733-9429(1989)115:3(289). *(Cited page 16)*

A. Journel and F. Alabert. New method for reservoir mapping. *Journal of Petroleum technology*, 42(2):212–218, 1990. doi: 10.2118/18324-PA. *(Cited page 38)*

A. Journel and T. Zhang. The Necessity of a Multiple-Point Prior Model. *Mathematical Geology*, 38(5):591–610, 2006. doi: 10.1007/s11004-006-9031-2. *(Cited page 32)*

P. Jussel, F. Stauffer, and T. Dracos. Transport modeling in heterogeneous aquifers: 1. Statistical description and numerical generation of gravel deposits. *Water Resources Research*, 30(6):1803–1817, 1994. doi: 10.1029/94WR00162. *(Cited pages xxxix and 2)*

G. M. Keevil, J. Peakall, J. L. Best, and K. J. Amos. Flow structure in sinuous submarine channels: Velocity and turbulence structure of an experimental submarine channel. *Marine Geology*, 229(3-4):241–257, 2006. doi: 10.1016/j.margeo.2006.03.010. *(Cited page 17)*

M. King and M. Mark. Flow Simulation of Geologic Models. *SPE Reservoir Evaluation & Engineering*, 2(4):351–367, 1999. doi: 10.2118/57469-PA. *(Cited page 38)*

R. Kinoshita. An investigation of channel deformation of the Ishikari River. Publication no. 36. *Natural Resources Division, Ministry of Science and Technology of Japan*, 1961. *(Cited page 147)*

B. Kneller and C. Buckee. The structure and fluid mechanics of turbidity currents: a review of some recent studies and their geological implications. *Sedimentology*, 47:62–94, 2000. doi: 10.1046/j.1365-3091.2000.047s1062.x. *(Cited page 3)*

V. Kolla. A review of sinuous channel avulsion patterns in some major deep-sea fans and factors controlling them. *Marine and Petroleum Geology*, 24(6-9):450–469, 2007. doi: 10.1016/j.marpetgeo.2007.01.004. *(Cited pages xxix, 9, 20, 24, 25, 30, and 215)*

V. Kolla, P. Bourges, J.-M. Urruty, and P. Safa. Evolution of Deep-Water Tertiary Sinuous Channels Offshore Angola (West Africa) and

Implications for Reservoir Architecture. *AAPG Bulletin*, 85(8):1373–1405, 2001. doi: 10.1306/8626CAC3-173B-11D7-8645000102C1865D. *(Cited pages xx, xxiii, 26, 147, and 148)*

V. Kolla, H. W. Posamentier, and L. J. Wood. Deep-water and fluvial sinuous channels—Characteristics, similarities and dissimilarities, and modes of formation. *Marine and Petroleum Geology*, 24(6-9):388–405, June 2007. doi: 10.1016/j.marpetgeo.2007.01.007. *(Cited pages 10 and 25)*

P. D. Komar. The channelized flow of turbidity currents with application to Monterey Deep-Sea Fan Channel. *Journal of Geophysical Research*, 74(18): 4544–4558, Aug. 1969. doi: 10.1029/JC074i018p04544. *(Cited page 3)*

A. A. Konstantinovskii. Perspectives of the discovery of complex (gold and platinum group metal) paleoplacers in the eastern Baltic Shield. *Lithology and Mineral Resources*, 40(1):9–20, 2005. doi: 10.1007/s10987-005-0002-3. *(Cited page 2)*

R. Labourdette. Integrated three-dimensional modeling approach of stacked turbidite channels. *AAPG Bulletin*, 91(11):1603–1618, 2007. doi: 10.1306/06210706143. *(Cited pages xxix, 2, 12, 13, and 14)*

R. Labourdette. 'LOSCS' Lateral Offset Stacked Channel Simulations: Towards geometrical modelling of turbidite elementary channels. *Basin Research*, 20(3):431–444, 2008. doi: 10.1111/j.1365-2117.2008.00361.x. *(Cited pages xxxv, 164, 165, 204, and 205)*

R. Labourdette and M. Bez. Element migration in turbidite systems: Random or systematic depositional processes? *AAPG Bulletin*, 94(3):345–368, 2010. doi: 10.1306/09010909035. *(Cited pages xx and 23)*

R. Labourdette, J. Poncet, J. Seguin, F. Temple, J. Hegre, and A. Irving. Three-dimensional modelling of stacked turbidite channels in West Africa: impact on dynamic reservoir simulations. *Petroleum Geoscience*, 12(4):335–345, 2006. doi: 10.1144/1354-079306-705. *(Cited pages 13, 14, 35, 38, and 162)*

E. Lajeunesse, L. Malverti, P. Lancien, L. Armstrong, F. Métivier, S. Coleman, C. E. Smith, T. Davies, A. Cantelli, and G. Parker. Fluvial and submarine morphodynamics of laminar and near-laminar flows: a synthesis. *Sedimentology*, 57(1):1–26, 2010. doi: 10.1111/j.1365-3091.2009.01109.x. *(Cited pages xx and 17)*

W. B. Langbein and L. B. Leopold. *River meanders – Theory of minimum variance*. US Government Printing Office, 1966. ISBN 978-1-288-97435-1. *(Cited page 147)*

D. K. Larue and J. Hovadik. Why Is Reservoir Architecture an Insignificant Uncertainty in Many Appraisal and Development Studies of Clastic Channelized Reservoirs? *Journal of Petroleum Geology*, 31(4):337–366, 2008. doi: 10.1111/j.1747-5457.2008.00426.x. *(Cited pages 14, 111, and 116)*

T. C. Lee, R. L. Kashyap, and C. N. Chu. Building Skeleton Models via 3-D Medial Surface Axis Thinning Algorithms. *CVGIP: Graphical Models and Image Processing*, 56(6):462–478, 1994. doi: 10.1006/cgip.1994.1042. *(Cited page 47)*

D. Leitner, S. Klepsch, G. Bodner, and A. Schnepf. A dynamic root system growth model based on L-Systems. *Plant and Soil*, 332(1-2):177–192, 2010. doi: 10.1007/s11104-010-0284-7. *(Cited page 86)*

J. Lin. Divergence measures based on the Shannon entropy. *Information Theory, IEEE Transactions on*, 37(1):145–151, 1991. doi: 10.1109/18.61115. *(Cited page 53)*

A. Lindenmayer. Mathematical models for cellular interactions in development I. Filaments with one-sided inputs. *Journal of Theoretical Biology*, 18(3):280–299, 1968. doi: 10.1016/0022-5193(68)90079-9. *(Cited pages xxxiv and 86)*

Y. Liu and A. Journel. Improving Sequential Simulation with a Structured Path Guided by Information Content. *Mathematical Geology*, 36(8):945–964, 2004. doi: 10.1023/B:MATG.0000048800.72104.de. *(Cited page 32)*

S. Longay, A. Runions, F. Boudon, and P. Prusinkiewicz. Treesketch: interactive procedural modeling of trees on a tablet. In *Proceedings of the international symposium on sketch-based interfaces and modeling*, pages 107–120. Eurographics Association, 2012. doi: 10.2312/SBM/SBM12/107-120. *(Cited page 107)*

S. Lopez. *Modélisation de réservoirs chenalisés méandriformes : une approche génétique et stochastique*. PhD thesis, Ecole Nationale Supérieure des Mines de Paris, 2003. *(Cited pages xxxv, 34, 38, 149, 164, 202, 203, 206, 207, 211, and 214)*

D. R. Lowe. Sediment gravity flows; II, Depositional models with special reference to the deposits of high-density turbidity currents. *Journal of Sedimentary Research*, 52(1):279–297, 1982. doi: 10.1306/212F7F31-2B24-11D7-8648000102C1865D. *(Cited page 7)*

S. M. Luthi and S. S. Flint. The application of outcrop-based research boreholes for reservoir modelling: potential, challenges and pitfalls. *Geological Society, London, Special Publications*, 387(1):233–246, 2014. doi: 10.1144/SP387.6. *(Cited page xl)*

R. V. Macauley and S. M. Hubbard. Slope channel sedimentary processes and stratigraphic stacking, Cretaceous Tres Pasos Formation slope system, Chilean Patagonia. *Marine and Petroleum Geology*, 41:146–162, 2013. doi: 10.1016/j.marpetgeo.2012.02.004. *(Cited page 7)*

K. L. Maier, A. Fildani, T. R. McHargue, C. K. Paull, S. A. Graham, and D. W. Caress. Punctuated Deep-Water Channel Migration: High-Resolution Subsurface Data from the Lucia Chica Channel System, Offshore California, U.S.A. *Journal of Sedimentary Research*, 82(1):1–8, 2012. doi: 10.2110/jsr.2012.10. *(Cited pages xx and 24)*

J.-L. Mallet. Space-Time Mathematical Framework for Sedimentary Geology. *Mathematical Geology*, 36(1):1–32, 2004. doi: 10.1023/B:MATG.0000016228.75495.7c. *(Cited pages xxii, 95, and 96)*

G. Mariethoz. *Geological stochastic imaging for aquifer characterization*. PhD thesis, Université de Neuchâtel, 2009. *(Cited page 44)*

G. Mariethoz and J. Caers. *Multiple-point Geostatistics: Stochastic Modeling with Training Images*. John Wiley & Sons, 2014. *(Cited page xlvi)*

G. Mariethoz, P. Renard, and J. Straubhaar. The Direct Sampling method to perform multiple-point geostatistical simulations. *Water Resources Research*, 46(11):W11536, 2010. doi: 10.1029/2008WR007621. *(Cited pages 30, 39, 58, and 175)*

G. Mariethoz, A. Comunian, I. Irarrazaval, and P. Renard. Analog-based meandering channel simulation. *Water Resources Research*, 50(2):836–854, 2014. doi: 10.1002/2013WR013730. *(Cited pages 33, 205, and 211)*

J. H. Martin. A review of braided fluvial hydrocarbon reservoirs: the petroleum engineer's perspective. *Geological Society, London, Special Pub-*

lications, 75(1):333–367, 1993. doi: 10.1144/GSL.SP.1993.075.01.20. *(Cited pages xxxix and 2)*

M. Mayall and C. O'Byrne. Reservoir Prediction and Development Challenges in Turbidite Slope Channels. In *Offshore Technology Conference*, Houston, Texas U.S.A., 2002. doi: 10.4043/14029-MS. *(Cited pages 12, 14, and 162)*

M. Mayall, E. Jones, and M. Casey. Turbidite channel reservoirs – Key elements in facies prediction and effective development. *Marine and Petroleum Geology*, 23(8):821–841, 2006. doi: 10.1016/j.marpetgeo.2006.08.001. *(Cited pages xxix, xxxix, 2, 7, 9, 12, 13, 14, and 35)*

P. J. McCabe, D. L. Gautier, M. D. Lewan, and C. Turner. The future of energy gases. USGS Numbered Series Circular 1115, Dept. of the Interior, U.S. Geological Survey, USGS Map Distribution ; U.S. G.P.O., 1993. *(Cited page xxxix)*

T. McHargue, M. Pyrcz, M. Sullivan, J. Clark, A. Fildani, B. Romans, J. Covault, M. Levy, H. Posamentier, and N. Drinkwater. Architecture of turbidite channel systems on the continental slope: Patterns and predictions. *Marine and Petroleum Geology*, 28(3):728–743, 2011. doi: 10.1016/j.marpetgeo.2010.07.008. *(Cited pages xx, xxix, 7, 12, 13, 23, 34, 133, and 164)*

E. Meerschman, G. Pirot, G. Mariethoz, J. Straubhaar, M. V. Meirvenne, and P. Renard. A Practical Guide to Performing Multiple-Point Statistical Simulations with the Direct Sampling Algorithm. *Computers & Geosciences*, 52:307–324, 2012. doi: 10.1016/j.cageo.2012.09.019. *(Cited pages 39 and 178)*

G. V. Middleton and M. A. Hampton. Sediment gravity flows: mechanics of flow and deposition. In G. Middleton and A. Bouma, editors, *Turbidites and Deep-water Sedimentation*, page 38. Pacific Section Society of Economic Paleontologists and Mineralogists, Los Angeles, 1973. *(Cited page 3)*

J. M. Moore, A. D. Howard, W. E. Dietrich, and P. M. Schenk. Martian Layered Fluvial Deposits: Implications for Noachian Climate Scenarios. *Geophysical Research Letters*, 30(24):2292, 2003. doi: 10.1029/2003GL019002. *(Cited page 2)*

T. Mulder and J. Alexander. The physical character of subaqueous sedimentary density flows and their deposits. *Sedimentology*, 48(2):269–299, 2001. doi: 10.1046/j.1365-3091.2001.00360.x. *(Cited page 3)*

T. Mulder and S. Etienne. Lobes in deep-sea turbidite systems: State of the art. *Sedimentary Geology*, 229(3):75–80, 2010. doi: 10.1016/j.sedgeo.2010.06.011. *(Cited page 10)*

A. E. Mulligan, R. L. Evans, and D. Lizarralde. The role of paleochannels in groundwater/seawater exchange. *Journal of Hydrology*, 335(3-4):313–329, 2007. doi: 10.1016/j.jhydrol.2006.11.025. *(Cited page 2)*

E. Mutti and W. R. Normark. An Integrated Approach to the Study of Turbidite Systems. In P. Weimer and M. H. Link, editors, *Seismic Facies and Sedimentary Processes of Submarine Fans and Turbidite Systems*, Frontiers in Sedimentary Geology, pages 75–106. Springer New York, 1991. ISBN 978-1-4684-8278-2 978-1-4684-8276-8. doi: 10.1007/978-1-4684-8276-8_4. *(Cited page 6)*

R. Mvech and P. Prusinkiewicz. Visual models of plants interacting with their environment. In *Proceedings of the 23rd annual conference on Computer graphics and interactive techniques*, pages 397–410, 1996. doi: 10.1145/237170.237279. *(Cited pages 86 and 94)*

T. Nakajima, J. Peakall, W. D. McCaffrey, D. A. Paton, and P. J. P. Thompson. Outer-Bank Bars: A New Intra-Channel Architectural Element within Sinuous Submarine Slope Channels. *Journal of Sedimentary Research*, 79(12):872–886, 2009. doi: 10.2110/jsr.2009.094. *(Cited pages 22, 162, 201, and 202)*

W. R. Normark, H. Posamentier, and E. Mutti. Turbidite systems: State of the art and future directions. *Reviews of Geophysics*, 31(2):91–116, 1993. doi: 10.1029/93RG02832. *(Cited page 6)*

D. S. Oliver. Conditioning Channel Meanders to Well Observations. *Mathematical Geology*, 34(2):185–201, 2002. doi: 10.1023/A:1014464202497. *(Cited pages 33 and 211)*

D. S. Oliver and Y. Chen. Recent progress on reservoir history matching: a review. *Computational Geosciences*, 15(1):185–221, 2010. doi: 10.1007/s10596-010-9194-2. *(Cited page 35)*

M. P. O'Neill and A. D. Abrahams. Objective identification of meanders and bends. *Journal of Hydrology*, 83(3):337–353, 1986. doi: 10.1016/0022-1694(86)90160-5. *(Cited page 203)*

F. Oriani and P. Renard. Binary upscaling on complex heterogeneities: The role of geometry and connectivity. *Advances in Water Resources*, 64:47–61, 2014. doi: 10.1016/j.advwatres.2013.12.003. *(Cited page 44)*

R. Ostermeier. Compaction Effects on Porosity and Permeability: Deepwater Gulf of Mexico Turbidite. *Journal of Petroleum Technology*, 53(02):68–74, 2001. doi: 10.2118/66479-JPT. *(Cited page 27)*

W. Palubicki, K. Horel, S. Longay, A. Runions, B. Lane, R. Měch, and P. Prusinkiewicz. Self-organizing Tree Models for Image Synthesis. In *ACM SIGGRAPH 2009 Papers*, SIGGRAPH '09, pages 58:1–58:10, New York, NY, USA, 2009. ACM. ISBN 978-1-60558-726-4. doi: 10.1145/1576246.1531364. *(Cited page 86)*

Paradigm. SKUA® Software Suite by Paradigm®. `http://www.pdgm.com/products/skua-gocad/`, 2015. *(Cited page 58)*

G. Parker, Y. Shimizu, G. V. Wilkerson, E. C. Eke, J. D. Abad, J. W. Lauer, C. Paola, W. E. Dietrich, and V. R. Voller. A new framework for modeling the migration of meandering rivers. *Earth Surface Processes and Landforms*, 36 (1):70–86, 2011. doi: 10.1002/esp.2113. *(Cited page 203)*

M. Parquer, J. Ruiu, G. Caumon, P. Collon, and G. Rongier. Towards more genetics concepts and data integration in channel simulation. In *Proc. 35th Gocad Meeting*, Nancy, France, 2015. *(Cited pages 158, 165, and 206)*

J. Peakall, B. McCaffrey, and B. Kneller. A Process Model for the Evolution, Morphology, and Architecture of Sinuous Submarine Channels. *Journal of Sedimentary Research*, 70(3):434–448, 2000. doi: 10.1306/2DC4091C-0E47-11D7-8643000102C1865D. *(Cited pages 21, 22, 25, and 162)*

L. Piegl and W. Tiller. *The NURBS book*. Springer, London, 1995. ISBN 978-3-642-59223-2. *(Cited page 97)*

D. J. W. Piper and W. R. Normark. Sandy Fans-From Amazon to Hueneme and Beyond. *AAPG Bulletin*, 85(8):1407–1438, Jan. 2001. doi: 10.1306/8626CACD-173B-11D7-8645000102C1865D. *(Cited page 4)*

D. J. W. Piper, P. Cochonat, and M. L. Morrison. The sequence of events around the epicentre of the 1929 Grand Banks earthquake: initiation of debris flows and turbidity current inferred from sidescan sonar. *Sedimentology*, 46(1): 79–97, 1999. doi: 10.1046/j.1365-3091.1999.00204.x. *(Cited page 3)*

C. Pirmez and J. Imran. Reconstruction of turbidity currents in Amazon Channel. *Marine and Petroleum Geology*, 20(6-8):823–849, June 2003. doi: 10.1016/j.marpetgeo.2003.03.005. *(Cited page 3)*

H. W. Posamentier. Depositional elements associated with a basin floor channel-levee system: case study from the Gulf of Mexico. *Marine and Petroleum Geology*, 20(6-8):677–690, 2003. doi: 10.1016/j.marpetgeo.2003.01.002. *(Cited pages xx, 21, 22, 25, 27, and 162)*

M. J. Pranter and N. K. Sommer. Static connectivity of fluvial sandstones in a lower coastal-plain setting: An example from the Upper Cretaceous lower Williams Fork Formation, Piceance Basin, Colorado. *AAPG Bulletin*, 95(6): 899–923, 2011. doi: 10.1306/12091010008. *(Cited pages xxxix and 2)*

A. Prélat, D. M. Hodgson, and S. S. Flint. Evolution, architecture and hierarchy of distributary deep-water deposits: a high-resolution outcrop investigation from the Permian Karoo Basin, South Africa. *Sedimentology*, 56(7):2132–2154, 2009. doi: 10.1111/j.1365-3091.2009.01073.x. *(Cited page 10)*

A. Prélat, J. A. Covault, D. M. Hodgson, A. Fildani, and S. S. Flint. Intrinsic controls on the range of volumes, morphologies, and dimensions of submarine lobes. *Sedimentary Geology*, 232(1-2):66–76, 2010. doi: 10.1016/j.sedgeo.2010.09.010. *(Cited pages xx and 11)*

P. Prusinkiewicz. Graphical applications of L-systems. In *Proceedings of graphics interface*, volume 86, pages 247–253, 1986. *(Cited page 90)*

P. Prusinkiewicz and A. Lindenmayer. *The Algorithmic Beauty of Plants*. Springer-Verlag, New York, NY, USA, 1996. ISBN 978-1-4613-8476-2. *(Cited pages xxii, 86, 89, 94, and 95)*

P. Prusinkiewicz, M. James, and R. Měch. Synthetic topiary. In *Proceedings of the 21st annual conference on Computer graphics and interactive techniques*, pages 351–358. ACM, 1994. doi: 10.1145/192161.192254. *(Cited page 94)*

P. Prusinkiewicz, L. Mündermann, R. Karwowski, and B. Lane. The use of positional information in the modeling of plants. In *Proceedings of the 28th annual conference on Computer graphics and interactive techniques*, pages 289–300, 2001. doi: 10.1145/383259.383291. *(Cited page 213)*

M. Pyrcz, J. Boisvert, and C. Deutsch. ALLUVSIM: A program for event-based stochastic modeling of fluvial depositional systems. *Computers & Geosciences*, 35(8):1671–1685, 2009. doi: 10.1016/j.cageo.2008.09.012. *(Cited pages xxxi, xxxv, 34, 38, 86, 97, 149, 164, 168, 202, 203, 211, and 214)*

M. J. Pyrcz and C. V. Deutsch. *Geostatistical reservoir modeling*. Oxford university press, 2014. *(Cited page xlvi)*

M. J. Pyrcz, T. McHargue, J. Clark, M. Sullivan, and S. Strebelle. Event-Based Geostatistical Modeling: Description and Applications. In P. Abrahamsen, R. Hauge, and O. Kolbjørnsen, editors, *Geostatistics Oslo 2012*, number 17 in Quantitative Geology and Geostatistics, pages 27–38. Springer Netherlands, Jan. 2012. ISBN 978-94-007-4152-2 978-94-007-4153-9. *(Cited page 33)*

R Core Team. *R: A Language and Environment for Statistical Computing*. R Foundation for Statistical Computing, Vienna, Austria, 2012. ISBN 3-900051-07-0. *(Cited page 58)*

C. R. Rao. Differential metrics in probability spaces. *Differential geometry in statistical inference*, 10:217–240, 1987. doi: doi:10.1214/lnms/1215467062. *(Cited page 53)*

H. G. Reading and M. Richards. Turbidite systems in deep-water basin margins classified by grain size and feeder system. *AAPG bulletin*, 78(5):792–822, 1994. *(Cited page 4)*

P. Renard, J. Straubhaar, J. Caers, and G. Mariethoz. Conditioning Facies Simulations with Connectivity Data. *Mathematical Geosciences*, 43(8):879–903, 2011. doi: 10.1007/s11004-011-9363-4. *(Cited pages 36, 40, and 43)*

M. Richards, M. Bowman, and H. Reading. Submarine-fan systems i: characterization and stratigraphic prediction. *Marine and Petroleum Geology*, 15(7): 689–717, 1998. doi: 10.1016/S0264-8172(98)00036-1. *(Cited page 4)*

G. Rongier, P. Collon, P. Renard, and J. Ruiu. Channel simulation using L-system, potential fields and NURBS. In *Proc. 35th Gocad Meeting*, Nancy, France, 2015. *(Cited pages xix and xxxiii)*

I. L. Rozovskiĭ. *Flow of water in bends of open channels*. Academy of Sciences of the Ukrainian SSR (translated from Russian by the Israel Program for Scientific Translations, Jerusalem, 1961), Kiev, 1957. *(Cited page 16)*

J. Ruiu, G. Caumon, and S. Viseur. Semiautomatic interpretation of 3D sedimentological structures on geologic images: An object-based approach. *Interpretation*, 3(3):SX63–SX74, 2015a. doi: 10.1190/INT-2015-0004.1. *(Cited pages 33, 111, and 167)*

J. Ruiu, G. Caumon, and S. Viseur. Modeling Channel Forms and Related Sedimentary Objects Using a Boundary Representation Based on Non-uniform Rational B-Splines. *Mathematical Geosciences*, pages 1–26, 2015b. doi: 10.1007/s11004-015-9629-3. *(Cited pages 31, 89, 97, 98, 133, 159, 165, 166, and 214)*

T. Salles. *Modélisation numérique du remplissage sédimentaire des canyons et chenaux sous-marins par approche génétique*. PhD thesis, Université Bordeaux 1, Bordeaux, 2006. *(Cited pages xx, 3, and 18)*

C. Scheidt and J. Caers. Representing Spatial Uncertainty Using Distances and Kernels. *Mathematical Geosciences*, 41(4):397–419, 2009. doi: 10.1007/s11004-008-9186-0. *(Cited page 39)*

Schlumberger. Petrel E&p Software Platform. `http://www.software.slb.com/products/platform/Pages/petrel.aspx`, 2015. *(Cited page 58)*

J. Schwenk, S. Lanzoni, and E. Foufoula-Georgiou. The life of a meander bend: connecting shape and dynamics via analysis of a numerical model. *Journal of Geophysical Research: Earth Surface*, page 2014JF003252, 2015. doi: 10.1002/2014JF003252. *(Cited pages 179, 180, 181, 182, and 206)*

J. Serra. *Image Analysis and Mathematical Morphology*. Academic Press, Inc., Orlando, FL, USA, 1983. ISBN 978-0-12-637240-3. *(Cited page 47)*

G. Shanmugam. Ten turbidite myths. *Earth-Science Reviews*, 58(3-4):311–341, 2002. doi: 10.1016/S0012-8252(02)00065-X. *(Cited page 3)*

G. Shanmugam and R. J. Moiola. Submarine fans: Characteristics, models, classification, and reservoir potential. *Earth-Science Reviews*, 24(6):383–428, 1988. doi: 10.1016/0012-8252(88)90064-5. *(Cited pages 10 and 12)*

G. Shanmugam, T. D. Spalding, and D. H. Rofheart. Process sedimentology and reservoir quality of deep-marine bottom-current reworked sands (sandy contourites); an example from the Gulf of Mexico. *AAPG Bulletin*, 77(7):1241–1259, 1993. *(Cited pages xix and 7)*

R. N. Shepard. The analysis of proximities: Multidimensional scaling with an unknown distance function. I. *Psychometrika*, 27(2):125–140, 1962a. doi: 10.1007/BF02289630. *(Cited page 39)*

R. N. Shepard. The analysis of proximities: Multidimensional scaling with an unknown distance function. II. *Psychometrika*, 27(3):219–246, 1962b. doi: 10.1007/BF02289621. *(Cited page 39)*

L. E. Shmaryan and C. V. Deutsch. Object-based modeling of fluvial/deepwater reservoirs with fast data conditioning: methodology and case studies. In *SPE annual technical conference*, pages 877–886, 1999. doi: 10.2118/56821-MS. *(Cited page 33)*

A. Shtuka, P. Samson, and J. L. Mallet. Petrophysical simulation within an object-based reservoir model. In *European 3-D reservoir modelling conference*, pages 47–56, 1996. *(Cited pages 33 and 40)*

J. W. Snedden. Channel-body basal scours: Observations from 3D seismic and importance for subsurface reservoir connectivity. *Marine and Petroleum Geology*, 39(1):150–163, 2013. doi: 10.1016/j.marpetgeo.2012.08.013. *(Cited page 2)*

A. R. G. Sprague,, M. D. Sullivan, K. M. Campion, G. N. Jensen, F. J. Goulding, T. R. Garfield, D. K. Sickafoose, C. Rossen, D. C. Jennette, R. T. Beaubouef, V. Abreu, J. A. Ardill, M. L. Porter, and F. B. Zelt. The Physical Stratigraphy of Deep-Water Strata: A Hierarchical Approach to the Analysis of Genetically Related Stratigraphic Elements for Improved Reservoir Prediction. In *AAPG Annual Meeting*, Houston, Texas, USA, 2002. *(Cited pages 6 and 7)*

D. a. V. Stow and A. J. Bowen. A physical model for the transport and sorting of fine-grained sediment by turbidity currents. *Sedimentology*, 27(1):31–46, 1980. doi: 10.1111/j.1365-3091.1980.tb01156.x. *(Cited page 3)*

J. Straubhaar. MPDS technical reference guide. Technical report, Centre d'hydrogéologie et géothermie, University of Neuchâtel, Neuchâtel, 2011. *(Cited page 58)*

J. Straubhaar, P. Renard, G. Mariethoz, R. Froidevaux, and O. Besson. An Improved Parallel Multiple-point Algorithm Using a List Approach. *Mathematical Geosciences*, 43(3):305–328, Mar. 2011. doi: 10.1007/s11004-011-9328-7. *(Cited pages xx, 29, 30, and 58)*

S. Strebelle. Conditional Simulation of Complex Geological Structures Using Multiple-Point Statistics. *Mathematical Geology*, 34(1):1–21, 2002. doi: 10.1023/A:1014009426274. *(Cited pages xxxi, 30, 39, and 86)*

S. Strebelle and N. Remy. Post-processing of Multiple-point Geostatistical Models to Improve Reproduction of Training Patterns. In O. Leuangthong and C. V. Deutsch, editors, *Geostatistics Banff 2004*, number 14 in Quantitative Geology and Geostatistics, pages 979–988. Springer Netherlands, 2005. ISBN 978-1-4020-3515-9 978-1-4020-3610-1. doi: 10.1007/978-1-4020-3610-1_102. *(Cited page 32)*

S. Strebelle, K. Payrazyan, and J. Caers. Modeling of a Deepwater Turbidite Reservoir Conditional to Seismic Data Using Principal Component Analysis and Multiple-Point Geostatistics. *SPE Journal*, 8(3), 2003. doi: 10.2118/85962-PA. *(Cited pages 35 and 111)*

L. Streit, P. Federl, and M. Sousa. Modelling Plant Variation Through Growth. *Computer Graphics Forum*, 24(3):497–506, Sept. 2005. doi: 10.1111/j.1467-8659.2005.00875.x. *(Cited page 86)*

L. Stright, J. Stewart, K. Campion, and S. Graham. Geologic and seismic modeling of a coarse-grained deep-water channel reservoir analog (Black's Beach, La Jolla, California). *AAPG Bulletin*, 98(4):695–728, 2014. doi: 10.1306/09121312211. *(Cited pages xix, 7, and 8)*

E. J. Sumner, J. Peakall, R. M. Dorrell, D. R. Parsons, S. E. Darby, R. B. Wynn, S. D. McPhail, J. Perrett, A. Webb, and D. White. Driven around the bend: Spatial evolution and controls on the orientation of helical bend flow in a natural submarine gravity current. *Journal of Geophysical Research: Oceans*, 119(2):898–913, 2014. doi: 10.1002/2013JC009008. *(Cited pages 20, 35, and 164)*

P. Tahmasebi, A. Hezarkhani, and M. Sahimi. Multiple-point geostatistical modeling based on the cross-correlation functions. *Computational Geosciences*, 16(3):779–797, 2012. doi: 10.1007/s10596-012-9287-1. *(Cited pages 32 and 39)*

P. Tahmasebi, M. Sahimi, and J. Caers. MS-CCSIM: Accelerating pattern-based geostatistical simulation of categorical variables using a multi-scale search in Fourier space. *Computers & Geosciences*, 67:75–88, June 2014. doi: 10.1016/j.cageo.2014.03.009. *(Cited page 210)*

P. J. Talling. On the triggers, resulting flow types and frequencies of subaqueous sediment density flows in different settings. *Marine Geology*, 352:155–182, 2014. doi: 10.1016/j.margeo.2014.02.006. *(Cited pages 3 and 4)*

P. J. Talling, R. B. Wynn, D. G. Masson, M. Frenz, B. T. Cronin, R. Schiebel, A. M. Akhmetzhanov, S. Dallmeier-Tiessen, S. Benetti, P. P. E. Weaver, and others. Onset of submarine debris flow deposition far from original giant landslide. *Nature*, 450(7169):541–544, 2007. doi: 10.1038/nature06313. *(Cited page 3)*

P. J. Talling, J. Allin, D. A. Armitage, R. W. Arnott, M. J. Cartigny, M. A. Clare, F. Felletti, J. A. Covault, S. Girardclos, E. Hansen, and others. Key future directions for research on turbidity currents and their deposits. *Journal of Sedimentary Research*, 85(2):153–169, 2015. doi: 10.2110/jsr.2015.03. *(Cited page 2)*

X. Tan, P. Tahmasebi, and J. Caers. Comparing Training-Image Based Algorithms Using an Analysis of Distance. *Mathematical Geosciences*, 46(2):149–169, 2014. doi: 10.1007/s11004-013-9482-1. *(Cited pages xxxi, 39, and 71)*

J. Taylor-Hell. Incorporating Biomechanics into Architectural Tree Models. In *18th Brazilian Symposium on Computer Graphics and Image Processing, 2005. SIBGRAPI 2005*, pages 299–306, Oct. 2005. doi: 10.1109/SIBGRAPI.2005.32. *(Cited pages 86 and 107)*

V. Teles, G. de Marsily, and E. Perrier. Sur une nouvelle approche de modélisation de la mise en place des sédiments dans une plaine alluviale pour en représenter l'hétérogénéité. *Comptes Rendus de l'Académie des Sciences - Series IIA - Earth and Planetary Science*, 327(9):597–606, 1998. doi: 10.1016/S1251-8050(99)80113-X. *(Cited pages xxxv, 165, and 201)*

W. S. Torgerson. Multidimensional scaling: I. Theory and method. *Psychometrika*, 17(4):401–419, 1952. doi: 10.1007/BF02288916. *(Cited pages 39, 54, and 55)*

W. S. Torgerson. *Theory and methods of scaling*. John Wiley & Sons, New York, 1958. ISBN 978-0-471-87945-9. *(Cited pages 54 and 55)*

T. T. Tran. Improving variogram reproduction on dense simulation grids. *Computers & Geosciences*, 20(7):1161–1168, 1994. doi: 10.1016/0098-3004(94)90069-8. *(Cited page 72)*

N. Tyler. New oil from old fields. *Geotimes*, 33(7):8–10, 1988. *(Cited page 2)*

S. Viseur. *Simulation stochastique basée-objet de chenaux*. PhD thesis, Institut National Polytechnique de Lorraine, Vandoeuvre-lès-Nancy, France, 2001. *(Cited pages xxxi, xxxv, 31, 33, 38, 86, 97, 154, 155, 156, 165, and 201)*

H. Wadell. Volume, shape, and roundness of quartz particles. *The Journal of Geology*, pages 250–280, 1935. *(Cited page 46)*

A. W. Western, G. Blöschl, and R. B. Grayson. Toward capturing hydrologically significant connectivity in spatial patterns. *Water Resources Research*, 37(1): 83–97, Jan. 2001. doi: 10.1029/2000WR900241. *(Cited page 44)*

H. E. Wheeler. Time-stratigraphy. *AAPG Bulletin*, 42(5):1047–1063, Jan. 1958. *(Cited page 96)*

H. Wickham. *ggplot2: elegant graphics for data analysis*. Springer, 2009. ISBN 978-0-387-98141-3. *(Cited page 58)*

L. Wietzerbin. *Modélisation et paramétrisation d'objets naturels de formes complexes en trois dimensions. Application à la simulation stochastique de la distribution d'hétérogénéités au sein des réservoirs pétroliers*. PhD thesis, Institut National Polytechnique de Lorraine, Vandoeuvre-lès-Nancy, France, 1994. *(Cited pages 31 and 97)*

D. R. Wilson and T. R. Martinez. Improved heterogeneous distance functions. *Journal of Artificial Intelligence Research*, 6:1–34, 1997. doi: 10.1613/jair.346. *(Cited page 53)*

R. B. Wynn, B. T. Cronin, and J. Peakall. Sinuous deep-water channels: Genesis, geometry and architecture. *Marine and Petroleum Geology*, 24(6-9):341–387, 2007. doi: 10.1016/j.marpetgeo.2007.06.001. *(Cited pages 4, 6, 8, and 215)*

L. Yang, W. Hou, C. Cui, and J. Cui. GOSIM: A multi-scale iterative multiple-point statistics algorithm with global optimization. *Computers & Geosciences*, 89:57–70, 2016. doi: 10.1016/j.cageo.2015.12.020. *(Cited page 210)*

Y. Yin, S. Wu, C. Zhang, S. Li, and T. Yin. A reservoir skeleton-based multiple point geostatistics method. *Science in China Series D: Earth Sciences*, 52(1): 171–178, 2009. doi: 10.1007/s11430-009-5004-x. *(Cited page 39)*

J. H. Youngson and D. Craw. Variation in placer style, gold morphology, and gold particle behavior down gravel bed-load rivers; an example from the

Shotover/Arrow-Kawarau-Clutha River system, Otago, New Zealand. *Economic Geology*, 94(5):615–633, 1999. doi: 10.2113/gsecongeo.94.5.615. *(Cited pages xxxix and 2)*